VIBRATIONAL ANALYSIS OF SMALL MOLECULES AT THE COMPLETE BASIS SET LIMIT

by

WHITNEY JAMES MORGAN

(Under the Direction of Henry F. Schaefer III)

ABSTRACT

Vibrational analysis is an *ab initio* technique that explains the infrared spectrum of a molecule by describing its internal motion. Spectroscopists and astronomers rely on this information to explore molecular vibrations observed in the laboratory or in the interstellar medium of space. In this work, we showcase computational chemistry methods that are able to predict anharmonic vibrational frequencies to sub-wavenumber, or spectroscopic, accuracy. We benchmarked this impressive capability with formaldehyde before applying similar methods to other small molecules of interest. The first is hydrogen sulfide cation; which has yet to be observed in space but is a likely contributor to interstellar sulfur depletion. Another important astronomical molecule, cyclopropenylidene, is then critically analyzed due to recent challenges in its theoretical description. Lastly, the fundamental vibrations and energy level splittings of the elusive methyl anion are explored with high-level methods.

INDEX WORDS: Computational chemistry, anharmonic, force field, potential energy surface, rovibrational, molecular vibrations, electronic structure, astrochemistry, interstellar medium, sulfur depletion, formaldehyde, hydrogen sulfide cation, cyclopropenylidene, methyl anion

VIBRATIONAL ANALYSIS OF SMALL MOLECULES AT THE COMPLETE BASIS SET LIMIT

by

WHITNEY JAMES MORGAN

B.S., Georgia Southern University, 2013

M.S., Georgia Southern University, 2015

A Dissertation Submitted to the Graduate Faculty
of the University of Georgia in Partial Fulfillment
of the Requirements for the Degree

Doctor of Philosophy

Athens, Georgia

2019

©2019

All Rights Reserved

WHITNEY JAMES MORGAN

VIBRATIONAL ANALYSIS OF SMALL MOLECULES AT THE COMPLETE BASIS SET LIMIT

by

WHITNEY JAMES MORGAN

Major Professors:	Henry F. Schaefer III
Committee:	Gary E. Douberly
	Steven E. Wheeler

Electronic version approved:

Suzanne Barbour

Dean of the Graduate School

University of Georgia

May 2019

ACKNOWLEDGEMENTS

I have had some unforgettable experiences at the Center for Computational Quantum Chemistry (CCQC) and the NASA Ames Research Center. None of these experiences would have been possible if Prof. Henry F. Schaefer III and Dr. Timothy J. Lee did not take a chance on me. Tim set aside time to talk to me each week for almost two years; the significance of which is not lost on me. Some of my fondest memories were made during my short time at NASA. I am forever grateful to the both of them for the opportunity to contribute this work as well as their constant support and patience. I would like to thank Dr. Devin A. Matthews and Prof. John F. Stanton for treating me like an equal throughout our collaboration; I certainly did not feel like one but I am grateful and learned a tremendous amount during that time. I would also like to thank Prof. Wesley D. Allen for his mentorship during the early stages of that work and for answering my countless questions during his amazing course. I would not been able to complete my degree without the help (and mercy) of some of my coworkers. Marissa, Sarah, Leon (Zhi), Kevin(s), and Avery were great allies; I will miss my friends. I have to thank Dr. Turney, Kathryn, and especially Sybil for listening to my sob stories and helping when they were able. Even the most challenging of past coworkers were able to impart important lessons that I will not forget. The continued support of my family was paramount to my success and without them I would have had the leave the program more than once. My girlfriend Kayla should be awarded her own doctorate for the amount of support she has shown me during this time. She is far tougher than I am and without her this ship would have sank. Lastly, Wishbone is the best dog. This is a physical truth of the universe that I hope to prove in my post-doctoral research.

TABLE OF CONTENTS

CHAPTER 1

GEOMETRIC ENERGY DERIVATIVES AT THE COMPLETE BASIS SET LIMIT: APPLICATION TO THE EQUILIBRIUM STRUCTURE AND MOLECULAR FORCE FIELD OF FORMALDEHYDE

[1] Morgan, W. James. Accepted by the *Journal of Chemical Theory and Computation*. Reprinted here with permission of publisher.

1.1 Abstract

Geometric energy derivatives which rely on core-corrected focal-point energies extrapolated to the complete basis set (CBS) limit of coupled cluster theory with iterative and noniterative quadruple excitations, CCSDTQ and CCSDT(Q), are used as elements of molecular gradients and, in the case of CCSDT(Q), expansion coefficients of an anharmonic force field. These gradients are used to determine the CCSDTQ/CBS and CCSDT(Q)/CBS equilibrium structure of the S_0 ground state of H_2CO where excellent agreement is observed with previous work and experimentally derived results. A fourth-order expansion about this CCSDT(Q)/CBS reference geometry using the same level of theory produces an exceptional level of agreement to spectroscopically observed vibrational band origins (VBOs) with a MAE of 0.57 cm^{-1}. Second-order vibrational perturbation theory (VPT2) and variational discrete variable representation (DVR) results are contrasted and discussed. Vibration-rotation, anharmonicity, and centrifugal distortion constants from the VPT2 analysis are reported and compared to previous work. Additionally, an initial application of a sum-over-states fourth-order vibrational perturbation theory (VPT4) formalism is employed herein, utilizing quintic and sextic derivatives obtained with a recursive algorithmic approach for response theory.

1.2 Introduction

Spectroscopic accuracy, where deviations from gas-phase vibrational band origins (VBO's) does not exceed 1 cm^{-1}, has been a longstanding goal of theoretical spectroscopy[1]. Empirically fit[2–5] potential energy surfaces (PESs) are capable of providing spectroscopic accuracy for a system if a very high-quality *ab initio* PES is available and hundreds of rotationally resolved spectroscopic observations about well-defined VBOs have been for reported for that system. Such empirical reliance obsfucates the powerful predictive ability of theory which most often seeks to describe the properties of systems that are difficult to study in the lab-

oratory. High-accuracy benchmark work[6–8] on the rovibrational spectrum of water shows that *ab initio* PESs alone are capable of spectroscopic accuracy for VBOs as long as complete basis set (CBS) extrapolations and extensive correlation energy corrections are utilized. Quantum chemistry has reached a point where fully *ab initio* PESs of this quality are now available for several small molecules[9–13] but the cost associated with higher-order correlation corrections has prevented their development as a routine practice.

The effectiveness of composite approaches to the total energy of a system is emphasized in the current work through the use of a focal-point analysis (FPA)[14–17] that provides a spectroscopically accurate PES through high-level, size-extensive coupled cluster computations. Recent advances involving a (spin-free) orbital representation of the cluster amplitudes combined with a spin summation technique have made otherwise prohibitive coupled cluster models tractable[18]. These models of correlation include the coupled cluster singles, doubles, iterative triples (CCSDT), noniterative quadruples (CCSDT(Q)), and iterative quadruples (CCSDTQ) methods. The benefits of including the complete $\hat{T}_3$ and $\hat{T}_4$ excitation operators[19–22] have been known for some time, but the noniterative quadruple-excitation model[23] is comparatively new. Due to its relative cost and exemplary performance, CCSDT(Q) has been suggested as the "platinum standard" of quantum chemistry for high-accuracy studies[24]. All of these high-level correlation methods have been shown to converge faster through sub- and micro-iterations, which further increases their applicability by decreasing the time to solution[25].

The progress made in high-level coupled cluster methods is leveraged in this work by determining the equilibrium geometry and fundamental VBOs of the ground state of formaldehyde (S_0 H_2CO), using geometric energy derivatives determined numerically from focal-point energies. Formaldehyde benefits from decades of research using high-resolution gas-phase spectroscopy to describe the vibrational[26–29] and rotational[30,31] (as well as rovibrational in databases such as HITRAN2016[32]) characteristics of the parent molecule and its isotopologues[33]. Multiple empirically refined PESs[2–5] for S_0 H_2CO have been generated over the

years which form an excellent basis of comparison to the current high-accuracy *ab initio* work. The ground-state equilibrium structure (r_e) of formaldehyde has been previously optimized at the CBS limit with high-level correlation energy corrections[34] but the effects of high-level corrections on molecular vibrations and higher-order spectroscopic constants have not been evaluated. The reason for this shortcoming is obvious: the computational cost of quadruple-excitation coupled cluster models has discouraged their use in the development of anharmonic force fields until now.

Molecular force fields of small polyatomic systems have been produced through quartic using CBS-extrapolated composite energies in the past,[35–39] but only benchmark computations on triatomic systems[9] have incorporated quadruple excitation contributions to the correlation energy. A quartic force field (QFF) for S_0 formaldehyde using correlated methods up to CCSDT(Q) and basis sets as large as cc-pV6Z is presented here. QFFs provide a tractable alternative to full-dimensional PESs, which can require 50-100 times the number of displaced nuclear configurations as a QFF, when only the near-equilibrium properties of a molecule, such as fundamental vibrational frequencies, are desired. Such tractability allows for the high-throughput production of accurate spectroscopic data that is critical in the detection and characterization of molecules, especially for larger systems.

Second-order vibrational perturbation theory (VPT2) is used in this work to provide higher-order spectroscopic constants and vibrational frequencies for S_0 H_2CO and compared to a discrete variable representation (DVR) variational approach. The convergence of the VPT2 fundamental frequencies of S_0 formaldehyde to the new CCSDT(Q)/CBS standard is examined using a series of lower level CCSD(T)/cc-pVXZ (X=T,Q,5) QFFs. Additionally, an initial application of vibrational perturbation theory to fourth order (VPT4) is presented, which relies on fifth- and sixth-order geometric energy derivatives provided by a recursive and general-order implementation of response theory[40]. A high-accuracy Morse-based PES generated here is used to fit another, complimentary, dimensionless coordinate PES for use with VPT4. Together, the two datasets offer a basis of comparison for follow-on studies in

nuclear motion theory.

1.3 Theoretical Methods

1.3.1 Complete Basis Set Extrapolation

All CBS extrapolation formulae assume the use of a hierarchy of basis sets that contain an increasing number of one-electron basis functions. As basis set size increases, an exact description of the Hartree-Fock electron density should be approached and diverse sets of virtual orbitals should be provided for the description of electron correlation. The correlation-consistent, polarized-valence, family of basis sets (cc-pVXZ, aug-cc-pVXZ, cc-pCVXZ, cc-pwCVXZ; X=D, T, Q, 5, 6)[41–43] were designed to have these properties. The Hartree-Fock energy extrapolation formula of Feller[44] as well as that of Helgaker et al. for the correlation energy[45] were developed using the correlation-consistent family of basis sets. The three-parameter exponential fit[44],

$$E_X^{\mathrm{HF}} = E_\infty^{\mathrm{HF}} + ae^{-bX}, \tag{1.1}$$

relies on a system of direct-fit or least-squares equations involving Hartree-Fock energies computed using at least three correlation-consistent basis sets. The slower convergence[46–48] of the correlation energy (regardless of ansatz used) relative to the Hartree-Fock energy prompted Helgaker et al. to develop a separate two-parameter fit[45] of the correlation energy,

$$E_X^{\mathrm{total}} - E_X^{\mathrm{HF}} = \varepsilon_\infty^{\mathrm{corr}} + aX^{-3}, \tag{1.2}$$

where X is the cardinality of the correlation consistent basis set, noting that a sequence of basis sets is required to solve for extrapolated energies. The extrapolation formulae used above are just two of the many approaches available in the literature for CBS energy

extrapolations[49]. Other popular methods for the extrapolation of energies include the three-point scheme of Martin and Lee[50] as well as numerous formulations from Schwenke[51].

1.3.2 The Focal-Point Approach

Focal point analysis (FPA) is a dual-extrapolation composite energy scheme that systematically approaches the full configuration interaction (FCI) complete basis set (CBS) limit. The one-particle basis set limit is targeted in both the reference (Hartree-Fock) energy as well as the correlation energy. In this way, errors associated with the basis set dependence of the CCSD(T) energy is minimized. The unrecovered correlation energy is primarily accounted for by more complete models of n-particle excitation. These high level contributions to the correlation energy are represented in FPA as energy increments and appear as high level corrections (E_{hlc}) in model chemistries such as HEAT[52–54]. Energy increments are defined as the difference in the correlation energy using two separate but "adjacent" methods in the coupled cluster (or Møller-Plesset) hierarchy which rely on the same one-particle basis set.

Table 1.1: Example Focal Point Table of CCSDT(Q)/CBS Energies

Basis Set	E_e [RHF]	$+\delta$ [MP2]	$+\delta$ [CCSD]	$+\delta$ [CCSD(T)]	$+\delta$ [CCSDT]	$+\delta$ [CCSDT(Q)]	$= E_e$ [Final]
cc-pVTZ	$\boldsymbol{E_3}$	E_3	E_3	E_3	E_3	$\boldsymbol{E_3}$	E_3
cc-pVQZ	$\boldsymbol{E_4}$	E_4	E_4	$\boldsymbol{E_4}$	$\boldsymbol{E_4}$	$\tilde{E}_4$	$\tilde{E}_4$
cc-pV5Z	$\boldsymbol{E_5}$	E_5	E_5	$\boldsymbol{E_5}$	$\tilde{E}_5$	$\tilde{E}_5$	$\tilde{E}_5$
cc-pV6Z	$\boldsymbol{E_6}$	E_6	E_6	$\boldsymbol{E_6}$	$\tilde{E}_6$	$\tilde{E}_6$	$\tilde{E}_6$
CBS limit	E_∞	E_∞	E_∞	E_∞	$\tilde{E}_\infty$	$\tilde{E}_\infty$	$\tilde{E}_\infty$
Fit	$a + bc^{-eX}$	$a + bX^{-3}$	$a + bX^{-3}$	$a + bX^{-3}$	additive	additive	
Points (X)	4,5,6	5,6	5,6	5,6			

Colored areas are provided using the fit and points in the last two rows or by additivity.
Bolded terms are the only energies required to compute the focal-point extrapolated energy.
Additive terms are determined as CC_n/cc-pVXZ = CC_{n-1}/cc-pVXZ + [CC_n/cc-pV(X-1)Z - CC_{n-1}/cc-pV(X-1)Z] where CC_{n-1} is the previous method in the hierarchy.

The correlation hierarchy of methods used in FPA, such as the HF→MP2→CCSD→CCSD(T)→CCSDT→CCSDT(Q) hierarchy used here, is used to determine method adjacency and is almost always reported explicitly or in the form of a FPA table such as the

example in Table 1.1. A common example of an energy increment is the one associated with the correlation energy recovered using the iterative triple excitations model of coupled cluster theory: $\delta E_X^{\mathrm{T}} = E_X^{\mathrm{CCSDT}} - E_X^{\mathrm{CCSD(T)}}$. The defining n-particle excitation model is used as the energy increment superscript to convey that the correlation energy being recovered by the additive difference term is, in this example, from the iterative triples (CCSDT) results using a cc-pVXZ basis set. These increments rely solely on the correlation energy components of the methods employed, since the reference energy cancels when using the same one-particle basis set.

The core-corrected focal-point energy used in this study is defined by five components; four of which define the FPA energy and one which corresponds to the core correction. In the equation below, E is an absolute energy and ΔE is the difference between two absolute energies.

$$\begin{aligned} E_{\mathrm{CBS}}^{\mathrm{CCSDT(Q)}} = & \left(E_6^{\mathrm{HF}} - \frac{\left(E_6^{\mathrm{HF}} - E_5^{\mathrm{HF}}\right)^2}{E_6^{\mathrm{HF}} - 2E_5^{\mathrm{HF}} + E_4^{\mathrm{HF}}} \right) + \left(\varepsilon_6^{(\mathrm{T})} - \frac{\varepsilon_6^{(\mathrm{T})} - \varepsilon_5^{(\mathrm{T})}}{1 - \left(\frac{6}{5}\right)^3} \right) \\ & + \left(E_4^{\mathrm{T}} - E_4^{(\mathrm{T})} \right) + \left(E_3^{(\mathrm{Q})} - E_3^{\mathrm{T}} \right) + \left(E_{4,\mathrm{ae}}^{(\mathrm{T})} - E_{4,\mathrm{fc}}^{(\mathrm{T})} \right) \\ & = E_\infty^{\mathrm{HF}} + \varepsilon_\infty^{(\mathrm{T})} + \delta E_4^{\mathrm{T}} + \delta E_3^{(\mathrm{Q})} + \Delta E_{\mathrm{core}} \end{aligned} \tag{1.3}$$

Any term represented by ε_X^n is the correlation energy of a given method defined as $E_X^n - E_X^{HF}$ where n represents the defining excitation term of the model such as (T) in CCSD(T). Energy increments described as δE^n or $\delta \varepsilon^n$ are equivalent. The final term in this energy is the core correlation correction which relies on the cc-pCVXZ basis set [43]. It is defined as the difference between the CCSD(T) energy with all electrons correlated and the energy within the frozen core approximation. Two energy increments are used in the present work, δE_4^{T} and $\delta E_3^{(\mathrm{Q})}$, to define the CCSDT(Q)/CBS focal-point energy as seen in Equation 1.3.

1.3.3 Equilibrium Structure Optimization

Molecular structures are optimized with numerical gradients determined through three-point or five-point central finite difference formulae using the findiff module of PSI4[55]. The C_{2v} ground state structure of formaldehyde requires 6 or 12 displaced geometries per numerical gradient. CCSDT(Q)/CBS core-corrected focal-point energies are computed at each displaced geometry required for calculation of the three and five-point gradient. The efficacy of core corrections in composite approaches is evaluated through comparison of the three-point CCSDT(Q)/CBS geometry to a three-point optimized ae-CCSDT(Q)/CBS structure. Additionally, a CCSDTQ/CBS geometry, which relies on iterative CCSDT/cc-pV5Z and CCSDTQ/cc-pVTZ additive corrections, is determined using five-point gradients. The CCSDTQ/CBS level of theory is shown below in the aforementioned notation.

$$E_{\mathrm{CBS}}^{\mathrm{CCSDTQ}} = E_{\infty}^{\mathrm{HF}} + \varepsilon_{\infty}^{(\mathrm{T})} + \delta E_{5}^{\mathrm{T}} + \delta E_{3}^{\mathrm{Q}} + \Delta E_{\mathrm{core}} \tag{1.4}$$

Relativistic corrections, Δ_{rel}, are determined as the difference between the simple internal coordinates of structures optimized at ae-CCSD(T)/cc-pCVQZ corrected with mass-velocity as well as one- and two-electron Darwin terms (MVD2)[56,57] and ae-CCSD(T)/cc-pCVQZ (referred to below as nonrel).

$$r_{\mathrm{CBS}+\Delta_{\mathrm{rel}}} = r_{\mathrm{CBS}} + (r_{\mathrm{MVD2}} - r_{\mathrm{nonrel}}) \tag{1.5}$$

The r coordinate shown in Eqn. 1.5 is representative of any corrected simple internal coordinate; angle or bond distance. A root-mean-square (RMS) force convergence threshold of $1{\times}10^{-7}$ E_h/a_0 is used for all CBS structures. Analytic gradients implemented in CFOUR 2.0 are used to optimize the reference structures for the CCSD(T)/cc-pVXZ (X=T,Q,5) levels of theory and are converged with a force RMS threshold of $1{\times}10^{-9}$ E_h/a_0.[58]

1.3.4 CBS Extrapolation of Analytic Gradients

Although the numerical gradients used here benefit from an clearly parallelized computational strategy, analytic gradients will always be preferred when available as they are much faster to compute, are independent of system size, and suffer much less from numerical errors[59,60]. A brief derivation of how common CBS formulae may be extended to include first-order geometric derivatives is presented below. Solution of the a, b, c coefficients in an exponential fit[44] produces an easily implemented form of the CBS extrapolation of Hartree-Fock energies by way of:

$$E_\infty = E_3 - \frac{(E_3 - E_2)^2}{E_3 - 2E_2 + E_1} = E_3 - \frac{A^2}{B}. \tag{1.6}$$

In the above form, Hartree-Fock energies computed using correlation-consistent basis sets are presented as E_n where the highest n corresponds to the largest basis set used. Differentiation of the extrapolation formula with respect to a generic variable x representing a nuclear coordinate in the Cartesian frame provides a direct method of extrapolation of analytic gradients to the complete one-particle basis set limit:

$$\frac{\partial E_\infty}{\partial x} = (1 - 2AB^{-1} + A^2B^{-2})\ \frac{\partial E_3}{\partial x} + 2(AB^{-1} - A^2B^{-2})\ \frac{\partial E_2}{\partial x} + A^2B^{-2}\ \frac{\partial E_1}{\partial x} \tag{1.7}$$

The same principles used for the above derivation can be applied to Helgaker et al.'s extrapolation formulae for the correlation energy[45].

$$E_\infty = E_2 - \frac{E_2 - E_1}{1 - (X_2/X_1)^3} = E_2 - Ac^{-1} \tag{1.8}$$

$$\frac{\partial E_\infty}{\partial x} = (1 - c^{-1})\frac{\partial E_2}{\partial x} + c^{-1}\frac{\partial E_1}{\partial x} \tag{1.9}$$

The denominator shown above is a simple constant term represented as c, whereas the

electronic energies that enter the extrapolation are described by the difference term A. In both the reference and correlated results, the A and B variables are linear with respect to the electronic energies and the $\partial E_n/\partial x$ terms are independent of one another. The formulae derived above are with respect to a general variable x where x is chosen to be a geometric variable in this study. Similar approaches have been employed in past studies[34,61,62] with great success. However, the extrapolation of other types of energy derivatives may be better suited to a parameterized extrapolation, such as those in Ref. 63, as suggested by recent work on hyperpolarizabilities[64].

1.3.5 Quartic Force Fields

A local expansion of the CCSDT(Q)/CBS potential with respect to a set of curvilinear internal coordinates is produced to fourth order about the five-point CCSDT(Q)/CBS optimized geometry. The set of coordinates chosen are redundant simple internal coordinates of formaldehyde: r_{CO}, r_{CH}, r'_{CH}, θ_{OCH}, θ'_{OCH}, τ_{HCOH}. Symmetry-adapted internal coordinates are formed following the set described by Martin et al.[65]:

$$\begin{aligned}
S_1(a_1) &= \frac{1}{\sqrt{2}}(r_{\mathrm{CH}} + r'_{\mathrm{CH}}) \\
S_2(a_1) &= r_{\mathrm{CO}} \\
S_3(a_1) &= \frac{1}{\sqrt{2}}(\theta_{\mathrm{OCH}} + \theta'_{\mathrm{OCH}}) \\
S_4(b_1) &= \tau_{\mathrm{HCOH}} \\
S_5(b_2) &= \frac{1}{\sqrt{2}}(r_{\mathrm{CH}} - r'_{\mathrm{CH}}) \\
S_6(b_2) &= \frac{1}{\sqrt{2}}(\theta_{\mathrm{OCH}} - \theta'_{\mathrm{OCH}})
\end{aligned} \tag{1.10}$$

This quartic force field (QFF) is generated by displacing the equilibrium symmetry-adapted internal coordinates by 0.01 Å for bond lengths and 0.02 rad for bond angles. The displaced internal coordinate configurations are then transformed to the 183 required symmetry unique

Cartesian geometries. The focal-point procedure is performed at each of the displaced geometries using the CCSDT(Q)/CBS level of theory. The INTDIF2008 *Mathematica* program[66] is used to generate the single-point geometries, as well as solve for the symmetry-adapted internal coordinate energy derivatives by central finite difference formulae. In the polynomial below, the symmetry-adapted force constants are represented as $\mathrm{F}_{ij} = \frac{\partial^2 V}{\partial S_i \partial S_j}$, $\mathrm{F}_{ijk} = \frac{\partial^3 V}{\partial S_i \partial S_j \partial S_k}$, and $\mathrm{F}_{ijkl} = \frac{\partial^4 V}{\partial S_i \partial S_j \partial S_k \partial S_l}$.

$$\mathrm{V}_4(\mathbf{S}) = \frac{1}{2}\sum_{ij} \mathrm{F}_{ij} S_i S_j + \frac{1}{6}\sum_{ijk} \mathrm{F}_{ijk} S_i S_j S_k + \frac{1}{24}\sum_{ijkl} \mathrm{F}_{ijkl} S_i S_j S_k S_l. \tag{1.11}$$

The coordinates in Eqn. 1.11 are understood to be displacement coordinates in $\mathbf{S}$. Up to four-mode coupling is considered (unrestricted summations up to fourth order) but force constants obviously related by symmetry are equivalent, such as $\mathrm{F}_{ij} = \mathrm{F}_{ji}$, and only computed once.

Relativistic corrections to the CCSDT(Q)/CBS QFF are evaluated as the difference between the symmetry-adapted internal coordinate force constants (Eqn. 1.11) from two additional QFFs. These are the ae-CCSD(T)/cc-pCVQZ (MVD2)[56,57] and ae-CCSD(T)/cc-pCVQZ (referred to as nonrel) levels of theory, $\Delta_{\mathrm{rel}} = \mathrm{V}_4(\mathbf{S}_{\mathrm{MVD2}}) - \mathrm{V}_4(\mathbf{S}_{\mathrm{nonrel}})$, where the QFFs in Δ_{rel} are expanded about a geometry optimized at their respective levels of theory. Corrections made directly to the CCSDT(Q)/CBS energy with the same methods, $E_{\mathrm{CBS}}^{\mathrm{CCSDT(Q)}} + (E_{\mathrm{MVD2}} - E_{\mathrm{nonrel}})$, are found inferior to those made at the force constant level due to increasingly large shifts observed in F_{22}, the diagonal C−O stretching force constant. The additive difference corrected CBS geometry, $r_{\mathrm{CBS}+\Delta_{\mathrm{rel}}}$ (Eqn. 1.5), is used as the equilibrium geometry in VPT2 calculations in both cases but is likely inferior to a geometry which is optimized using a numerical gradient that explicitly contains scalar relativistic corrections. All QFFs are generated in the same procedure described at the beginning of this section and, thus, displace the corresponding CCSDT(Q)/CBS, MVD2, and nonrel equilibrium structures

along the same set of internal coordinate displacements. A diagonal Born-Oppenheimer correction (DBOC) was determined negligible for the present work but Refs. 6, 67, and 68 show how the magnitude of DBOCs can grow with the number of vibrational quanta in energy levels of water and how DBOC surfaces are needed for spectroscopic quality results for systems such as H_3^+.

Variational results for anharmonic vibrational frequencies are provided (using the full extrapolated surface) through discrete variable representation (DVR) with P. B. Changala's NITROGEN program[69]. A series of 9, 12, 12, 12, 12, and 9 potential-optimized grid points are chosen for NITROGEN from an initial basis spanning 1.7 Å, 1.2 Å, 1.2 Å, 90°, 90°, 120° in redundant simple internal coordinates (see above). Standard thick restart was used with a Lanczos tolerance of 1.0×10^{-6} cm^{-1} where the reported energy levels are converged to machine precision (approximately 1.0×10^{-12} cm^{-1} in this case). Coordinate transformations are performed with respect to the simple internal bond displacement coordinates, Δr_{CH} and Δr_{CO}, that comprise $S_{i=1-2,5}$ to generate a Morse[70], $\mu = 1 - \exp(-\alpha\Delta r)$, representation of the PES, $\alpha = -f_{iii}/3f_{ii}$, before prediction of vibrational eigenvalues. The simple internal coordinate derivatives used in α are defined as $f_{ii} = \frac{\partial^2 V}{\partial r_i^2}$ and $f_{iii} = \frac{\partial^3 V}{\partial r_i^3}$. The final surface maintains the symmetry of the original.

Second-order vibrational perturbation theory (VPT2) is used to provide vibrational frequencies and spectroscopic constants with the SPECTRO program[71] based on the quartic potential, $\mathrm{V}_4(\mathbf{q})$. The non-linear transformation of geometric derivatives, required to go from curvilinear internal coordinate space to Cartesian space, is performed using the INTDER2005 program[72] before transformation to reduced normal coordinates[73].

$$\mathrm{V}_4(\mathbf{q}) = \frac{1}{2}\sum_r \omega_r q^2 + \frac{1}{6}\sum_{rst}\phi_{rst}q_r q_s q_t + \frac{1}{24}\sum_{rstu}\phi_{rstu}q_r q_s q_t q_u \tag{1.12}$$

Additional anharmonic force fields are generated for the CCSD(T)/cc-pVXZ (X=T,Q,5) levels of theory with the procedure noted above where SPECTRO is used to provide vibra-

tional frequencies and anharmonicity constants. The first and second harmonic derivatives are calculated using the GUINEA module of CFOUR 2.0. Fermi resonances are treated in both SPECTRO and GUINEA where results are confirmed consistent to the reported values.

1.3.6 Recursive Calculation of Response Properties

For the analytic calculation of response properties at the Hartree-Fock (HF) level, a recently developed formulation of response theory[74] and its recursive implementation[75] in a local version of the DALTON2013 program suite[76,77] was employed, where differentiated one- and two-electron integrals were obtained using the GEN1INT[78,79] and CGTO-DIFF-ERI[80,81] modules, respectively, and where the response equation solver of Jørgensen *et al.*[82] was used. The method has previously been described extensively[74,75], and we refer the interested reader to this earlier work for further details about the underlying theory and its implementation. In the present manuscript, we will only outline the main features of the approach.

In this formulation, an arbitrary response property $\langle\langle A; B, C, \ldots\rangle\rangle_{\omega_{bc\cdots}}$ involving perturbations $a, b, c \ldots$, associated with a collection of frequencies $\omega_{bc\cdots}$, where $\omega_a = -\sum_{i\in\{b,c,\ldots\}} \omega_i$, is expressed as a quasienergy derivative $\mathcal{L}^{abc\cdots}_{k,n}$. Using a generalization of Wigner's $(2n+1)$ rule expressed by integers k and n and permitting truncation rule choices between and including the well-known $(n+1)$ and $(2n+1)$ rules[83], response properties can be expressed compactly as

$$\begin{aligned}\langle\langle A; B, C, \ldots\rangle\rangle_{\omega_{bc\cdots}} = \mathcal{L}^{abc\cdots}_{k,n} \overset{\{\mathrm{Tr}\}_T}{=} E^{abc\cdots}_{k,n} - (\mathbf{SW})^{abc\cdots}_{n_W} - (\mathbf{S}^a\mathbf{W})^{bc\cdots}_{k_S,n'_W} \\ - (\boldsymbol{\lambda}^a\mathbf{Y})^{bc\cdots}_{k_\lambda,n'_Y} - (\boldsymbol{\zeta}^a\mathbf{Z})^{bc\cdots}_{k_\zeta,n'_Z},\end{aligned} \tag{1.13}$$

where E in this work is the HF energy, $\mathbf{S}$ is the overlap matrix, $\mathbf{W}$ is a generalization of the so-called energy-weighted density matrix, and $\boldsymbol{\lambda}$ and $\boldsymbol{\zeta}$ are Lagrange multipliers for respectively the time-dependent self-consistent field and idempotency conditions, expressed as $\mathbf{Y}$ and $\mathbf{Z}$, respectively. The notation $\overset{\{\mathrm{Tr}\}_T}{=}$ signifies that the trace and time-average over

the collective oscillation period of the applied perturbations will be taken for the terms on the right-hand side of Eq. (1.13), and superscripts $abc\cdots$ denotes perturbation-strength differentiation and subsequent evaluation at zero perturbation strength for the collection of perturbations thus indicated. The integers k and n, taking various forms in Eq. (1.13), indicate a particular choice of the generalized Wigner rule, placing certain conditions on which terms must be evaluated to yield the desired response property. We remark that in this work, which involves only perturbations that represent displacement of the Cartesian coordinates of the system, the maximum value of k and n for a given property notably determines the maximum order of such perturbation to which the density matrix $\mathbf{D}$ and Fock matrix $\mathbf{F}$ must be evaluated during the course of the calculation. For further details, we refer to the original works[74,75]; noting, however, that it is the $(2n+1)$ rule which for all properties in this work will result in the lowest computational costs and is therefore here the one chosen. The $(2n+1)$ rule choice is equivalent to setting $(k,n)=(2,2)$ and $(k,n)=(2,3)$ for the fifth- and sixth-order force constants, respectively, and the fifth-order force constants $\mathcal{L}^{ggggg}$, where g denotes displacement of the Cartesian nuclear coordinates, are thus obtained by evaluating the expression

$$\begin{aligned}\mathcal{L}^{ggggg}_{2,2} \overset{\{\mathrm{Tr}\}_T}{=} E^{ggggg}_{2,2} - (\mathbf{SW})^{ggggg}_{2_W} - (\mathbf{S}^g\mathbf{W})^{gggg}_{2_S,2'_W} \\ - (\boldsymbol{\lambda}^g\mathbf{Y})^{gggg}_{2_\lambda,2'_Y} - (\boldsymbol{\zeta}^g\mathbf{Z})^{gggg}_{2_\zeta,2'_Z},\end{aligned} \tag{1.14}$$

for the fifth-rank tensor containing all combinations of the components of such displacements, while the corresponding expression for sixth-order force constants $\mathcal{L}^{gggggg}$ is

$$\begin{aligned}\mathcal{L}^{gggggg}_{2,3} \overset{\{\mathrm{Tr}\}_T}{=} E^{gggggg}_{2,3} - (\mathbf{SW})^{gggggg}_{3_W} - (\mathbf{S}^g\mathbf{W})^{ggggg}_{2_S,3'_W} \\ - (\boldsymbol{\lambda}^g\mathbf{Y})^{ggggg}_{2_\lambda,3'_Y} - (\boldsymbol{\zeta}^g\mathbf{Z})^{ggggg}_{2_\zeta,3'_Z}.\end{aligned} \tag{1.15}$$

1.3.7 4th-order Vibrational Perturbation Theory

Using the recursive approach of the previous subsection, a set of fully analytic HF/cc-pVTZ quintic and sextic geometric derivatives are determined in the Cartesian reference frame with an S_0 H_2CO structure optimized at the HF/cc-pVTZ level of theory. An analytic HF/cc-pVTZ Hessian produced about this equilibrium structure is used to transform the Cartesian derivatives into a reduced normal coordinate (dimensionless) system. For clarity, CCSDT(Q)/CBS reduced normal coordinates are referred to as **q** whereas HF/TZ reduced normal coordinates are denoted by **q'**. The set of HF/TZ reduced normal coordinate fifth- and sixth-order derivatives determined from the recursive approach is referred to as V_6(**q'**) as shown in Eqn. 1.16.

$$V_6(\mathbf{q'}) = \frac{1}{120}\sum_{rstu}\phi_{rrstu}q_r^2 q_s q_t q_u + \frac{1}{720}\sum_{rtu}\phi_{rrttuu}q_r^2 q_t^2 q_u^2 \tag{1.16}$$

Additionally, the improved convergence radius of the aforementioned CCSDT(Q)/CBS Morse-based QFF is exploited to produce another set of reduced normal coordinate force constants up to sixth-order by LSQ fitting energies to displacements along **q**, the CCSDT(Q)/CBS reduced normal coordinates. It may be noted that only the expansion coefficients known to contribute in VPT4 are used to define the quintic and sextic portions of both force fields.

Fundamental frequencies computed with fourth order vibrational perturbation theory (VPT4) are determined using both the quartic (V_4(**q**)) and quintic and sextic (V_6(**q**) or V_6(**q'**)) force fields, as well as vibrational corrections to the instantaneous moments of inertia $\mu_{\alpha\beta}$. The mass-dependent pseudopotential term U(**q**) which appears in the Watson Hamiltonian has not been included fully to fourth order. We use standard Rayleigh-Schrödinger perturbation theory and a direct sum-over-states formalism, in contrast to other work on analytical[84] and numerical[85,86] contact transformations. This approach has been incorporated into the GUINEA module of the CFOUR program suite[58]. VPT4 is also capable of generating additional vibrational corrections to the rotational constants, centrifugal distor-

tion constants, etc. We expect that these additional corrections could account for some of the residual differences with respect to experiment that we observe (see for example, Table 1.5); however, we have not yet implemented them.

All electronic structure computations are based on restricted Hartree-Fock (RHF) reference wavefunctions. The Molpro 2010.1.67 computational chemistry suite[87] is used for single-point coupled cluster computations up to CCSD(T). One and two electron integral cutoffs are 1×10^{-14} E_h where the HF and coupled cluster energies are converged to 1×10^{-11} E_h. The NCC module[24] of the CFOUR 2.0 package[58] is used for the CCSDT and CCSDT(Q) computations in the spin-adapted non-orthogonal coupled cluster framework[18]. CCSD(T)/aug-cc-pVQZ (aQZ) electronic contributions to the rotational constants of the CCSDT(Q)/CBS reference structure are provided through CFOUR 2.0. Coupled cluster energies and amplitudes are converged to better than 1×10^{-9} E_h in the CFOUR interfaced computations.

1.4 Results and Discussion

1.4.1 Equilibrium Structures and Rotational Constants

The change in predicted geometries is a function of both basis set and treatment of electron correlation[61,88–93]. These trends can be summarized succinctly with respect to the C_{2v} ground state of formaldehyde as: 1) bonds contract and angles grow with increasing basis set cardinality as well as with the inclusion of core correlation; and 2) bonds lengthen and angles shrink slightly as the description of the n-particle space improves. These relationships are explored here using the *ab initio* structures of S_0 H_2CO predicted at various levels of theory as shown in Table 1.2. The CCSD(T)/TZ predicted structure displays the longest bonds and smallest HCH bond angle; the only unique bond angle in the system due to symmetry. This bond angle widens significantly, from 116.185 to 116.442°, in the CCSD(T)/QZ structure where the characteristic contraction of bond lengths is observed. The contraction is especially prominent in r_e(CO) which decreases by 0.003 Å. The r_e(CO) bond is rela-

tively converged in the included CCSD(T)/cc-pVXZ, X = T, Q, 5, sequence (referred to as T→Q→5 hereafter) at the CCSD(T)/5Z geometry which only shrinks by 0.00024 Å compared to the cc-pVQZ geometry. However, a modest contraction of r_e(CH) is accompanied by an increase in θ_e(HCH) as the basis set grows from cc-pVQZ to cc-pV5Z.

The focal-point gradients used to optimize the CBS structures in this paper rely on extrapolation of CCSD(T)/cc-pVXZ (X=Q,5,6) energies and are corrected for higher-order electron correlation using up to the CCSDT/5Z and CCSDTQ/TZ levels of theory as seen in Eqns. 1.3 and 1.4. The $E_\infty^{\rm HF} + \varepsilon_\infty^{\rm (T)} + \Delta E_{\rm core}$ and $\delta E_5^{\rm T} + \delta E_3^{\rm Q}$ or $\delta E_4^{\rm T} + \delta E_3^{\rm (Q)}$ components of the composite energy are anticipated to shift the geometry in opposite directions within the established trends. It is apparent from the results in Table 1.2 that the former, CBS, components of the composite energy dominate in this context where large contractions of the bond lengths and a modest widening of the HCH bond angle are observed in the CBS results when compared to the CCSD(T)/cc-pVXZ (X=T,Q,5) structures.

Table 1.2: Computed *ab initio* H_2CO Geometries (Å,°)

Method	Basis	Gradient	r_e(CO)	r_e(CH)	θ_e(HCH)
CCSD(T)	cc-pVTZ	Analytic	1.209 57	1.103 28	116.185
CCSD(T)	cc-pVQZ	Analytic	1.206 58	1.102 18	116.442
CCSD(T)	cc-pV5Z	Analytic	1.206 34	1.101 79	116.597
ae-CCSDT(Q)	CBS	3-point	1.204 62	1.100 40	116.688
CCSDT(Q)	CBS	3-point	1.204 84	1.100 53	116.695
CCSDT(Q)	CBS	5-point	1.204 84	1.100 53	116.695
CCSDTQ	CBS	5-point	1.204 57	1.100 52	116.694
Err($\Delta_{\rm core}$)			-0.000 12	-0.000 13	-0.007
$\Delta_{\rm rel}$			-0.000 13	-0.000 11	+0.004

Frozen core computations unless otherwise denoted as all-electron (ae).
Err($\Delta_{\rm core}$) = ae-CCSDT(Q)/CBS- CCSDT(Q)/CBS
$\Delta_{\rm rel}$ = ae-CCSD(T)/pCVQZ (MVD2) - ae-CCSD(T)/pCVQZ

The three-point finite difference optimized ae-CCSDT(Q)/CBS geometry correlates all electrons and is used to gauge the error associated with the core correlation correction, $\Delta E_{\rm core}$, used in the frozen core CCSDT(Q)/CBS results. The differences between these two geometries are listed in Table 1.2 as Err($\Delta_{\rm core}$). A slight contraction of the bond lengths, as well as HCH bond angle, is observed in the three-point optimized all-electron

ae-CCSDT(Q)/CBS results when compared to the three-point optimized CCSDT(Q)/CBS core-corrected structure. Coincidentally, both the r_e(CO) and r_e(CH) bonds are shorter by an equivalent amount of 0.00012 Å and 0.00013 Å, respectively. As such, a core-corrected valence focal point structure may exhibit slightly longer bond lengths and angles than its all-electron counterpart. The three-point and five-point optimized CCSDT(Q)/CBS structures agree within the reported number of significant digits and show negligible differences (deviations on the order of 1×10^{-6} Å for bond lengths and 1×10^{-4} degrees for bond angles) for the core-corrected results.

The authors are not aware of any previous work which use a more complete composite method than the CCSDTQ/CBS level of theory shown in Eqn. 1.4 to determine the equilibrium geometry of this system. The energy increments used to correct the CBS energies use basis sets which are two cardinality higher for the iterative triples correction, δE_5^{T}, and one cardinality higher for the iterative quadruples correction, δE_3^{Q}, than previous results[34]. As described earlier in this section, longer bond lengths are expected from more complete models of correlation whereas contractions of these bonds are expected from increases in the cardinality of the basis set. However, Halkier et al. have shown that the iterative triples coupled cluster model (CCSDT) tends to give bond lengths slightly shorter than those of CCSD(T)[94].

Similar behavior is observed here for iterative quadruples upon comparison of the CCSDTQ/CBS and CCSDT(Q)/CBS geometries in Table 1.2. The CCSDT(Q) model exhibits a slight over-estimation of the total energy as first reported in Bomble et al.'s introduction of the method[23]. Eriksen et al.[95] recently evaluated a number of non-iterative quadruple excitation coupled cluster models and determined the correlation energy recovery of CCSDT(Q), using a cc-pVTZ basis set, to be ∼10% above that of the iterative CCSDTQ model. Thus, the r_e(CO) bond length of the CCSDT(Q)/CBS structure, which is longer than the CCSDTQ/CBS result by 0.00027 Å, is likely a consequence of the overestimation of the quadruples component present in the CCSDT(Q) model. The r_e(CH) bond length

and θ_e(HCH) bond angle, on the other hand, appear converged at this level of theory as seen in Table 1.2.

Despite the well-studied nature of S_0 formaldehyde, there are very few equilibrium structures which are determined at a comparable level of theory as the present results. The equilibrium structure of Puzzarini et al.[34], shown in Table 1.4, was determined in a similar method as the present work as it relies on CBS-extrapolated (analytic) gradients which are corrected with an additive difference scheme. Exemplary agreement is seen for the calulated bond lengths of S_0 formaldehyde between the CCSDTQ/CBS structure computed in this work and the cc-pVDZ-based CCSDTQ/CBS structure of Puzzarini et al. The C−O bond length differs by a negligible 0.00003 Å (1.20457 - 1.20454 Å) between the two geometries with an even smaller difference of 0.00002 Å (1.10052 - 1.10050 Å) for the C−H bonds. The assumption of a diminishing basis set dependence for this system is reasonable considering only r_e(CO) shows significant change amongst the CCSDT(Q)/CBS and CCSDTQ/CBS geometries computed in this work.

Table 1.3: CCSDT(Q)/CBS Vibration-Rotation α Constants (MHz)

	A	B	C
α_1	4909.417	11.067	67.110
α_2	89.510	217.061	266.381
α_3	-1894.655	-252.883	78.093
α_4	4300.901*	373.052	-39.664
α_5	2710.134	44.366	43.244
α_6	-3644.134*	-75.243	190.938

* treated for Coriolis resonance.

The convergence of individual structural parameters relies not only on the reported *ab initio* results but also requires validation through empirical findings. At present, Lohilahti reports the most recent (and certain) experimentally derived r_e structure of S_0 formaldehyde[96]. As shown in Table 1.4, both the CCSDT(Q)/CBS and CCSDTQ/CBS equilibrium structures provided in this work show exceptional agreement with that of Lohilahti's experimental structure. Both CBS geometries fall within experimental uncertainty for the

CH bond lengths and HCH bond angle, differing less than 0.0001 Å from experiment in r_e(CH) for both structures. CCSDTQ/CBS predicts a r_e(CO) bond length within experimental uncertainty, only 0.00004 Å from Lohilahti's value, whereas CCSDT(Q)/CBS mildly overestimates the length, landing slightly outside the error bounds. The additive difference relativistic corrections shown in Table 1.2 and described in the theoretical methods appear effective here in the case of CCSDT(Q)/CBS, moving the corrected geometry closer in every case, with r_e(CO) = 1.20471 Å, r_e(CH) = 1.10042 Å, and θ_e(HCH) = 116.698 degrees. For CCSDTQ/CBS, both the relatively converged CH bond lengths and HCH bond angle improve when including relativistic corrections but the CO bond length moves away from the experimental structure (although still within experimental uncertainty) at r_e(CO) = 1.20444 Å.

Further validation of the quality of the provided structure is found through the analysis of rotational constants. The equilibrium rotational constants, B_e, provided in Table 1.4 are computed by CFOUR from the internal coordinates of the listed structure if they are otherwise unreported in the corresponding literature. The B_e of the present work are corrected for vibrational and electronic (magnetic) effects as $B_0 = B_e + \Delta B_{\text{vib}} + \Delta B_{\text{el}}$, where B corresponds to A, B, or C, as described in previous work[34]. Vibrational corrections, Δ_{vib}, to the equilibrium rotational constants are determined with VPT2 from the CCSDT(Q)/CBS force field whereas electronic contributions, ΔB_{el}, are predicted at the CCSDT(Q)/CBS geometry using the CCSD(T)/aQZ level of theory. These are ΔA_{vib} = -3235.6 MHz, ΔB_{vib} = -158.7 MHz, and ΔC_{vib} = -303.0 MHz for vibrational corrections and ΔA_{el} = -438.4 MHz, ΔB_{el} = -4.7 MHz, and ΔC_{el} = -1.8 MHz for the magnetic corrections.

The magnetic correction, $\Delta B_{el} = \frac{m_e}{m_p} g B_e$ (m_e and m_p are the masses of an electron and proton, respectively), appears particularly large for A when compared to past studies of halogen cynanides[98] where a correlation between mass and molecular magnetic moment (g-value) was emphasized. In the present case, the electronic contribution to the rotational **g**-tensor dominates the nuclear contribution (especially in the case of the a-principal axis)

Table 1.4: Equilibrium Molecular Structures (Å,°) of $\tilde{\boldsymbol{X}}\ ^1\boldsymbol{A}_1(S_0)$ H_2CO

	Present Work		Rauhut[a]	Puzzarini[b]	Carter[c]	Yachmenev [d]	Experiment[e,f]
	CCSDT(Q)/CBS	CCSDTQ/CBS	*ab initio*	*ab initio*	Spec. Fit	Spec. Fit	
r_e(CO)	1.204 84	1.204 57	1.206 0	1.204 54	1.202 96	1.203 67	1.204 61(19)
r_e(CH)	1.100 53	1.100 52	1.101 9	1.100 50	1.100 64	1.102 90	1.100 46(16)
θ_e(HCH)	116.694	116.694	116.66	116.690	116.704	116.438	116.722(93)
A_e	285 686.8	285 691.3	285 082.7	285 715.9	285 600.5	285 248.4	285 598.2
B_e	38 977.7	38 992.9	38 896.2	38 994.4	39 086.7	38 997.2	38 996.8
C_e	34 298.2	34 310.0	34 226.4	34 311.6	34 381.4	34 307.0	34 308.6
A_0	282 012.8	282 017.3	-	282 033.7	281 955.8	-	281 970.557 8(61)
B_0	38 814.3	38 829.5	-	38 832.1	38 846.3	-	38 833.987 15(31)
C_0	33 993.4	34 005.2	-	34 008.0	34 003.8	-	34 004.243 49(31)

[a] CCSD(T)-F12b/aQZ result from Ref. 97. [b] CCSDTQ/CBS result from Ref. 34.
[c] CCSD(T)/TZ results from Ref. 65 fit to spectroscopically observed vibrational lines in Ref. 4.
[d] CCSD(T)/aQZ PES result fit to spectroscopically observed vibrational lines from Ref. 5.
[e] Experimentally derived equilibrium results from Ref. 96.
[f] A, B, and C from THz and IR results fit to the S reduction in Ref. 30.

producing g-values in line with past experimental work[99]. The g-values are g_{aa} = -2.8177, g_{bb} = -0.2201, and g_{cc} = -0.0952 here whereas Flygare[99] reports g_{aa} = -2.9017(8), g_{bb} = -0.2243(1), and g_{cc} = -0.0994(1). Other planar systems with a central double bond show a similar pattern where the g-value along the double bond axis is much larger than the others. This is the case for the isoeletronic methanimine[100,101] (g_{aa} = -1.27099(22), g_{bb} = -0.18975(7), and g_{cc} = -0.03440(8)) as well as the isovalent thioformaldehyde[99] (g_{aa} = -5.6202(68), g_{bb} = -0.1337(4), and g_{cc} = -0.0239(4)). The interested reader is encouraged to review the supporting information of Ref. 34 for a tabulation of *ab initio* ΔB_{el} values for first-row polyatomics and their isotopes.

A recent study of S_0 H_2CO in the terahertz (THz) regime reports high-accuracy A, B, C constants 281970.5558(61), 38833.98715(31), and 34004.24349(31) MHz, respectively[30]. A difference of 42.3, 19.7, and 10.9 MHz is observed between the experimental A, B, and C constants of Brunken et al. and the theoretical A_0, B_0, and C_0 constants of the CCSDT(Q)/CBS structure[30]. This represents a mean absolute percent error (MAPE; shown below where Y is relative to X) of 0.033% with respect to the experimental values.

$$\mathrm{MAPE}(\%) = \frac{100\%}{n} \sum_{i=1}^{n} \left| \frac{X_i - Y_i}{X_i} \right| \tag{1.17}$$

Improvement on the MAPE is found by applying the same corrections to the equilibrium rotational constants computed using the CCSDTQ/CBS structure. Both B_0 and C_0 show better agreement with B_0 differing by 4.7 MHz and C_0 by 1.0 MHz from experiment but a slight decrease in accuracy is observed in A_0 which varies by 46.9 MHZ. This level of accuracy produces a MAPE a third of the original value at 0.010%. Inclusion of the CCSDT(Q)/CBS quartic and sextic centrifugal distortion constants effects shifts A_0, B_0, and C_0 by 0.0, -1.3, and 1.3 MHz, respectively, which moves both the CCSDT(Q)/CBS and CCSDTQ/CBS rotational constants slightly away from experiment. Although beyond the scope of this work, a better comparison here would be to compute the actual ground state rotational level positions

variationally using our potential, and then fit them to the same rotational Hamiltonian used by Brunken et al. However, this would not alter the qualitative result observed here: that the rotational constants computed here via VPT2 are in excellent agreement with experiment. The present VPT4 framework will soon allow for further correction of these spectroscopic constants through higher-order contributions, once implemented, and should provide even more accurate results by refining ΔB_{vib} as well as providing a more complete description of centrifugal distortion.

1.4.2 Vibrational Band Origins

1.4.2.1 Convergence of VBOs

The easily applied and well-documented convergence patterns of structural parameters seen in subsection A do not generally extend to the vibrational properties of polyatomic molecules. A number of studies have shown that no systematic trend can be applied to anticipate change associated with basis set cardinality as individual harmonic frequencies may increase or decrease independent of one another[104–106]. However, previous work regarding the effects of electron correlation on the harmonic frequencies of diatomics[89,107] and small polyatomics[108,109] suggest that convergence of ω_i follows that of the energy itself. A very narrow selection of literature exists on the convergence of anharmonic frequencies[36,110–113] due to the cost associated with benchmarking large potential expansions. Most anharmonic force field studies focus on reporting a set of spectroscopic constants which provide the best agreement to experimentally observed VBOs rather than analyze the convergence properties of the system being investigated.

For these reasons, a progression of CCSD(T)/cc-pVXZ (X=T,Q,5) harmonic and anharmonic fundamental vibrational frequencies is shown in Table 1.6 for S_0 formaldehyde alongside the modern CCSDT(Q)/CBS results. Martin has shown the convergence of ω_i for S_0 H_2CO in the CCSD(T)/cc-pVXZ (X=D,T,Q) sequence[105]. The present CCSD(T)/cc-

Table 1.5: Quartic and Sextic Centrifugal Distortion Constants (in MHz) from the S and A Reductions

Parameter	Experiment[a]		This work	Parameter	Experiment[a]	This Work	Martin[b]	Carter[c]
$D_J \times 10^3$	70.321 00(68)	70.320 5(50)	70.254 96	$\Delta_J \times 10^3$	75.322 46(75)	74.566 94	72.730	76.807 3
$D_{JK} \times 10^3$	1 321.101(15)	1 321.107 3(93)	1 319.308	$\Delta_{JK} \times 10^3$	1 291.220(23)	1 293.436	1 265.2	1 275.365
$D_K \times 10^3$	19.390 89(72)	19.39 136(53)	18.617 20	$\Delta_K \times 10^3$	19.415 83(73)	18.638 76	18.609	18.113 38
$d_1 \times 10^3$	−10.437 98(18)	−10.437 877(47)	−9.903 52	$\delta_J \times 10^3$	10.454 11(21)	9.903 52	9.563	10.960 4
d_2	−2.501 461(58)	−2.501 496(33)	−2.155 991	δ_K	1.028 291(34)	0.917 961	0.896	-
$H_J \times 10^9$	3.92(47)	3.54(33)	3.40	$\Phi_J \times 10^9$	97.45(53)	85.09	89.94	-
$H_{JK} \times 10^6$	7.453(31)	7.465(16)	7.403	$\Phi_{JK} \times 10^6$	32.802(60)	26.815	25.812	-
$H_{KJ} \times 10^6$	10.72(16)	10.865(79)	12.66	$\Phi_{KJ} \times 10^6$	−74.10(43)	−53.28	−58.19	-
$H_K \times 10^3$	4.021(25)	4.027(22)	3.759	$\Phi_K \times 10^3$	4.077(25)	3.805	3.789	3.428
$h_1 \times 10^9$	32.33(14)	32.272(58)	29.59	$\phi_J \times 10^9$	48.04(18)	41.27	29.98	-
$h_2 \times 10^6$	47.87(13)	47.942(74)	40.84	$\phi_{JK} \times 10^6$	16.26(44)	14.33	13.76	-
$h_3 \times 10^3$	15.946(31)	15.966(15)	11.686	$\phi_K \times 10^3$	1.543 2(31)	1.189 6	1.156 0	-

[a] Terahertz spectroscopy results from Ref. 30 with revised results from Ref. 102.
[b] CCSD(T)/TZ QFF results from Ref. 65.
[c] Empirically fit PES from Ref. 103.

pVXZ (X=T,Q) results match those of Martin showing an increase in $\omega_1(a_1)$ and $\omega_5(b_2)$ (C−H stretching modes) with decreases in $\omega_3(a_1)$, $\omega_4(b_1)$, and $\omega_6(b_2)$ (bending modes) from T→Q. At first sight, it is appealing to assume that the geometric changes associated with increasing basis set cardinality (contraction of bonds and widening of angles) explain these frequency changes on the basis of nuclear-nuclear repulsion. However, such a simple argument is incomplete with respect to the changes seen in $\omega_2(a_1)$ which is dominated by the C=O stretch (86.7% $S_2(a_1)$, 13.7% $-S_3(a_1)$, -0.4% $S_1(a_1)$). Inclusion of the present CCSD(T)/5Z results shows a rise and fall from T→Q→5 in $\omega_2(a_1)$ despite the slightly shorter bond length (0.00023 Å contraction) in the 5Z results relative to the QZ results.

The internal coordinate diagonal quadratic force constants, F_{ii}, provide some insight as they follow directly from the energies and are the dominant terms in the symmetrized **F** matrix[114]. It is obvious from Table 1.6 that the trends seen in ω_i follow those seen in F_{ii}. The change seen in the T→Q→5 sequence of ω_2 is captured by F_{22} as 13.03486 → 13.08516 → 13.06267 aJ/Å^2. Inspection of the CCSDT(Q)/CBS results shows this analysis to be consistent with the aforementioned trend of increases in C−H stretching modes and decreases in bending modes with improved basis set. While the F_{22} constant of CCSD(T)/TZ is similar to the CCSDT(Q)/CBS value, the off-diagonal F_{21}, F_{31}, and F_{32} constants in the A_1 symmetry block are larger in the latter CBS-extrapolated results and, thus, care must be taken comparing the magnitudes of force constants outside of a sequence. The internal coordinates used here are representative of the normal modes of vibration of formaldehyde, as a total energy distribution (TED) shows only two vibrational modes, $\omega_2(a_1)$ and $\omega_3(a_1)$, which correspond to <99.9% of the associated symmetry-adapted coordinate. The former has been described above but the latter $\omega_3(a_1)$ is represented by 86.4% $S_3(a_1)$ and 13.4% $S_2(a_1)$ with a miniscule contribution from $S_1(a_1)$. Previous work on ethylene does not reveal a similar relationship between harmonic force constants and frequencies, reinforcing the system specific nature of these properties.[110]

The anharmonicity constants, x_{ij}, comprise contributions from the cubic and quartic PES

Table 1.6: Basis Set Dependence of S_0 H_2CO VBOs

Theory	5 (b_2)*	1 (a_1)*	2 (a_1)	3 (a_1)	6 (b_2)	4 (b_1)
CCSDT(Q)/CBS						
F_{ii}	4.803 847	4.957 790	13.036 335	1.657 386	0.821 508	0.262 751
w_i	3 008.63	2 936.05	1 776.83	1 534.91	1 271.10	1 186.70
$2x_{ii}$	−75.16	−64.14	−19.53	−1.51	−3.89	−5.62
$\frac{1}{2}\sum_{i\neq j}x_{ij}$	−109.50	−89.04	−11.76	−33.47	−18.26	−13.97
ν_i	2 823.98	2 782.87	1 745.54	1 499.93	1 248.96	1 167.11
$\%w$	6.14	5.22	1.76	2.28	1.74	1.65
CCSD(T)/cc-pV5Z						
F_{ii}	4.797 530	4.952 077	13.062 667	1.662 347	0.823 216	0.263 664
w_i	3 006.43	2 934.70	1 779.05	1 535.16	1 271.10	1 188.18
$2x_{ii}$	−74.58	−63.93	−19.25	−1.31	−4.32	−5.61
$\frac{1}{2}\sum_{i\neq j}x_{ij}$	−108.91	−88.67	−11.82	−33.39	−18.51	−13.85
ν_i	2 822.93	2 782.09	1 747.98	1 500.45	1 248.27	1 168.73
$\%w$	6.10	5.20	1.75	2.26	1.80	1.64
CCSD(T)/cc-pVQZ						
F_{ii}	4.789 586	4.947 730	13.085 162	1.670 461	0.825 754	0.264 194
w_i	3 003.69	2 933.52	1 781.45	1 537.64	1 272.90	1 190.25
$2x_{ii}$	−74.36	−63.85	−19.20	−1.43	−4.38	−5.84
$\frac{1}{2}\sum_{i\neq j}x_{ij}$	−108.77	−88.49	−11.99	−33.41	−18.49	−13.86
ν_i	2 820.56	2 781.17	1 750.25	1 502.80	1 250.03	1 170.55
$\%w$	6.10	5.19	1.75	2.27	1.80	1.65
CCSD(T)/cc-pVTZ						
F_{ii}	4.764 287	4.931 374	13.034 858	1.691 586	0.830 064	0.264 728
w_i	2 995.85	2 929.23	1 780.76	1 543.21	1 274.88	1 192.20
$2x_{ii}$	−74.01	−63.10	−18.76	−1.85	−4.44	−6.36
$\frac{1}{2}\sum_{i\neq j}x_{ij}$	−108.05	−87.47	−12.70	−33.11	−18.19	−14.23
ν_i	2 813.80	2 778.66	1 749.31	1 508.24	1 252.24	1 171.60
$\%w$	6.08	5.14	1.77	2.27	1.78	1.73

* deperturbed for $2_1 6_1(b_2) \approx 5_1(b_2)$ and $3_1 6_1(b_2) \approx 5_1(b_2)$ or $3_2(a_1) \approx 1_1(a_1)$ Fermi resonance. Structural parameters for the cc-pVXZ (X=T,Q,5) progression are: r_e(CO) = 1.20957, 1.20658, 1.20634 Å; r_e(CH) = 1.10328, 1.10218, 1.10179 Å; and θ_e(HCH) = 116.185, 116.442, 116.597°.

expansion coefficients and are related to the anharmonic vibrational fundamental frequencies, ν_i, by[115]:

$$\nu_i = \omega_i + 2x_{ii} + \frac{1}{2}\sum_{i \neq j} x_{ij}. \tag{1.18}$$

Convergence of individual anharmonicity constants in the T→Q→5 progression shows the x_{ii} values steadily decreasing for $i = 1, 2, 5$ and increasing for $i = 3, 4, 6$, suggesting that, in smaller basis sets, diagonal anharmonicity is underestimated for stretching modes and overestimated for bending modes. Both the diagonal and off-diagonal anharmonic corrections (the second and third terms in Eqn. 1.18, respectively) for the antisymmetric and symmetric C−H stretching modes, $\nu_5(b_2)$ and $\nu_1(a_1)$, decrease in the T→Q→5 progression as well as in the CCSDT(Q)/CBS results. These decreases serve to offset the increases seen in $\omega_1(a_1)$ and $\omega_5(b_2)$ but both modes are affected by first-order resonances which affect their overall accuracy as discussed later. The remaning off-diagonal coupling constants do not show a similar trend overall but many x_{ij} tend toward a certain change even into the CCSDT(Q)/CBS results. It should be noted that the CCSD(T)/TZ results show large changes from T→Q relative to the rest of the progression series changes especially in the case of the resonance-affected x_{52} and x_{65} constants. The $\%\omega$ term listed in Table 1.6 is defined as $(1 - \nu/\omega) * 100\%$ and describes the anharmonicity of the fundamental with respect to its corresponding harmonic frequency.

1.4.2.2 VPT2 and the $5_1, 2_16_1, 3_16_1$ Triad

The treatment of anharmonic resonances which affect the vibrational frequencies of a molecule in VPT2 involves two steps; the reformulation of affected anharmonicity constants, x_{ii} and/or x_{ij}, to accomodate the removal of resonance denominators (or the equivalent sum-over-states alternative) and the subsequent diagonalization of an effective Hamiltonian which contains the deperturbed frequencies along with appropriate interaction constants[115–119].

Resonance interactions are most often identified in a VPT2 analysis by the differences in the energy of symmetry-related combinations of harmonic vibrational frequencies which correspond to first-order (Fermi) and second-order resonances. However, critical interactions which may otherwise cause large shifts in the anharmonicity constants and, thus, anharmonic vibrational frequencies may be overlooked due to arbitrarily defined tolerances[119]. The CCSDT(Q)/CBS fundamentals of S_0 formaldehyde serve as an example of this concept where a generous threshold of 200 cm^{-1} would fail to identify the well-documented[2,29] $\omega_3(a_1)+\omega_6(b_2) \approx \omega_5(b_2)$, 1534.91 + 1271.10 $\approx$ 3008.63 cm^{-1}, component of the $5_1, 2_16_1, 3_16_1$ resonance triad as $\Delta\omega = 202.62$ cm^{-1}. It is interesting to note that the failure of this detection method for S_0 formaldehyde is an emergent property of the high-level CBS treatment as the previously mentioned convergence pattern of the harmonic frequencies pushes $\Delta\omega$ beyond the (arbitrary but oft-applied) threshold.

A complete description of this three-state interaction in VPT2 requires the diagonalization of the effective Hamiltonian, $\mathbf{H}_{\text{eff}}$, shown in Eqn. 1.19. The diagonal terms correspond to the deperturbed values of the corresponding energies and are denoted with an asterisk where combination levels are determined as $\nu_i+\nu_j+x_{ij}$. Off-diagonal matrix elements serve as a measure of coupling between states where first-order interaction constants easily follow from the cubic force constants. A trivial representation of the matrix element describing the second-order interaction between the 2_16_1 and 3_16_1 combination levels, denoted K below, is $K = 0$ as the coupling between these two states is expected to be limited[118].

$$\mathbf{H}_{\text{eff}} = \begin{array}{c} \begin{array}{ccc} 5_1 & 2_16_1 & 3_16_1 \end{array} \\ \begin{pmatrix} \nu_5^* & \frac{1}{\sqrt{8}}\phi_{652} & \frac{1}{\sqrt{8}}\phi_{653} \\ \frac{1}{\sqrt{8}}\phi_{652} & \nu_2+\nu_6+x_{62}^* & K \\ \frac{1}{\sqrt{8}}\phi_{653} & K & \nu_3+\nu_6+x_{63}^* \end{pmatrix} \end{array} \tag{1.19}$$

However, a more thoughtful solution to the matrix element denoted by K, shown in Eqn. 1.20,

follows from the second-order contact transformation. Such relationships have been carefully explored elsewhere.[118,120–123]

$$K = \frac{1}{4}(K_{21,31} + K_{22,23} + K_{23,33} + K_{24,34} + K_{25,35} + 3K_{26,36}) \tag{1.20}$$

The expression above can be derived from the 1-1 resonance equations found in Ref. 122 where the necessary numerical factors follow from harmonic oscillator matrix elements in reduced normal coordinates.

The eigenvalue of Eqn. 1.19 whose largest eigenvector coefficient belongs to the 5_1 state is listed in Table 1.7 for both solutions of K alongside the contributions (coefficients squared) from the other two states for the non-trivial K solution of $\mathbf{H}_{\text{eff}}$. A complete treatment of the $5_1, 2_16_1, 3_16_1$ resonance triad through deperturbation of $5_1 \approx 2_16_1$ and $5_1 \approx 3_16_1$ followed by the diagonalization of $\mathbf{H}_{\text{eff}}$ in Eqn. 1.19 provides a superior result for $\nu_5(b_2)$ only in the case of the CCSD(T)/TZ data where the trivial solution of K provides the best experimental agreement as discussed in the following section. McCaslin et al. have recently produced the Full K solutions of $\nu_5(b_2)$ for CCSD(T)/XZ (X = D, T, Q) as well as benchmarking the more complete NASA Ames atomic natural orbital (ANO) basis sets[124]. The Full K solutions in Table 1.7 match the fundamental values reported by McCaslin et al. for CCSD(T)/XZ (X = T, Q) where the current work extends the data to show convergence onto the CCSDT(Q)/CBS result of 2850.05 cm^{-1}. The CCSD(T)/ANO0 (2855 cm^{-1}) and CCSD(T)/ANO2 (2852 cm^{-1}) results of McCaslin et al. are in excess of the CCSD(T)/CBS result but the CCSD(T)/ANO1 $\nu_5(b_2)$ value of 2849 cm^{-1} is promising. In either case, the ANO basis sets suffer from the same overestimation of $\nu_5(b_2)$ relative to experiment, without exception, when using the full treatment of the Fermi resonance.

The treatment of isolated Fermi ($\nu_i \sim 2\nu_j$ and $\nu_i \sim \nu_j + \nu_k$) resonances in VPT4 is a straightforward extension of the treatment for VPT2: the diagonal elements of the effective Hamiltonian are deperturbed VPT4 energies, and the off-diagonal element is the sum of the

Table 1.7: Effects of the 5_1, $2_1 6_1$, $3_1 6_1$ (b_2) Resonance Triad on $\nu_5(b_2)$ (cm^{-1})

	$\boldsymbol{\Delta\omega}$			$\boldsymbol{\nu_5(b_2)}$		**Contribution**		
Theory	$5_1 \approx 2_1 6_1$	$5_1 \approx 3_1 6_1$	Deperturbed	K=0	Full K	5_1	$2_1 6_1$	$3_1 6_1$
CCSD(T)/TZ	-59.79	177.77	2813.80	2844.70	2845.60	0.586	0.065	0.349
CCSD(T)/QZ	-50.65	193.16	2820.56	2847.99	2848.78	0.621	0.073	0.306
CCSD(T)/5Z	-43.72	200.17	2822.93	2848.62	2849.40	0.631	0.080	0.290
CCSDT(Q)/CBS	-39.29	202.63	2823.98	2849.35	2850.04	0.628	0.083	0.289
				Spectroscopic Constants				
Theory	$\frac{1}{\sqrt{8}}\phi_{652}$	$\frac{1}{\sqrt{8}}\phi_{653}$	K	x_{52}	x_{53}	x_{62}	x_{63}	x_{65}
CCSD(T)/TZ	51.921	63.546	-2.932	-1.54 (-47)	-33.47 (-11)	-6.81 (38)	1.59 (-21)	-30.14 (-53)
CCSD(T)/QZ	51.410	65.231	-2.621	-0.97 (-53)	-34.25 (-12)	-6.91 (45)	1.86 (-20)	-30.48 (-61)
CCSD(T)/5Z	51.435	65.998	-2.527	-0.85 (-61)	-34.41 (-13)	-6.90 (54)	1.99 (-20)	-30.54 (-69)
CCSDT(Q)/CBS	51.651	66.225	-2.205	-0.70 (-69)	-34.63 (-13)	-6.78 (61)	2.26 (-19)	-30.70 (-77)

$\nu_2(a_1) + \nu_6(b_2) \approx \nu_5(b_2)$ and $\nu_3(a_1) + \nu_6(b_2) \approx \nu_5(b_2)$ related denominators removed.
Values in parentheses correspond to x_{ij} without removal of resonance denominators.
K=0 and Full K values correspond to the ν_5 eigenvalue of $\mathbf{H_{eff}}$ in Eqn. 1.7.

first- and third-order Hamiltonian matrix elements. For formaldehyde, the coincidence of the $5_1 \sim 2_1 6_1$ and $5_1 \sim 3_1 6_1$ Fermi resonances requires inclusion of an off-diagonal Darling-Dennison term (the K term in VPT2). For VPT4, this requires evaluation of the fourth-order once-transformed off-diagonal Hamiltonian, which we have not yet derived. Instead, we substitute the second-order K constants, as this coupling element has a rather small effect on the diagonalized energies. The interaction between $\nu_1(a_1)$ and $2\nu_4(a_1)$ is relatively weak with $\Delta\omega = 133.76$ cm^{-1} but is included as a Fermi resonance in the following VPT2 and VPT4 analysis as its treatment as such improves agreement to experiment in both cases.

Table 1.8: First ($\boldsymbol{D}^5_{\omega}$) and Second ($\boldsymbol{D}^5_{\omega,\omega'}$) Harmonic Derivatives of $\boldsymbol{\nu_5(b_2)}$

(Q)/CBS*	ν_5	ν_5	ω_5	ω_2	ω_3	ω_6
ω_5	-1.826	ω_5	-0.0869	0.0880	-0.0011	-0.0869
ω_2	1.726	ω_2	0.0880	-0.0880	0.0000	0.0880
ω_3	0.110	ω_3	-0.0011	0.0000	0.0011	-0.0011
ω_6	1.835	ω_6	0.0869	-0.0880	0.0011	0.0869
(T)/5Z	ν_5	ν_5	ω_5	ω_2	ω_3	ω_6
ω_5	-1.484	ω_5	-0.0622	0.0633	-0.0011	0.0622
ω_2	1.382	ω_2	0.0633	-0.0633	0.0000	-0.0633
ω_3	0.112	ω_3	-0.0011	0.0000	0.0011	0.0011
ω_6	1.493	ω_6	0.0622	-0.0633	0.0011	-0.0622
(T)/QZ	ν_5	ν_5	ω_5	ω_2	ω_3	ω_6
ω_5	-1.135	ω_5	-0.0395	0.0407	-0.0012	0.0395
ω_2	1.028	ω_2	0.0407	-0.0407	0.0000	-0.0407
ω_3	0.117	ω_3	-0.0012	0.0000	0.0012	0.0012
ω_6	1.144	ω_6	0.0395	-0.0407	0.0012	-0.0395
(T)/TZ	ν_5	ν_5	ω_5	ω_2	ω_3	ω_6
ω_5	-0.873	ω_5	-0.0238	0.0252	-0.0014	-0.0238
ω_2	0.752	ω_2	0.0252	-0.0252	0.0000	-0.0252
ω_3	0.131	ω_3	-0.0014	0.0000	0.0014	0.0014
ω_6	0.882	ω_6	0.0238	-0.0252	0.0014	-0.0238

Unitless and cm for first and second derivatives, respectively.
*CCSDT(Q)/CBS results, see Eqn. 1.3.

1.4.2.3 Comparison to Experiment

Comparison to previous theoretical and experimental work of S_0 H_2CO's fundamental frequencies is shown in Table 1.9. Theoretical results are evaluated against the analysis of Tchana et al.[126] and Bouwens et al.[29]. It is clear from the VPT2 results that as basis set

Table 1.9: $\tilde{\boldsymbol{X}}\ ^1\boldsymbol{A}_1(S_0)$ H_2CO Fundamental Vibrational Frequencies (cm^{-1})

		1 (a_1)	2 (a_1)	3 (a_1)	4 (b_1)	5 (b_2)	6 (b_2)		
Experiment									
Bouwens[a]		2782.2(10)	1746.1(10)	1500.2(10)	1167.4(10)	2843.0(10)	1249.6(10)		
Tchana[b]		2782.4569(10)	1746.00928(49)	1500.1747(4)	1167.2563(4)	2843.3256(10)	1249.0948(3)		
This work	**Method**	***Difference from experiment[b]***						**MAE**	**MAPE**
CCSD(T)/TZ	VPT2	-5.13*	3.30	8.07	4.34	2.27*	3.15	4.38	0.269
CCSD(T)/QZ	VPT2	-2.80*	4.24	2.63	3.29	5.45*	0.94	3.22	0.178
CCSD(T)/5Z	VPT2	-2.00*	1.97	0.28	1.47	6.07*	-0.82	2.10	0.101
CCSDT(Q)/CBS	VPT2	-1.25*	-0.47	-0.24	-0.14	6.71*	-0.14	1.49	0.058
$+\Delta_{rel}$	VPT2	-1.71*	-1.48	-0.19	-0.34	6.10*	-0.26	1.68	0.119
CCSDT(Q)/CBS	DVR	1.18	-0.32	-0.03	-0.80	1.06	0.03	0.57	0.029
$+\Delta_{rel}$	DVR	0.49	-1.48	0.01	-0.95	0.25	-0.08	0.54	0.034
Previous Theory									
CCSD(T)/aTZ[c]	VCI	0.94	-11.11	-5.48	-4.76	0.27	-8.49	5.18	0.355
CCSD(T)-F12b/aTZ[c]	VCI	1.74	1.29	-2.48	-0.06	6.07	-3.29	2.49	0.131
CCSD(T)/TZ[d]	VPT2	-5.56	3.89	8.13	4.14	-51.63	3.51	12.81	0.569
CCSD(T)/TZ[d]	VCI	6.74	2.99	4.12	-1.56	-1.33	-1.19	2.99	0.161
Empirical Fit[e]	CVPT	-0.16	0.09	-0.67	0.04	-0.83	-0.19	0.33	0.017
CCSD(T)/aQZ[f]	TROVE	-0.72	-1.40	-1.08	-1.16	-0.96	-3.49	1.47	0.098
Empirical Fit[f]	TROVE	0.00	0.02	0.01	0.04	-0.02	-0.02	0.02	0.001

* treated for the Fermi resonances.

[a] DF spectroscopy results from Ref. 29. [b] Analysis from multiple sources as seen in Refs. 125,126.

[c] Ref. 97. [d] Untreated VPT2 and VSCF-CI "raw" results from Ref. 65.

[e] Empirical fit of Martin et al.'s SPF CCSD(T)/TZ QFF from Ref. 2.

[f] Yachmenev et al.'s variational results from fit of CCSD(T)/aQZ PES in Ref. 5.

cardinality increases in the CCSD(T)/cc-pVXZ (X = T, Q, 5) sequence that the individual errors relative to experiment are reduced or left unchanged as in the case of $\nu_6(b_2)$. The exception to this is $\nu_5(b_2)$ which is involved in the aforementioned $5_1, 2_1 6_1, 3_1 6_1$ resonance triad where the large difference seen between CCSD(T)/TZ and CCSD(T)/QZ are emphasized in previous sections and detailed in Table 1.7. Overall error decreases despite this exception as evidenced by the MAEs ($\frac{1}{n}\sum_{i=1}^{n}|X_i - Y_i|$) and MAPEs (Eqn. 1.17).

Extrapolation to the basis set limit with corrections for higher-order dynamic and core correlation, as represented by the CCSDT(Q)/CBS level of theory, shows a significant improvement in most but not all fundamentals. Substantial decreases in the absolute errors of the C−O stretch, $\nu_2(a_1)$, and torsion, $\nu_4(b_1)$, which drop from 1.97 to 0.47 cm^{-1} and 1.47 to 0.14 cm^{-1}, respectively, are seen when moving from the CCSD(T)/5Z to CCSDT(Q)/CBS results. The accuracy of the anti-symmetric OCH bend, $\nu_6(b_2)$, and symmetric C−H stretch, $\nu_1(a_1)$, improve by similar amounts where error is reduced by over half a wavenumber. Comparable accuracy is observed in both the CCSDT(Q)/CBS and CCSD(T)/5Z results for the symmetric OCH bend, $\nu_3(a_1)$, where errors for both are approximately a quarter wavenumber (but on either side) from the experimental result of 1500.1747(4) cm^{-1}. Keeping with the trend of increasing error with increasing basis set cardinality, the CCSDT(Q)/CBS VPT2 prediction of $\nu_5(b_1)$ shows the worst agreement to experiment of the included results but of course this is a resonant fundamental. Despite this, the MAE of the CCSDT(Q)/CBS VPT2 fundamentals approach spectroscopic accuracy at 1.49 cm^{-1} where the MAPE is approximately halved relative to the CCSD(T)/5Z results.

The CCSDT(Q)/CBS anharmonicity constants produced in the VPT2 analysis are shown in Table 4.5. The results vary in accuracy relative to the experimental values reported by Reisner et al[26]. Some constants are surprisingly well-described, such as the x_{22}, x_{42}, x_{44} where the CCSDT(Q)/CBS value of x_{42}, -7.19 cm^{-1}, reproduces Reisner et al.'s experimental value of -7.199(39) cm^{-1}. The utility of this agreement is obvious, as the CCSDT(Q)/CBS prediction of the $2_1 4_1(b_1)$ combination level is 2905.46 cm^{-1} compared to the experimental

Table 1.10: Anharmonicity Constants (cm^{-1})

	This work[a]				**Martin**[b]	**Reisner**[c]	**Bouwens**[c]
x_{ij}	CBS	5Z	QZ	TZ	TZ	Exp.	
11	-32.07	-31.97	-31.93	-31.55	-31.51	-28.95(14)	-50.65(139)
21	-1.78	-1.86	-1.92	-2.27	-2.27	1.15(19)	0.40(92)
22	-9.77	-9.63	-9.60	-9.38	-9.95	-9.926(23)	-10.00(20)
31	-27.16*	-27.08*	-26.96*	-26.06*	-30.05	-23.03(14)	-26.80(137)
32	-7.07	-6.97	-7.08	-7.50	-7.49	-8.26(11)	-8.27(31)
33	-0.75*	-0.66*	-0.72*	-0.93*	0.08	-0.164(97)	-0.55(39)
41	-7.64	-7.56	-7.54	-7.51	-7.44	-10.099(65)	-8.67(81)
42	-7.19	-7.07	-7.10	-7.27	-7.26	-7.199(39)	-7.12(15)
43	-0.34	-0.32	-0.38	-0.79	-0.80	-1.769(52)	-1.59(19)
44	-2.81	-2.80	-2.92	-3.18	-3.41	-3.157(12)	-2.91(8)
51	-133.14	-132.49	-132.25	-131.32	-131.15	-193.32(24)	-88.47(473)
52	-0.70*	-0.85*	-0.97*	-1.54*	-46.62	-17.23(23)	-14.38(334)
53	-34.63*	-34.41*	-34.25*	-33.47*	-10.73	6.00(37)	-5.86(287)
54	-19.84	-19.55	-19.57	-19.63	-19.57	-13.35(17)	-10.26(219)
55	-37.58	-37.29	-37.18	-37.00	-36.95	-17.97(13)	-14.66(245)
61	-8.37	-8.36	-8.31	-7.78	-7.74	-49.78(33)	-15.72(136)
62	-6.78*	-6.90*	-6.91*	-6.81*	38.30	6.581(49)	3.82(186)
63	2.26*	1.99*	1.86*	1.59*	-21.07	-29.861(88)	-33.36(275)
64	7.07	6.79	6.87	6.74	7.09	-2.860(70)	2.40(66)
65	-30.70*	-30.54*	-30.48*	-30.14*	-52.42	-17.63(33)	-7.65(283)
66	-1.94	-2.16	-2.19	-2.22	-2.20	-1.567(56)	-2.35(254)

* computed with resonance denominators removed.
[a] CCSDT(Q)/CBS and CCSD(T)/cc-pVXZ (X=T,Q,5) results.
[b] CCSD(T)/TZ *ab initio* results from Ref. 65.
[c] SEP or DF spectroscopy in Ref. 26 or Ref. 29.

value of 2905(1) cm^{-1}. However, perfect agreement to Reisner et al.'s derived constants is unnecessary to successfully predict extremely accurate combination levels as exhibited by the VPT2 prediction of $2_1 3_1(a_1)$. The x_{23} constant varies by 1.19 cm^{-1}, nearly 20%, from Reisner et. al.'s result yet a CCSDT(Q)/CBS prediction of $2_1 3_1(a_1)$ at 3238.40 cm^{-1} is only 0.06 cm^{-1} away from the experimental result of 3238.4548(20) cm^{-1} of Perrin et. al.[125].

A better example of this point, and the difficulties associated with the empirical determination of anharmonicity, comes from the $4_1 6_1(a_2)$ and $1_1 6_1(b_2)$ energy levels whose x_{ij}'s are wildly different from their experimental counterparts with x_{64} = 7.07 v.s. -2.860(70) cm^{-1} and x_{61} = -8.37 v.s. -49.78(33) cm^{-1}. CCSDT(Q)/CBS predicts $4_1 6_1(a_2)$ at 2423.14 cm^{-1} from VPT2 which is only 0.17 cm^{-1} from the high-resolution observations of Perrin et. al.[125]

despite x_{64} having the opposite sign and being over twice the magnitude of Reisner et. al's empirical value. Reisner et. al's x_{61} constant is six times that of the CCSDT(Q)/CBS result yet the CCSDT(Q)/CBS $1_1 6_1(b_2)$ prediction of 4023.46 cm^{-1} is only a couple wavenumbers from Flaud et. al.'s gas phase observation[127] at 4021.08066(60) cm^{-1}. It is not surprising that these two empirically determined anharmonicity constants vary so much from the current high-accuracy study, as Reisner et. al. had to determine five and eleven x_{ij}'s before extracting x_{64} and x_{61}, respectively, where the analysis relied on accurate assignment of the $1_1 4_2 6_1(b_2)$ and $3_1 4_3 6_1(a_2)$ combination levels. A more updated fit of the anharmonicity constants is found from Bouwens et. al.[29] which is shown in Table 4.5 but the agreement is similar and the conclusion remains with regard to theoretical and empirical findings. The present data serves as an excellent example, along the lines of previous work in the literature[118], of how high-accuracy *ab initio* force fields relying on convergent quantum chemistry can use VPT2 to its fullest by generating a set of spectroscopic constants with predictable accuracy and leverage this in the determination of overtones and combination bands.

The obvious exception to this statement is resonance-affected energy levels where vibrational perturbation theory encounters difficulties that inevitably affect the accuracy of predictions. As previously discussed, the $\nu_5(b_2)$ fundamental is a classic case of this and is qualitatively inaccurate if its interaction with the $2_1 6_1(b_2)$ and $3_1 6_1(b_2)$ combination levels is treated with VPT2. The accuracy of the energy levels directly involved in the triad benefits from an effective Hamiltonian treatment (as shown in Eqn. 1.19) following deperturbation, but x^*_{25}, x^*_{35}, and x^*_{65} and their corresponding unmixed energy levels do not. Errors are over 40 cm^{-1} for CCSDT(Q)/CBS VPT2 predictions of $3_1 5_1(b_2) = 4289.28$ cm^{-1} and $5_1 6_1(a_1) = 4042.24$ cm^{-1} relative to the gas-phase observations of 4335.09709(60) and 4083.1(10) cm^{-1}, respectively[29,127]. Even the errors for the eigenvalues of $\mathbf{H}_{\text{eff}}$ are far too high relative to the rest of the dataset. Only $2_1 6_1(b_2)$ shows error under 5 cm^{-1} from experiment with a prediction of 3003.79 cm^{-1} which is 3.73 cm^{-1} from the experimental value[26] of 3000.0656(10) cm^{-1}. The relative lack of accuracy in the prediction of resonance-affected energy levels with

VPT2 logically leads to variational approaches for predicting vibrational energy levels.

Variational (DVR) solutions to the CCSDT(Q)/CBS vibrational energy levels are shown in Table 1.9 below their VPT2 counterparts. Individual errors are equivalent or superior to VPT2 for all fundamentals but $\nu_4(b_1)$, the torsional mode, which displays an increase from 0.14 to 0.80 cm^{-1}. Predicted values for $\nu_3(a_1)$ and $\nu_6(b_2)$ are essentially exact with the CCSDT(Q)/CBS potential, where errors are both 0.03 cm^{-1}. The largest error is seen in the C−H stretching modes which are 1.18 and 1.06 cm^{-1} for $\nu_1(a_1)$ and $\nu_5(b_2)$, respectively. The error in $\nu_5(b_2)$ is vastly improved relative to the 6.71 cm^{-1} error from the CCSDT(Q)/CBS VPT2 fundamental, which can largely be attributed to issues associated with treating the resonance discussed earlier. Excellent agreement is seen for the fundamentals overall with a MAE of 0.57 cm^{-1} where the MAPE is half that of the VPT2 results. It is important to recognize these results are exemplary for purely *ab initio* predictions of VBOs, especially for a QFF, but modern high-resolution spectroscopy experiments are capable of obtaining far more accurate rovibrational results for simple systems such as formaldehyde. The beauty of the present work presents itself in situations where experiment cannot isolate, detect, or analyze the molecular species of interest. CCSDT(Q)/CBS VPT2 and DVR fundamentals of D_2CO and HDCO are shown in Table 1.11.

It should be noted that the original quartic expansion in symmetry-adapted internal coordinates is completely unsuitable for variational solutions to the vibrational problem here. Originally, transformation of the PES to Simons-Parr-Finland (SPF) coordinates was performed but the error was found to be too high for $\nu_1(a_1)$ and $\nu_5(b_2)$, the C−H stretching fundamentals. Rauhut has reported this exact issue previously with variational approaches using many-mode expansions, noting the C−H stretching fundamentals of formaldehyde were sensitive to vibrational coupling and prone to errors which were associated with an incomplete description of the potential in its outer regions[132]. Morse coordinates are found to be superior for providing quantitatively accurate, spectroscopic, predictions of the fundamentals; a topic which has been studied previously[37,133].

Table 1.11: CCSDT(Q)/CBS VBOs of D_2CO and HDCO (cm^{-1})

	D_2CO			HDCO		
	VPT2	DVR	Exp[a]	VPT2	DVR	Exp[b]
$\nu_1(a_1)$	2063.94*	2061.53	2054.694000(81)	2097.37*	2095.95	2104.4[c]
$\nu_2(a_1)$	1701.27	1701.11	1701.619103(32)	1723.90	1723.83	1724.0
$\nu_3(a_1)$	1099.98	1100.22	1100.44254(74)	1396.18	1396.49	-
$\nu_4(b_1)$	937.75	937.32	938.03549(68)	1058.60	1058.03	1059.6
$\nu_5(b_2)$	2166.47*	2163.15	2162.923385(66)	2854.57*	2845.31	-[d]
$\nu_6(b_2)$	988.86	988.92	989.25028(59)	1027.92	1028.01	1027.1

HDCO (C_s) modes described with H_2CO (C_{2v}) spectroscopic ordering.
[a] FTIR results from Refs 128, 129, and 130.
[b] DF spectra from Ref 131 (~2 cm^{-1} linewidth in spectra).
[c] Vibrational admixture with a DF spectra assignment of $-4_2 + 1_1 + 6_2$.
[d] Unobserved in the DF spectra; not to be confused with $5_1 + 3_2 = 2846.8$ cm^{-1}.
Values with asteriks treated for resonance interactions with eigenvalues shown below.
$5_1 \approx 3_1 6_1(b_2)$ eigenvalues are: 2068.15, 2166.47 cm^{-1}.
$4_2, 6_2, 1_1, 3_2(a_1)$ eigenvalues are: 1864.91, 1972.75, 2063.94, 2201.79 cm^{-1}.
$5_1, 2_1 6_1, 3_2(a')$ triad eigenvalues are: 2729.43, 2754.03, 2854.57 cm^{-1}.
$1_1, 4_2, 6_2(a')$ triad eigenvalues are: 2032.29, 2097.37, 2135.51 cm^{-1}.

1.4.2.4 Comparison to Previous Theory

There are no known PESs which use high levels of theory (those including CBS extrapolations and higher-order dynamic electron correlation) for this system. Previous theoretical work on formaldehyde is extensive but generally limited to CCSD(T) using the (aug-)cc-pVTZ or (aug-)cc-pVQZ basis sets. It is clear from the variation seen in the error of previous *ab initio* results (Table 1.9) that the accuracy of predicted VBOs goes beyond choice of theory alone; the form of the PES and solution of the vibrational energy levels is equally important. Results from three types of PES are compared to those of this work: the CCSD(T)/aTZ (and F12b variant) 3-mode (many-mode) expansion of Rauhut et al.[97,132], which relies on interpolation of intrinsic potentials, the CCSD(T)/TZ SPF QFF of Martin et al.[65], and the CCSD(T)/aQZ Morse coordinate 6D (full-dimensionality) PES of Yachmenev et al.[5] Almost the entire literature on S_0 formaldehyde (that compares to experimental observations) uses variational approaches for nuclear motion to avoid the resonance denominator issue associated with VPT2.

None of the previous *ab initio* results show accuracy comparable to the present

CCSDT(Q)/CBS DVR fundamental VBOs which have a MAE of 0.57 cm^{-1} relative to gas-phase observations. The variational CCSD(T)-F12b/aTZ many-mode results of Rauhut et al. have a respectable MAE of 2.49 cm^{-1} but show the greatest range of error of any of the included results and actually performs worse than its traditional CCSD(T)/aTZ counterpart in predicting an accurate value of $\nu_5(b_2)$ (errors of 6.07 cm^{-1} and 0.27 cm^{-1}, respectively). The *ab initio* CCSD(T)/aQZ 6D PES of Yachmenev et. al., on the other hand, proves more consistent with a MAE of 1.47 cm^{-1} despite unusually large error in the torsion, $\nu_4(b_1)$, of 3.49 cm^{-1}. Such performance is similar to the resonance-affected CCSDT(Q)/CBS VPT2 results (MAE = 1.49 cm^{-1}) where the Yachmenev et. al.'s 6D PES addresses challenges previously noted by Rauhut by using a far more expansive surface and full unconstrained coupling between vibrational modes[132]. A more relevant comparison would be beteween the variational results, DVR and TROVE, where the CCSDT(Q)/CBS QFF clearly shows its strength with a MAE less than half that of the *ab initio* 6D PES.

Fitting of the expansive full-dimensionality 6D surface of Yachmenev et al. to high-quality experimental results is understandably superior to all of the included *ab initio* VBO predictions[5] where MAE relative to experiment is an order of magnitude better than the purely *ab initio* sources. Constructing a semi-empirical PES such as this one obviously requires a great deal of high-resolution gas-phase observations in tandem with significant refinement and is a service to theorists and experimentalists alike, but such treatments are only available for extensively studied and small chemical species. The fact that spectroscopically accurate VBOs can be variationally computed for fundamentals using an unaltered, purely *ab initio*, surface that spans only 183 geometries is quite agreeable when compared to the 30840 geometries used by Yachmenev et al. Moreso, the CCSDT(Q)/CBS DVR results carry a MAE which is only twice that of the semi-empirical fit of Burleigh et al. which relies on the older SPF QFF of Martin et al.[2,65] Individual errors from CCSDT(Q)/CBS DVR are actually superior in some cases ($\nu_3(a_1)$, $\nu_6(b_2)$) to those predicted variationally with canonical Van Vleck vibrational perturbation theory (CVPT) using Burleigh et al.'s empirically

fit QFF. An interesting topic for further study would be investigating the accuracy of a semi-empirical QFF produced through refinement of the CCSDT(Q)/CBS QFF used here.

1.4.2.5 Relativistic Corrections to the PES

Results for fundamental vibrational frequencies using Δ_{rel} corrections to the CCSDT(Q)/CBS equilibrium geometry and PES are shown in Table 1.9. A negligible decrease of 0.05 cm^{-1} in the error of $\nu_3(a_1)$ is met with increased error in all other fundamentals with the exception of $\nu_5(b_2)$ which is lowered by approximately 0.5 cm^{-1}; a very small effect considering the convergence of the $\nu_5(b_2)$ eigenvalue of $\mathbf{H}_{\text{eff}}$ as shown in Table 1.7. Closer inspection of the results shows that the magnitude of the shifts between CCSDT(Q)/CBS and the CCSDT(Q)/CBS+Δ_{rel} results are largest in the Fermi-affected C−H modes ($\nu_1(a_1)$, $\nu_5(b_2)$) and, most importantly, the C−O stretch ($\nu_2(a_1)$). The latter fundamental, $\nu_2(a_1)$, drops from 1745.54 to 1744.53 cm^{-1} which increases the error against the experimental value of 1746.00928(49) cm^{-1} by 1.01 cm^{-1}. Such a shift is almost entirely explained by the change in the harmonic force constant of the C−O stretching coordinate, $\Delta_{\text{rel}}(F_{22})$ = -0.01605 aJ/Å^2, which lowers the harmonic vibrational frequency of 1776.83 to 1775.85 cm^{-1}; almost exactly a wavenumber. The Morse-based variational CCSDT(Q)/CBS+Δ_{rel} predictions behave similarly to VPT2 with respect to the increased error in the C−O stretch ($\nu_2(a_1)$) but, unlike VPT2, the Δ_{rel} shifts to $\nu_1(a_1)$ and $\nu_5(b_2)$ vastly improve agreement to experiment as these modes are predicted with equivalent accuracy in the absence of resonance problems.

1.4.2.6 4$^{\text{th}}$-order Vibrational Perturbation Theory

VPT2 is a successful, and the most used, approach to vibrational anharmonicity in molecular physics. It is exceptionally easy to use in conjunction with Taylor series representations of the potential energy surface and is familiar to theorists and experimentalists alike. Perhaps VPT2's most obvious limitation is quasi-degeneracies (resonances) but the effective Hamiltonian approach is a solution, albeit an imperfect one, to that problem. What VPT2 cannot

do is take advantage of more expansive swaths of the nuclear potential which can be used to produce better predictions of vibrational energy levels. A natural extension to higher-order contributions (those arising from derivatives beyond quartic in normal coordinates) of the PES follows by taking VPT to 4^{th}-order *via* VPT4.

VPT4 requires derivatives of the potential through sextic. Most quantum chemistry packages do not have the automated generation of quartic force fields implemented, let alone to sextic, making the production of these surfaces a challenge. The neccessary quintic and sextic geometric derivatives can be calculated at the HF level by a routine execution of the recursive response theory implementation described in Section 1.3.6. This is one of the few, if not the only, method(s) of providing arbitrary-order force constants without recourse to numerical methods which are much less reliable at high order than their analytic counterparts. It is straight-forward to extend existing force fields in this way to generate a mixed-theory sextic force field such as the $V_4(\mathbf{q})$[CCSDT(Q)/CBS] + $V_6(\mathbf{q'})$[HF/TZ] one used here. Another strategy used in this study is to LSQ fit displacements along the CCSDT(Q)/CBS reduced normal coordinates ($\mathbf{q}$) to energies from the Morse-based symmetry-adapted internal coordinate QFF to generate $V_6(\mathbf{q})$[CCSDT(Q)/CBS] directly.

The difference in VPT4 vibrational energy levels predicted with these PES is shown as ΔVPT4‡ in Table 1.12, where VPT4† are the Morse-based results and VPT4‡ are the results relying on the recursively solved $V_6(\mathbf{q'})$[HF/TZ] (see theoretical details). Only the fundamentals, overtones, and combination level of $\nu_2(a_1)$ and $\nu_4(b_1)$ show agreement under a wavenumber between the two VPT4 datasets. The exception to this is the $2_1 6_1(b_2)$ combination level which is part of the discussed resonance triad with $\nu_5(b_2)$ and qualitatively incorrect in VPT. Overall, HF/TZ does not describe the required quintic and sextic regions of the force field with enough accuracy to improve upon the CCSDT(Q)/CBS VPT2 results as most levels are shifted further away from experimental observations in the corresponding VPT4‡ results.

It is immediately obvious from Table 1.12 that the differences between the DVR and

Table 1.12: Comparison of VPT4 H_2CO VBOs (cm^{-1})

Level	Symm.	Exp	ΔExp	DVR(Exact)	ΔVPT2†	VPT2†	ΔVPT4†	VPT4†	ΔVPT4‡	VPT4‡
4_1	b_1	1167.26	-0.80	1166.46	0.23	1166.69	0.05	1166.51	-0.42	1166.08
6_1	b_2	1249.09	0.03	1249.13	-0.27	1248.86	0.03	1249.16	-1.15	1248.01
3_1	a_1	1500.17	-0.03	1500.15	-0.25	1499.90	0.02	1500.17	-1.22	1498.95
2_1	a_1	1746.01	-0.32	1745.69	-0.28	1745.41	0.03	1745.71	-0.15	1745.56
4_2	a_1	2327.52	-3.06	2324.47	3.09	2327.56	0.17	2324.63	0.17	2324.80
4_16_1	a_2	2422.97	-0.32	2422.65	-0.10	2422.55	0.17	2422.82	-2.02	2420.80
6_2	a_1	2494.35	0.52	2494.87	-1.07	2493.81	0.13	2495.00	-2.63	2492.37
3_14_1	b_1	2667.05	-0.17	2666.88	-0.67	2666.21	0.10	2666.98	-2.75	2664.23
3_16_1*	b_2	2719.16	1.32	2720.47	8.88	2729.36	3.77	2724.25	-3.86	2720.39
1_1*	a_1	2782.46	1.18	2783.64	-3.71	2779.93	1.57	2785.21	-2.03	2783.18
5_1*	b_2	2843.33	1.06	2844.39	-66.90	2777.49	260.77	3105.16	-4.16	3101.00
2_14_1	b_1	2905.97	-1.24	2904.73	0.09	2904.82	0.10	2904.83	-0.95	2903.87
2_16_1*	b_2	3000.07	-0.17	2999.90	55.47	3055.37	-264.49	2735.41	0.08	2735.49
2_13_1	a_1	3238.45	-0.15	3238.31	-0.08	3238.16	-0.14	3238.16	-1.52	3236.64
2_2	a_1	3471.6	-0.5	3471.07	0.19	3471.26	0.01	3471.08	-0.13	3470.95
4_3	b_1	3480.7	-6.3	3474.42	8.19	3482.60	-0.90	3473.51	1.47	3474.98

* Fermi resonance affected energy levels. See text for details.
Level assignment from VPT4† results. Experimental results from Refs. 5 and 29.
ΔVPTn† = VPTn† - DVR and ΔVPT4‡ = VPT4‡ - VPT4†.
† V(**q**) LSQ fit from the CCSDT(Q)/CBS PES used in DVR(Exact).
‡ HF/TZ V_6(**q'**) from a local version of DALTON2013.

Morse-based VPT4† data is much smaller than those between the two VPT4 datasets, and that between VPT2† and VPT4†. Excellent agreement is anticipated due to the construction of the VPT4† PES through LSQ fitting, and is indeed observed. VPT4 predicts vibrational energy levels virtually identical to those from exact (variational) methods based on the same potential. An order of magnitude increase in agreement is seen between the DVR fundamentals and those predicted from VPT4† when compared to VPT2† for non-resonant levels (to include multi-quanta states). Large shifts from VPT2† to VPT4† in $4_2(a_1)$ and $6_2(a_1)$ clearly show that a lack of vibrational anharmonicity in VPT2 is reponsible for the disagreement with DVR and not a resonance interaction[29]. The treatment of resonances in VPT4 is an open topic but a successful approach has been applied here. Extending the effective Hamiltonian treatment from VPT2 to VPT4 is done by defining the Fermi-interaction terms as the sum of the first-order and third-order Hamiltonian elements while retaining the transformed second-order term (discussed in previous sections) that couples combination levels, if present. Determination of the VPT4 $\nu_5(b_2)$ fundamental in this way shows a value of 2852.11 cm^{-1} which is a vast improvement on the original value of 3105.16 cm^{-1}. The VPT4 Fermi resonance treatment of the questionable interaction between $1_1(a_1)$ and $4_2(a_1)$ slightly improves ($\sim$0.2 cm^{-1}) experimental agreement over the VPT2 result as 2782.25 cm^{-1}.

1.5 Conclusions

The application of CCSDT(Q)-based focal-point analysis[14–16] to geometric energy derivatives is now feasible due to the implementation and optimization of non-orthogonal spin-adapted coupled cluster theory[18,24,25]. Optimization of the equilibrium geometry of S_0 formaldehyde using numerical CCSDT(Q)/CBS and CCSDTQ/CBS gradients provides structures that show smooth convergence patterns expected of the quantum chemical methods which define the composite focal-point energy. The gradient-based approach allows high-level geometries

to be produced in a straightforward way without fitting structural parameters to a PES at an equivalent level of theory. A brief derivation of how CBS extrapolation formulae may be applied to analytic forms of the molecular gradient is provided to allow subsequent studies to benefit from currently implemented formulations and further advances in the development of high-level coupled cluster approaches.

The CCSDT(Q)/CBS anharmonic force field based on focal-point energies shows the best experimental agreement to date for purely *ab initio* fundamental VBOs of S_0 H_2CO with a MAE of 0.57 cm^{-1} and MAPE of 0.029%. Fermi resonances which affect the fundamentals of S_0 have been explored in detail with emphasis on the interesting emergent behavior of the $5_1, 2_1 6_1, 3_1 6_1 (b_2)$ triad at the CCSDT(Q)/CBS level of theory. A series of anharmonic force fields at the CCSD(T)/cc-pVXZ (X=T,Q,5) levels of theory show that the system-specific basis set convergence of harmonic vibrational frequencies, anharmonicity constants, and their anharmonic counterparts leads smoothly to the current high-level CBS-extrapolated results. A full set of spectroscopic constants computed at the CCSDT(Q)/CBS level which include rotational, centrifugal distortion, and vibration-rotation interaction constants provides a point of comparison for previous and future work. The availability of fully analytic arbitrary-order HF force constants through the recently published recursive approach contributes to the ability to evaluate vibrational perturbation theory corrections beyond second order without recourse to finite difference methods.

The results provided here are proof of concept that state-of-the-art quantum chemistry is capable of providing very accurate (within $\sim$1 cm^{-1} of experiment) fundamental positions of a prototypical tetra-atomic system using a very small PES (183 geometries) which is defined by high-level composite energies. This accuracy is obtained without the use of smaller auxiliary corrections normally seen in composite schemes reiterating that the critical components of any composite method resides in the CBS extrapolation(s) and core correlation treatment. The present purely *ab initio* results rival last-generation empirically fit PES where the theory presented here may lead to unprecedented levels of accuracy through empirical

refinement in the future. The obvious advantage of the present, purely *ab initio*, approach over semi-empirical PES is that it enables high-throughput production of accurate geometric and spectroscopic data which has zero experimental reliance using the most trusted, time-tested, methods in quantum chemistry. It is the hope of the authors that the present work provides sufficient example of the capabilities of well-defined *ab initio* methodologies which display easily understood convergence properties and that the methods will be applied to less understood molecules in the future.

CHAPTER 2

ASTROPHYSICAL SULFUR IN DIFFUSE AND DARK CLOUDS: THE FUNDAMENTAL VIBRATIONAL FREQUENCIES AND SPECTROSCOPIC CONSTANTS OF HYDROGEN SULFIDE CATION (H_2S^+)

[1] Morgan, W. James. Accepted by the *Monthly Notices of the Royal Astronomical Society.* Reprinted here with permission of publisher.

2.1 Abstract

The abundance of hydrogen sulfide, H_2S, is underpredicted in standard astrophysical models and, thus, so are the effects of its rich chemistry. Its cation, H_2S^+, may have a similarly understated effect on the interstellar medium (ISM) but, unlike its neutral parent, its presence in the ISM is unconfirmed. Advancing the search for H_2S^+ requires the accurate characterization of its spectroscopic properties; both in the infrared (IR) and microwave regimes. Past spectroscopy experiments were unable to resolve its rotational structure to high-accuracy and could not observe one of its fundamental vibrations. In this research, the H_2S^+ species has been studied at the highest available levels of electronic structure theory. Molecular structures, vibrational frequencies, rotational constants, and other rovibrational spectroscopic constants are predicted for H_2S^+ and eleven of its isotopologues. Previous *ab initio* studies fail to predict a separation of at least 5 cm^{-1} between the fundamental S−H stretching vibrations; a value equivalent to the uncertainty of previous photoelectron spectroscopy experiments. The characteristically different rotational properties of H_2S and H_2S^+ are established concluding that most, if not all, large-dish telescopes and interferometers can easily discern the cation from the neutral. The best possible candidates for interstellar detection of H_2S^+ in the IR are determined to be the fundamental S−H stretches, due to their intensity and unique region in the IR. JWST is best equipped for this search whereas the EXES instrument on SOFIA is better suited to find the bending fundamental of H_2S^+ and all fundamentals of its deuterated isotopologues.

2.2 Introduction

The sulfur depletion problem in dark clouds persists, as the primary reservoir of sulfur in these regions remains unidentified[134–136]. However, recent models which consider the rich chemistry of sulfur suggest SH and H_2S as primary candidates. Both species form on

grain surfaces through hydrogenation of atomic sulfur and eventually sink into the bulk of the grain or, in the case of H_2S, can desorb into the gas-phase *via* reaction-diffusion competition[137]. The recent astronomical detection of NS^+, S_2H, HCS, and HSC demonstrates that the sulfur chemical network is diverse, with gas-phase species more abundant than once thought[135,138,139]. For example, the abundance ratio of NS to NS^+ is 50 toward Barnard 1-b (B1b) and 33 in Taurus Molecular Cloud-1 (TMC-1)[138]. Abundances of H_2S are of the same order of magnitude as NS in both of these dense molecular clouds as well as in L134N[140,141]. In diffuse clouds, abundances are observed to be an order of magnitude higher for H_2S where grain interactions are expected to be reduced but the possibility of forming H_2S^+ directly by photoionization exists[142].

Unlike its neutral counterpart, the spectroscopic properties of H_2S^+ have not been painstakingly characterized despite its potential importance in the sulfur network[143]. One obvious reason for this is due to the difficulty in studying radical cations, whose categorization inevitably relies on limited resolution photoelectron spectroscopy experiments. Much of the past work on the H_2S^+ system has focused on the non-adiabatic Renner-Teller coupling between the $^2B_1$ ground and $^2A_1$ excited states, which manifests itself in the rovibronic spectrum when energies approach or surpass the barrier to linearity[144–146]. Despite this complexity, several experiments have provided ionization energies (ca. 10.5 eV) and rotational constants for $^2B_1$ H_2S^+, but with a limited number of significant figures[147,148]. Reliable answers for the vibrational band origins, on the other hand, seem to source from only one vacuum ultraviolet (VUV) pulsed-field ionization-photoelectron (PFI-PE) experiment, which reports a minimum resolution of 5 cm^{-1}[147]. Previous *ab initio* results provide a relatively complete picture of the room temperature spectrum but rely on incomplete models of electron correlation and only consider deuterated isotopologues[149]. Thus, the present work seeks to provide definitive predictions for the ground state fundamental vibrations of H_2S^+ and its isotopologues as well as to evaluate the accuracy of rotational constants derived from various experimental sources.

Table 2.1: H_2S^+ Symmetry Coordinates

Coord.	Symm.	Norm.	Formula
S_1	a_1	$1/\sqrt{2}$	$(r_{\mathrm{SH}} + r_{\mathrm{SH'}})$
S_2	a_1		θ_{HSH}
S_3	b_2	$1/\sqrt{2}$	$(r_{\mathrm{SH}} - r_{\mathrm{SH'}})$

2.3 Computational Methods

Potential energy surfaces (PESs) are constructed using both unrestricted and restricted Hartree-Fock reference wavefunctions (UHF and ROHF, respectively) where spin-contamination in the UHF case is negligible as indicated by $< S^2 - S_z^2 - S_z > < 0.005$. Electron correlation is described *via* coupled cluster theory with non-iterative triple excitations, CCSD(T), as well as up to non-iterative quadruple excitations, CCSDT(Q)[23,150]. The correlation-consistent polarized-valence basis sets[151,152], cc-pV(X+d)Z (X = T, Q, 5), are used in all computations except for core-correlation corrections where the Martin-Taylor (MT) uncontracted basis set is employed instead[153,154]. An initial, near-equilibrium, geometry is optimized with the CCSD(T)/cc-pV(5+d)Z method and corrected for core-correlation by adding the difference between geometries optimized using CCSD(T)/MT with and without core electrons correlated (referred to as MTc and MT, respectively) as defined in Equation 3.1. The CCSD(T)/cc-pV5Z $\mathcal{T}_1$ diagnostic is 0.009 and the $\mathcal{D}_1$ diagnostic is 0.016 for UHF and ROHF. The root-mean-square of the computed forces were converged better than 1×10^{-8} a.u.

$$r_{\mathrm{ne}} = r_{\mathrm{5Z}} + (r_{\mathrm{MTc}} - r_{\mathrm{MT}}) \tag{2.1}$$

A grid of nuclear configurations is generated from this reference structure by displacing along each of its symmetry-adapted internal coordinates (Equation 2.1) up to fourth-order in step sizes of 0.005 Å or 0.005 rad. The total energy at each point is defined as a sum of four separate components; the CCSD(T) energy extrapolated to the complete-basis set (CBS)

limit and three energy increments. Each increment represents a source of electron correlation omitted from the above CBS energy: core-correlation, scalar-relativistic correlation, and higher-order dynamic correlation. A nomenclature has been used in the past to describe this composite theory by its components where C represents CBS-extrapolation, cC represents core-correlation, R represents scalar-relativity, and E represents higher-order correlation[155]. For example, the CcCRE potential surface (Equation 3.3) includes all of the corrections, but the CcCR omits the higher-order correlation correction.

$$E_{\mathrm{CcCRE}} = E_{\mathrm{CBS}} + \Delta E_{\mathrm{core}} + \Delta E_{\mathrm{rel}} + \Delta E_{\mathrm{hlc}} \tag{2.2}$$

Two different procedures are used to extrapolate the CCSD(T) energy to the CBS limit. The first scheme used is the three-point total energy extrapolation shown in Equation 3.4[50].

$$E(X) = E_{\mathrm{CBS}} + A(X + 1/2)^{-4} + B(X + 1/2)^{-6} \tag{2.3}$$

The second scheme extrapolates the Hartree-Fock energy and the correlation energy, represented here as ε, separately using Equations 2.4 and 2.5, respectively[44,45].

$$E^{\mathrm{HF}}(X) = E^{\mathrm{HF}}_{\mathrm{CBS}} + A\ e^{BX} \tag{2.4}$$

$$\varepsilon^{(\mathrm{T})}(X) = \varepsilon^{(\mathrm{T})}_{\mathrm{CBS}} + A\ X^{-3} \tag{2.5}$$

The resulting CCSD(T)/CBS energy in this latter scheme is $E'_{\mathrm{CBS}} = E^{\mathrm{HF}}_{\mathrm{CBS}} + \varepsilon^{(\mathrm{T})}_{\mathrm{CBS}}$ where the prime is simply used to distinguish the two CBS extrapolations. Each energy correction (increment) is defined as the difference between the energy with the correlation effect considered and the energy without it when using the same basis set. The core-correlation correction, ΔE_{core}, is $E_{\mathrm{MTc}} - E_{\mathrm{MT}}$ as defined with the geometry correction. Scalar relativity is incorporated through ΔE_{rel} which is taken as the difference in the all-electron CCSD(T)/cc-pCV(T+d)Z-DK energy with and without the Douglas-Kroll-Hess (DKH) corrections to

second-order[156]. The energy contribution from non-iterative quadruple excitations in the coupled cluster wavefunction, ΔE_{hlc}, is defined as the difference between CCSDT(Q)/cc-pV(T+d)Z and CCSD(T)/cc-pV(T+d)Z at each point.

The expansion coefficients which define the C, CcC, CcCR, and CcCRE PESs are determined through a least-squares fitting of their corresponding composite energies at each displaced geometry. All fits display a sum-of-square residuals (SSR) better than 2×10^{-18} a.u. where no qualitative difference is observed between ROHF or UHF methods nor the two extrapolation schemes. INTDER was used to transform internal coordinate derivatives into Cartesian ones before subsequent normal mode analysis[72]. Second-order vibrational perturbation theory (VPT2) is used to predict spectroscopic constants of H_2S^+ as well as its vibrationally-averaged geometry with the SPECTRO program[71]. Transformation into Morse-cosine coordinates from symmetry-adapted internal coordinates is performed before variationally predicting vibrational band origins using VTET[133,157]. Energies are converged to better than $1.\times10^{-12}$ a.u. and integrals are included if $> 1.\times10^{-15}$. All single-point energy computations are performed with Molpro 2010.1.67[158] with the exception of ΔE_{hlc}. The purely *ab initio* ΔE_{hlc} increment is determined with MRCC 2018[159] because a majority of quantum chemistry packages do not implement CCSDT(Q) theory due to its expensive nature, let alone implement it for use with both ROHF and UHF. The CCSD(T)/cc-pV(5+d)Z, CCSD(T)/MTc, and CCSD(T)/MT geometries were optimized in Molpro 2010.1.67 using 5-pt central finite difference gradients. UHF-CCSD(T)/cc-pV(Q+d)Z anharmonic infrared intensities are computed *via* finite-differences of analytic seconds, as well as the equilibrium and vibrationally-averaged dipole moments, using CFOUR 2.0[58].

2.4 Results and Discussion

Units of cm^{-1} (referred to as wavenumbers) are used here when discussing vibrational frequencies even though this is technically a unit of inverse length. This choice is made because

wavenumbers are one of the two common units, the other being microns, which is used in IR spectroscopy and astronomy to describe the vibrational transitions of a molecule. It is easier to compare the magnitude and thus, accuracy of both the anharmonic (fundamental and overtone) and harmonic vibrational frequencies relative to previous results in the scientific literature using this convention.

A minimum basis set for hydrogen sulfide will be similar to that for water in the valence space, as it shares a common set of symmetry-adapted molecular orbitals in C_{2v} point-group symmetry. That is, atomic orbitals of the central atom, S, interacting with symmetric and anti-symmetric combinations of the 1σ orbitals of H_2. What results from this set, at equilibrium, are stabilizing interactions with the atomic S($3p_z$) and $\frac{1}{\sqrt{2}}(1\sigma+1\sigma')$ as well as S($3p_y$) and $\frac{1}{\sqrt{2}}(1\sigma\text{-}1\sigma')$; a_1 and b_2 combinations, respectively. No symmetry-allowed combinations exist for the out-of-plane S($3p_x$) atomic orbital within this basis, so it persists as a primarily atomic lone-pair molecular orbital. It is from this highest occupied molecular orbital (HOMO) that the lowest energy electronic state of H_2S^+ is derived. The $^1A_1$ H_2S Hartree-Fock wavefunction may be qualitatively described as

$$(1a_1)^2(2a_1)^2(1b_2)^2(3a_1)^2(1b_1)^2\underline{(4a_1)^2(2b_2)^2(5a_1)^2(2b_1)^2},$$

where ionization of the HOMO results in the $^2B_1$ H_2S^+ wavefunction,

$$(1a_1)^2(2a_1)^2(1b_1)^2(1b_2)^2(3a_1)^2\underline{(4a_1)^2(2b_2)^2(5a_1)^2(2b_1)},$$

noting that the rearrangement of MOs in the core (not underlined) reflects slight energetic changes in the primarily atomic S core orbitals.

The ionization of a non-bonding, primarily atomic, MO is not anticipated to cause a large geometric change within the system. Preliminary CCSD(T)/cc-pV(T+d)Z optimizations performed here shows the geometry expands from $r_{\mathrm{SH}} = 1.338$ Å in H_2S to $r_{\mathrm{SH}} = 1.357$ Å in H_2S^+, and the angle expands from $\theta_{\mathrm{HSH}} = 92.26°$ to $\theta_{\mathrm{HSH}} = 93.08°$. Such a change represents

Table 2.2: Molecular Structures and Rotational Constants of H_2S^+ (Å , degrees, and cm^{-1})

	C	CcC	CcCR	CcCRE	CEPA-1[a]	Emission[b]
r_e	1.35672	1.35496	1.35546	1.35594	1.357	-
θ_e	93.080	93.035	92.927	92.894	93.0	-
r_0	1.37336	1.37161	1.37212	1.37267	-	1.358*
θ_0	93.039	92.995	92.882	92.846	-	92.9
A_e	10.20866	10.22660	10.19889	10.18541	10.1869	-
B_e	8.62388	8.65276	8.66183	8.66041	8.6201	-
C_e	4.67480	4.68704	4.68386	4.68060	4.6691	-
A_0	10.20101	10.21889	10.18943	10.17457	10.1749	-
B_0	8.59786	8.62647	8.63655	8.63501	8.5920	-
C_0	4.58173	4.59356	4.59046	4.58684	4.5746	-

$E_{\mathrm{CcCRE}} = E_{\mathrm{CBS}} + \Delta E_{\mathrm{core}} + \Delta E_{\mathrm{rel}} + \Delta E_{\mathrm{hlc}}$
Remove terms from right to left for previous level of theory.
Equation 3.4 was used for CBS extrapolation.
[a] *ab initio* results from [149].
[b] Emission spectroscopy from [160].
* See text for a description of discrepancies.

Table 2.3: S-reduced Watson Hamiltonian parameters of H_2S^+ (cm^{-1})

	C	CcC	CcCR	CcCRE	Emission [a]	PFI-PE [b]
10^4 D_J	59.035	97.901	97.538	97.639	-	-
10^4 D_{JK}	-206.84	-164.76	-164.37	-164.62	-	-
10^4 D_K	336.17	72.945	72.913	73.062	-	-
10^4 d_1	-24.686	20.784	20.244	20.141	-	-
10^4 d_2	1.8067	-24.660	-24.505	-24.516	-	-
10^6 H_J	2.495	3.704	3.668	3.674	-	-
10^6 H_{JK}	-21.78	-12.07	-12.01	-12.04	-	-
10^6 H_{KJ}	36.16	13.73	13.67	13.72	-	-
10^6 H_K	-5.708	-5.356	-5.325	-5.342	-	-
10^6 h_1	0.7179	-1.528	-1.477	-1.471	-	-
10^6 h_2	-0.2838	1.924	1.898	1.900	-	-
10^6 h_3	0.2436	-0.2981	-0.2878	-0.2867	-	-
A	10.19995	10.22022	10.19074	10.17588	10.177(21)	10.170
B	8.59942	8.62698	8.63707	8.63553	8.631(16)	8.652
C	4.58119	4.59221	4.58912	4.58550	4.601(60)	4.611

$E_{\mathrm{CcCRE}} = E_{\mathrm{CBS}} + \Delta E_{\mathrm{core}} + \Delta E_{\mathrm{rel}} + \Delta E_{\mathrm{hlc}}$
Remove terms from right to left for previous level of theory.
Equation 3.4 was used for CBS extrapolation.
[a] Emission spectroscopy from [160].
[b] Pulsed-field ionization-photoelectron spectroscopy from [147].

an increase of approximately 1.5% in the bonds and 1% in the angle for the ionized geometry at equilibrium. This low level of theory is fine for a relative comparison to other *ab initio* results but achieving quantitative accuracy (that is, comparable to experimental results) requires significantly more costly approaches[161]. Table 2.2 contains such high-level results for the equilibrium geometries r_e, vibrationally-averaged zero-point geometries r_0, and the rotational constants of H_2S^+.

Here we see that the CBS extrapolation using cc-pV(X+d)Z (X = T, Q, 5) does not significantly change the equilibrium geometry from the previously mentioned CCSD(T)/cc-pV(T+d)Z values of $r_{SH} = 1.357$ Å and $\theta_{HSH} = 93.08°$. This suggests that basis set effects on the equilibrium geometry are not as prominent as those seen in similarly sized systems[161]. Small effects of electron correlation follow established trends with core-correlation (CcC) contracting the geometry and additional dynamic correlation (CcCR and CcCRE) lengthening bond distances and shrinking bond angles. All of the high-level equilibrium geometries (r_e, θ_e) in Table 2.2 have slightly shorter bond lengths than the past *ab initio* work by[149] whose CEPA-1 geometry is instead closer to the aforementioned CCSD(T)/cc-pV(T+d)Z structure. No experimentally determined equilibrium structures exist for comparison.

However, a somewhat dated zero-point structure (r_0, θ_0) from[160] was derived through emission spectroscopy of the system. The bond length of this experimental structure is more similar to the *ab initio* equilibrium structures than our zero-point predictions which have approximately 0.01 Å longer bond lengths in all cases.[160] discusses this discrepancy noting that their values are too short to reproduce rotational constants in the original text. Only small changes are observed between the equilibrium and zero-point structures with respect to the bond angle where the current work agrees well with past experiment and theory[149]. Equilibrium rotational constants about the a rotation axis are consistent between the present work and past theory but differences of 0.05% and 0.025% are observed in B_e and C_e. These errors persist into the vibrationally-averaged rotational constants (A_0, B_0, C_0) where the present complete-basis set extrapolated results, which include core-correlation, scalar

relativistic, and CCSDT(Q)-based contributions, are taken to be the correct predictions.

The accuracy of the CcCRE results relative to past theoretical studies is established by comparing our CcCRE rotational constants in the S-reduction (Table 2.3) to those provided by[160]. All of the constants fall within the uncertainty of[160] only varying in the third decimal place for A and B whereas those of[149] appear to systematically underestimate B (B_0). Further comparison is difficult as few rotationally-resolved experiments exist for H_2S^+.[148] produced a rotationally-resolved spectrum but was focused on the $^2A_1$ electronic and highly vibrationally excited $^2B_1$ states of H_2S^+ without reporting ground state rotational constants. The photoelectron experiments of[147] are consistent with our prediction of the rotational constant A to four significant digits, $A = 10.17$ cm^{-1}, but the uncertainty of their rotational constants is unclear.

While relatively small changes are observed between the geometries found with the different composite theories (C, CcC, CcCR, and CcCRE), much more significant changes make an apperance in the molecular vibrations. Table 2.4 reports the harmonic and fundamental vibrational frequencies of H_2S^+ (as predicted by VPT2) and their relative CCSD(T)/cc-pV(Q+d)Z integrated band intensities. The inclusion of core-correlation (CcC) increases the harmonic frequencies up to 4 cm^{-1} (ω_3) which is offset by slightly larger decreases in the CcCRE results due to contributions from quadruple excitations, CCSDT(Q). Scalar relativistic corrections play a more subtle role, despite sulfur's larger core, only decreasing harmonic frequencies by ca. 1 cm^{-1} from CcC to CcCR. The harmonic vibrational frequencies of[149] compare reasonably well, within ca. 6 cm^{-1}, to our CBS theories, with the exception of their possible typographical error swapping the magnitudes of the symmetric (ω_1) and anti-symmetric (ω_3) S$-$H stretching modes which in all cases should be $\omega_3 > \omega_1$.

Inclusion of anharmonicity does little to change how the CBS theories compare to one another with the exception of the CcCR results. The CcCR ν_2 fundamental increases by 3 cm^{-1} from CcC. This difference is not represented by changes in the harmonics. Reasonable agreement is seen again between our results and the older *ab initio* results of[149] but their

Table 2.4: VPT2 Vibrational Frequencies of H_2S^+ (cm^{-1}) and their Intensities (km/mol)

	C	CcC	CcCR	CcCRE	I^a_{rel}	I^a	CEPA-1[b]	PFI-PE[c]
$\omega_1(a_1)$	2600.1	2603.6	2601.7	2596.9	71	77.69	2602.88	-
$\omega_2(a_1)$	1192.7	1194.1	1194.5	1192.4	5	5.66	1195.41	-
$\omega_3(b_2)$	2606.7	2610.5	2609.6	2604.9	100	109.74	2604.61	-
$\nu_1(a_1)$	2496.5	2498.7	2497.1	2491.6	69	77.71	2495.60	2496(5)
$\nu_2(a_1)$	1161.1	1162.3	1165.7	1163.0	6	7.33	1159.21	1161(5)
$\nu_3(b_2)$	2500.0	2502.5	2502.4	2497.2	100	112.84	2495.92	-

$E_{\text{CcCRE}} = E_{\text{CBS}} + \Delta E_{\text{core}} + \Delta E_{\text{rel}} + \Delta E_{\text{hlc}}$
Remove terms from right to left for previous level of theory.
Equation 3.4 was used for CBS extrapolation.
[a] This work: CCSD(T)/cc-pV(Q+d)Z where I_{rel} is $100(I/I_{\omega_3/\nu_3})$.
[b] *ab initio* results from [149].
[c] Pulsed-field ionization-photoelectron spectroscopy from [147].

work fails to resolve a difference between the two S−H stretching fundamentals. Our CcCRE results predict the difference between ν_1 and ν_3 to be 5.8 cm^{-1} with the VPT2 method.[147] were not able to observe ν_3 in their PFI-PE experiment despite assigning a band origin for the other two fundamentals. The perceived absence of this band in their spectrum may be partly due to their full-width half-max (FWHM) resolution of 5 cm^{-1} which is very close to the expected separation of ν_1 and ν_3. The frequencies they do provide for comparison, ν_1 and ν_2, agree well with our own where the CcCRE results are within the uncertainty of their experiment.

[147] have also suggested a first-order anharmonic resonance between ν_1 and the overtone of the bend, $2\nu_2$. The interaction constant for these modes is $\frac{1}{4}\phi_{233}$, where $\phi_{233} = 95.144$ cm^{-1}, and serves as the off-diagonal element of an effective Hamiltonian $\boldsymbol{H}_{\text{eff}}$. The deperturbed diagonal of this 2×2 matrix is $2\nu_2^* = 2318.5$ cm^{-1} and $\nu_1^* = 2488.9$ cm^{-1}. Determination of any Fermi resonance shift from this coupling follows as $\boldsymbol{v} = \boldsymbol{U}^{\boldsymbol{T}}\boldsymbol{H}_{\text{eff}}\boldsymbol{U}$, where $\boldsymbol{v}$ contains the shifted levels (considered a vector where off-diagonal elements $<< 0$) and $\boldsymbol{U}$ their mixing coefficients. Diagonalization of this matrix moves the CcCRE VPT2 predictions of ν_1 from 2492.7 to 2492.2 cm^{-1} and $2\nu_2$ from 2315.8 to 2315.2 cm^{-1}; approximately half of a wavenumber shift downward for the fundamental. An interaction of this magnitude is gener-

Table 2.5: CcCRE VTET fundamentals of H_2S^+ and D_2S^+ (cm^{-1})

	$\nu_1(a_1)$	$\nu_2(a_1)$	$\nu_3(b_2)$
$H^{32}SH^+$	2491.3	1162.2	2497.2
$H^{33}SH^+$	2490.3	1161.7	2496.0
$H^{34}SH^+$	2489.4	1161.2	2494.9
$H^{36}SH^+$	2487.7	1160.2	2492.9
$D^{32}SD^+$	1808.2	840.7	1816.2
$D^{33}SD^+$	1806.7	840.0	1814.5
$D^{34}SD^+$	1805.3	839.3	1813.0
$D^{36}SD^+$	1802.8	838.1	1810.1

$E_{\mathrm{CcCRE}} = E_{\mathrm{CBS}} + \Delta E_{\mathrm{core}} + \Delta E_{\mathrm{rel}} + \Delta E_{\mathrm{hlc}}$
Equation 3.4 was used for CBS extrapolation.
See Supporting Information for HSD^+ VPT2 results.

ally not considered a Fermi resonance and would not have a significant effect on the infrared spectrum, where intensity borrowing from ν_1 to $2\nu_2$ would be proportional to their mixing coefficient from $\boldsymbol{U}$ which is 1.8%. The variational, VTET, predictions of vibrational band origins in Table 2.5 do not suffer the accidental degeneracy problem of perturbation theory and thus represent resonance-free frequencies. Good agreement, within ca. 1 cm^{-1}, is seen between the CcCRE fundamentals from VTET and those from VPT2, where the former are preferred to the latter because they do not experience anharmonic resonances.

Up to this point, our predictions only rely on the ROHF reference using the CBS-extrapolation of Martin and Lee[50]. This extrapolation scheme has seen great success and results based on it have been used to guide laboratory astrophysics studies on other cations[36,37,162,163]. However, additional VPT2 predictions using UHF and another popular extrapolation scheme have been considered in light of the ambiguous nature of the H_2S^+ fundamentals as shown in Table 2.6. No difference is seen between the values of ν_2 between the two extrapolation schemes and only a small difference, ca. 1 cm^{-1}, exists for the S−H stretching fundamentals. A similar trend is seen for the ROHF and UHF references where no difference in seen in ν_3 and a similarly small ca. 1 cm^{-1} difference exists for the remaining modes. The mean values of the CcCRE VPT2 fundamentals agree very well with the CcCRE VTET results (Table 2.5), where VPT2 may overestimate ν_2 slightly. A standard deviation less than a

wavenumber is observed between the combination of two reference wavefunctions and extrapolation schemes. Such agreement provides confidence that the present CBS results are highly-consistent and reliable predictions.

Table 2.6: CcCRE VPT2 Fundamentals of H_2S^+

HF	CBS*	$\nu_1(a_1)$	$\nu_2(a_1)$	$\nu_3(b_2)$
UHF	HF/CC	2491.3	1164.3	2498.4
UHF	Total	2490.4	1164.6	2497.2
ROHF	HF/CC	2492.7	1163.0	2498.5
ROHF	Total	2491.6	1163.0	2497.2
Mean		2491.5	1163.7	2497.8
Std. Dev.		0.9	0.8	0.7

$E_{\mathrm{CcCRE}} = E_{\mathrm{CBS}} + \Delta E_{\mathrm{core}} + \Delta E_{\mathrm{rel}} + \Delta E_{\mathrm{hlc}}$
* HF/CC ≡ Equations 2.4 and 2.5
* Total ≡ Equation 3.4

The relative abundance of sulfur isotopes is ^{32}S [0.9499(26)] > ^{34}S [0.0425(24)] > ^{33}S [0.0075(2)] > ^{36}S [0.0001(1)][164]. Differences in the mass of sulfur have a clear effect on the sulfur isotopologues of H_2S^+, where the change in center-of-mass effects all vibrations by 1-4 cm^{-1}. Double-deuteration retains the C_{2v} symmetry of the system while decreasing all vibrations by approximately 30%. The separation between the symmetric and anti-symmetric S−H (here, S−D) modes grows with double deuteration; something that[149] noted in their D_2S^+ harmonic frequency predictions. Mixed isotopologues in this category, D_2S^+, show similar shifts as those seen in their hydrogen-only, H_2S^+, counterparts. Only high-resolution experiments will be able to resolve the differences between the most abundant H_2S^+ isotopologues based on frequency differences alone (neglecting intensity concerns). The singly-deuterated, H^{32}SD$^+$, and doubly-deuterated, D^{32}SD$^+$, isotopologues should be discernable by their categorically different set of fundamentals.

It should be noted that the permanent dipole of H_2S^+ at equilibrium, μ_e, is predicted to be 1.6160 D and its vibrationally-averaged counterpart, μ_0, is predicted to be 1.6598 D using CCSD(T)/cc-pV(Q+d)Z. The cation's dipole moment was computed with respect to its center-of-mass. Both of these values are much smaller than the CEPA-1 prediction of 2.1334 D from[149] where only the electronic contribution to the total dipole moment may have

been reported. In either case, the present values of the dipole moment suggest H_2S^+ will have a significantly larger, almost twice, the experimentally determined value of 0.978325(10) D of neutral H_2S[165].

2.5 Astrophysical Implications

Neutral hydrogen sulfide and its isotopologues have been detected in a number of astronomical sources, but its cation has yet to be observed in such environments[166,167]. It is logical to assume H_2S^+ would be present in the same regions as H_2S, especially in diffuse molecular clouds, where cations are more prevalent[168,169]. However, these cation features are perhaps masked by its neutral parent due to the similarities of structure between H_2S and H_2S^+. The spectroscopic constants of neutral H_2S and its sulfur isotopologues have been experimentally determined to unprecedented levels by multiple groups in the past[170–173]. Maintaining enough significant figures for illustrative purposes, the H_2S rotational constants of[172] are $A_0 = 10.3600$ cm^{-1}, $B_0 = 9.0185$ cm^{-1}, and $C_0 = 4.7306$ cm^{-1}. We can use our H_2S^+ CcCRE rotational constants of $A_0 = 10.1746$ cm^{-1}, $B_0 = 8.6350$ cm^{-1}, and $C_0 = 4.5868$ cm^{-1} in a simple example to demonstrate that clear differences should be apparent in the rotational spectra of hydrogen sulfide and its cation.

In the simplest approximation, for an asymmetric top in its ground vibrational state, the lowest rotational energy levels, $E(J_{K_a,K_c})$, are $E(1_{0,1}) = B + C$, $E(1_{1,1}) = A + C$, and $E(1_{1,0}) = A + B$. Using the rotational constants presented above, the differences in the $J = 1$ energy levels between the neutral and cation are 0.5689 (13.7491-13.2218), 0.3291 (15.0906-14.7614), and 0.5273 (19.3785-18.8096) cm^{-1} which correspond to tens of GHz. The pure rotational spectra of H_2S and H_2S^+ should both be predominantly *b*-type transitions, $\Delta K_a = \pm 1$ and $\Delta K_c = \pm 1$, due to the nature of their dipole moments. The lowest energy transition of this category would be the $1_{1,1} \leftarrow 0_{0,0}$ transition that directly corresponds to the energy of $1_{1,1}$. This energy difference is already established here as 0.3291 cm^{-1} or 9.867

GHz which is clearly distinguishable with most, if not all, large-dish telescopes (IRAM 30m) and interferometers (ALMA). The neutral and cation should be sufficiently different in this sense where the cation's transitions are anticipated to be stronger due to its larger permanent dipole moment.

The consideration of centrifugal distortion would slightly lower term energies, changing transition frequencies, but not so much as to change the conclusion that the pure rotational spectrum of the neutral and cation should be considerably different. In the case of H_2S, this is confirmed by reviewing the experimentally observed frequency of $1_{1,1} \leftarrow 0_{0,0}$ from[172] which is 452390.3314(10) MHz. This value is 15.0901 cm^{-1} which is only 0.0005 cm^{-1} lower than the simple $A + C = 15.0906$ cm^{-1} predicts. Centrifugal distortion effects in H_2S^+ are anticipated to be more significant than in the neutral, at least for this transition, where the prediction of $1_{1,1} \leftarrow 0_{0,0}$ using the S-reduced results of Table 2.3 produces 14.7592 cm^{-1}, which is 0.0022 cm^{-1} lower than $A + C = 14.7614$ cm^{-1}.

However, the spectrum of H_2S^+ is more complicated than this example suggests due to fine and hyperfine structure, the former of which results from spin-rotation coupling. Energy levels with $K > 0$ are split because of this coupling where $J = N \pm \frac{1}{2}$. In this way, $1_{1,1} \leftarrow 0_{0,0}$ leads to two separate transitions (the ground state is not split by spin-rotation), a doublet, which is not captured in the simplistic analysis above. The magnitude of splittings between these peaks will obviously vary with N but the analysis of[174] (see Table VI and Figure 3 of the cited work) shows the $1_{1,1} \leftarrow 0_{0,0}$ transition of the water cation, H_2O^+, is split through spin-rotation coupling by ca. 2% of the magnitude of the unsplit level. In the case of H_2S^+, this amounts to $\Delta = 0.2952$ cm^{-1} (8.851 GHz) where $E(J = \frac{3}{2})$ would lie ca. 0.4Δ below $E(1_{1,1})$. Similarly, $E(J = \frac{1}{2})$ would lie ca. 0.6Δ higher when using[174] as an estimate. Such fine, and further hyperfine, structure would obviously not limit astronomical detection of H_2S^+ as evident by the Herschel/HIFI detection of H_2O^+ in dense star-forming regions of space through hyperfine transitions[175]. Even more complicated hyperfine structure arises for the related SH^+, a diradical cation, which was recently detected toward Sgr B2 using

Table 2.7: Some Instruments Capable of Detecting H_2S^+ in IR

Platform	Instrument	Isotopologue[a]	Fundamentals
SOFIA	EXES	H_2S^+	ν_2
		D_2S^+	ν_1, ν_2, ν_3
JWST	NIRSpec	H_2S^+	ν_1, ν_3
	MIRI/Med	H_2S^+	ν_2
		D_2S^+	ν_1, ν_2, ν_3
	MIRI/Low	H_2S^+	ν_2
		D_2S^+	ν_1, $\nu_2{}^*$, ν_3

[a] By deuteration where all sulfur variations are included.
* Close to 833.3 cm^{-1} limit of MIRI/Low.

APEX as well as W3 IRS5 using Herschel/HIFI[168,176]. Nuclear spin statistics must also be considered due to the equivalent hydrogens of the system where the nuclear spin functions, but not electronic wavefunction symmetry, are shared with water.

Detection of H_2S^+ by infrared absorption should also be possible. The vibrational band origin of ν_2 is predicted to be 1162.2 cm^{-1} which is within the instrument range of the Echelon-Cross-Echelle Spectrograph (EXES) aboard the Stratospheric Observatory for Infrared Astronomy (SOFIA). EXES is capable of very high spectral resolution (50,000-100,000) and should reveal the rovibrational nature of the band if detected. This is unfortunately the least intense fundamental, displaying an integrated band intensity only 5-6% that of the anti-symmetric S−H stretch (ν_3) which is predicted to be the brightest band. However, the James Webb Space Telescope (JWST) will be able to search for both S−H stretching fundamentals (ν_1 and ν_3) using its Near Infrared Spectrograph (NIRSpec). The spectral resolution of such a search is expected to be limited compared to EXES (i.e., rovibrational structure absent). This is despite the benefit of NIRSpec's highest resolution capabilities

(G395H/F290LP), but the higher sensitivity of JWST, combined the more intense features, makes detection with this platform more likely. Neither operating mode of JWST's Mid-Infrared Instrument (MIRI) will be able to aid in this search for the S−H stretches but MIRI will be able to look for the bending fundamental if SOFIA is unable to detect it. The symmetric stretch, ν_1, is predicted to be ca. 30% less intense than its anti-symmetric counterpart which will hopefully aid in its discovery despite the potential overlap of the S−H stretching bands. The infrared region of the S−H stretches (2450-2550 cm^{-1}) is also devoid of common molecular vibrations which incorporate the far more abundant carbon and oxygen such as C=O, C=C, C−H, and O−H which makes the ν_1 and ν_3 modes of H_2S^+ unique targets for interstellar detection. However, the bending modes of similarly small molecules, such as the ν_4 fundamental of H_2CO[161], are likely to cause congestion near hydrogen sulfide cation's own bending fundamental, ν_2.

The neutral parent, H_2S, exhibits S−H stretching frequencies that are well-separated, by over 100 cm^{-1}, from those of H_2S^+.[177] report the symmetric stretching fundamental of H_2S to be ν_1 = 2614.409(90) cm^{-1} and its anti-symmetric countepart to be ν_3 = 2628.440(20) cm^{-1}. This represents a vibrational band origin separation of 123.1 cm $^{-1}$ for ν_1 and 131.2 cm $^{-1}$ for ν_3 between the neutral and the cation. The bending fundamental of the two species is separated by 20.4 cm^{-1} as[178] observes 1182.575(30) cm^{-1} for the ν_2 fundamental of H_2S. Thus, H_2S^+ will be harder to identify by its ν_2 using low-resolution instruments, but its ν_1 and ν_3 stretching modes should be easily discerned from its parent neutral at any resolution.

Singly and doubly-deuterated forms of hydrogen sulfide are known to exist in a number of dense clouds, implying its cation may be present as well[167]. All fundmamental vibrational frequencies of the doubly-deuterated isotopologues fall within detection ranges of SOFIA's EXES as well as both operating modes of MIRI, albeit on the high end of the low-resolution mode for ν_2. The differences in D_2S and D_2S^+ will be proportional to their non-deuterated counterparts by a factor related to the change in mass. Using the results of[179] (Table 2 of the cited work) and the results in Table 2.5, the differences are 72% of those between H_2S

and H_2S^+; 88.2, 14.7, 94.0 cm^{-1} for ν_1, ν_2, and ν_3, respectively. This leads to the same conclusions about D_2S^+; that is, the stretching fundamentals are well separated from the neutral but the bend is much closer. The shift in overall magnitude for the vibrational frequencies of D_2S^+ puts these SD stretching vibrations into a region of ketone (C=O) and alkene (C=C) stretches. This will limit their visibility in the infrared. The HSD^+ cation has a similar relationship to its neutral counterpart, but only one of its stretching fundamentals is significantly shifted; the symmetric stretch ν_1. Our CcCRE VPT2 results for $H^{32}SD^+$, Table 1 in the electronic supporting information (ESI), provide values of 1812.0, 1015.5, and 2494.3 cm^{-1} for ν_1, ν_2, and ν_3, respectively. This means the presence of HDS^+ ν_3 will likely overlap the region of H_2S^+ ν_1 so high-resolution analysis in regions where chemical fractionation is suspected will help delineate observed peaks. The last potential interaction amongst all of the considered isotopologues is that of $2\nu_2$ of H_2S which was observed at 2353.967(10) cm^{-1} by[178]. This band is ca. 100 cm^{-1} below the H_2S^+ stretches and HSD^+ ν_3, as well as far removed from the other fundamentals of all isotopologues. Thus, it should not lead to any overlap or interaction in the infrared spectrum of H_2S^+ in insterstellar, or laboratory environments.

2.6 Conclusions

The hydrogen sulfide cation, H_2S^+, may be of critical importance to the astrophysical sulfur network in diffuse and dark clouds, where it can interact with a variety of species including atomic oxygen[142]. Despite this, a discrepancy has persisted in the literature regarding its fundamental vibrational frequencies. The anti-symmetric S−H stretching fundamental, ν_3, of H_2S^+ is perceived to be absent in limited resolution photoelectron experiments, and it is predicted to be coincident with the symmetric S−H stretching fundamental ν_1 from previous theoretical studies[149]. In the present work, we have addressed this discrepancy by providing high-level, CBS-extrapolated, PES capable of determining vibrational band origins with

ca. 1 cm^{-1} consistency. Using both perturbation theory and variational methods, we have determined a clear separation of the two stretching fundamentals of this system on the order of 6 cm^{-1}. Variational predictions of the fundamentals are provided for all sulfur isotopologues of H_2S^+ and D_2S^+. In addition to this, high-level equilibrium geometries, vibrational frequencies, and spectroscopic constants for all combinations of S, H, and D have been reported. It is determined from these predictions that astronomical observation of H_2S^+ should be possible in the microwave and infrared regimes with multiple instruments.

CHAPTER 3

VIBRATIONAL ANALYSIS OF THE UBIQUITOUS INTERSTELLAR MOLECULE CYCLOPROPENYLIDENE (c-C_3H_2): THE IMPORTANCE OF NUMERICAL STABILITY

[1] Morgan, W. James. Accepted by *Molecular Physics*. Reprinted here with permission of publisher.

3.1 Abstract

Recent work on cyclopropenylidene, c-C_3H_2, sought to improve on past *ab initio* results with a complete basis set (CBS) quartic force field method capable of predicting fundamental bands to within 5 cm^{-1} accuracy of gas-phase spectroscopy experiments for semirigid molecules. It was suggested that a problematic coupling between n-body correlation and 1-particle basis set effects prevented a proper application of this method for the out-of-plane bending vibrations of c-C_3H_2. We establish here that the actual source of this anomalous behavior is numerical instability in the out-of-plane bending quartic force constants. It is found that the use of the normal equations to solve for the quartic force field, as well as a bending coordinate grid which is too compact, leads to errors of ca. 20 cm^{-1} in ν_5 and ν_9. Our revised analysis shows ν_5 and ν_9 to be 980 cm^{-1} and 777 cm^{-1}, respectively.

3.2 Introduction

Cyclopropenylidene, c-C_3H_2, was the first organic ring compound detected in space where its large dipole moment enabled the observation and assignment of its rotational spectrum[180]. It has been observed in most astrophysical environments, even in areas where harsh radiation would suggest the destruction of polyatomic molecules[181,182]. Most recently, it has been detected in multiple star-forming regions as well as the Helix Nebula (NGC 7293) where its role in the chemistry of high molecular weight polycyclic aromatic hydrocarbons (PAHs), such as C_{60}, remains an open topic[182,183]. Despite its prevalence in space, a high-resolution characterization of cyclopropenylidene's infrared (IR) spectrum has yet to be experimentally realized. Four fundamental vibrational bands remain unobserved in the laboratory and only a single fundamental (ν_3) has been observed in high-resolution gas-phase experiments. The determination of reliable, and accurate, IR results for c-C_3H_2 will enable a better understanding of PAH chemistry through detections with the next-generation of IR instruments

such as the James Webb Space Telescope (JWST) and the Wide Field IR Survey Telescope (WFIRST).

Quantum chemistry has provided insight into those bands which elude spectroscopic detection with predictions at various levels of theory[180,184]. Recent research[185,186] sought to improve on these past *ab initio* results by using a complete basis set (CBS) quartic force field (QFF) method capable of predicting fundamental bands to within 5 cm^{-1} accuracy of gas-phase spectroscopy experiments for semirigid molecules. However, an unphysical reduction of the out-of-plane bending fundamental vibrations, $\nu_5(a_2)$ and $\nu_9(b_2)$, relative to previous work was observed[185,186]. It was suggested that a problematic coupling between n-body correlation and 1-particle basis set effects prevented a proper application of this method. Fortenberry et al. focus on a situation where atom-centered s orbitals on the H_2 moiety bend out-of-plane to interact with π and π^* molecular orbitals (MOs) of c-C_3H_2. This interaction was suggested to lower the relative energy (c-C_3H_2 + H_2 relative to c-C_3H_4 along a similar pair of coordinate scans) of the out-of-plane bending potentials. This was attributed to the aforementioned reduction of the out-of-plane bending fundamentals.

While this past research[185,186] has provided a thorough consideration of electronic structure, it did not fully explore the possible numerical issues associated with the generation of a QFF. In the present research, the original quantum chemical results of Fortenberry et al. are re-analyzed with an emphasis on the linear least-squares problem solved to generate QFFs[185,186]. A wholly original set of QFFs is provided to supplement the original findings and these highlight the numerical consequences of displacement size and coordinate system. Lastly, a suggestion for the best theoretical prediction of cyclopropenylidene's fundamental frequencies is provided with a second-order vibrational perturbation theory (VPT2) analysis.

Figure 3.1: Simple Internal Coordinates of c-C_3H_2

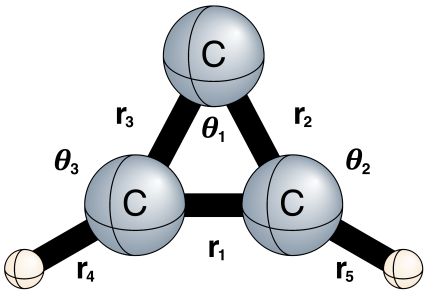

3.3 Computational Methods

All computations are performed using MOLPRO 2010 unless otherwise noted[87]. The correlation-consistent polarized-valence basis sets, (aug-)cc-pVXZ, are used in all computations except for core-correlation corrections, where the Martin-Taylor (MT) uncontracted basis set is employed[151,153,154]. An initial, near-equilibrium, geometry is optimized with the CCSD(T)/(aug-)cc-pV5Z method and corrected for core-correlation by adding the difference between geometries optimized using CCSD(T)/MT with and without core electrons correlated (referred to as MTc and MT, respectively).

$$r_{\mathrm{ne}} = r_{5\mathrm{Z}} + (r_{\mathrm{MTc}} - r_{\mathrm{MT}}) \tag{3.1}$$

The root-mean-square (RMS) of the computed forces are converged better than 1×10^{-8} a.u. for all three geometries which define this near-equilibrium structure (Equation 3.1). The near-equilibrium structure is then displaced up to four times, using standard displacement sizes, along each symmetry-adapted internal coordinate (Equation 2). All bond stretching coordinates, S_i (i = 1,2,3,6,7), rely on a displacement size of 0.005 Å whereas displacement sizes of 0.005 rad and 0.010 rad are tested for the bending coordinates, S_i (i=4,5,8,9).

Referring to Figure 1, the top most carbon is atom 1 where the remaining carbons moving clockwise from atom 1 are atoms 2 and 3, respectively. The hydrogen atom on the right, connected to atom 2, is atom 4 and the hydrogen on the left, connected to atom 3, is atom 5. We note here that the out-of-plane bending coordinates, $S_5(a_2)$ and $S_9(b_2)$, are defined by τ_1 and τ_2 which are more precisely characterized as the torsional angles τ_{4213} and τ_{5312}, respectively.

$$
\begin{aligned}
S_1(a_1) &= r_1 \\
S_2(a_1) &= (r_2 + r_3)/\sqrt{2} \\
S_3(a_1) &= (r_4 + r_5)/\sqrt{2} \\
S_4(a_1) &= (\theta_2 + \theta_3)/\sqrt{2} \\
S_5(a_2) &= (\tau_1 - \tau_2)/\sqrt{2} \\
S_6(b_1) &= (r_2 - r_3)/\sqrt{2} \\
S_7(b_1) &= (r_4 - r_5)/\sqrt{2} \\
S_8(b_1) &= (\theta_2 - \theta_3)/\sqrt{2} \\
S_9(b_2) &= (\tau_1 + \tau_2)/\sqrt{2}
\end{aligned}
\tag{3.2}
$$

A composite energy (CcCR) that is defined as the sum of the CBS-extrapolated CCSD(T) energy (C) as well as an additive correction for core-correlation (cC) and scalar-relativity (R) is determined at each displaced geometry. Scalar relativistic corrections are performed with Douglas–Kroll–Hess (DKH) corrections to second-order[156]. Results are presented as either CcCR or CcC where the latter omits the scalar relativistic correction. Equation 3.3 shows this summation, which is referred to as the CcCR energy in this research.

$$E_{\mathrm{CBS}} + (E_{\mathrm{MTc}} - E_{\mathrm{MT}}) + (E_{\mathrm{rel}} - E_{\mathrm{nonrel}}) \tag{3.3}$$

A three-point formula, shown in Equation 3.4, is used to extrapolate the CCSD(T) total energy to the CBS limit using the (aug-)cc-pVXZ (X=3,4,5) sequence of basis sets[50].

$$E(X) = E_{\mathrm{CBS}} + A(X + 1/2)^{-4} + B(X + 1/2)^{-6} \tag{3.4}$$

An initial set of CCSD(T)/CBS force constants is determined through a linear least-squares (LLS) fit of 1585 composite energies to a fourth-order Taylor-series polynomial V(S) with 235 unknowns using two methods described in Equation 3.4. Symmetry-adapted internal coordinate force constants are presented here as F_i where i is the coordinate(s) involved and the number of indices corresponds to the order of the constants. For example, F_{123} is the cubic force constant which describes the coupling between coordinates S_1, S_2, and S_3. An in-depth description of the use of such polynomials for QFFs is provided elsewhere[161,187]. This initial set of force constants has a non-zero gradient, g = $\{F_1, F_2, F_3, F_4\}$, due to the nature of r_{ne}. A Newton-Raphson optimization of the QFF is performed to minimize g and determine the minimum energy structure from the potential. In practice, this is done as $\mathrm{x}_{i+1} = \mathrm{x}_i + \mathrm{gH}^{-1}$ where g and H are the analytic first and second derivatives of V(S). The initial dataset is then biased by subtracting the optimized minimum displacement coordinates from each of the 1585 sets of displacement coordinates. This shift creates a new dataset which is used to refit the potential. The refit force constants are then transformed from symmetry-adapted internal coordinates to Cartesian coordinates using INTDER2005[?]. Fundamental vibrational frequencies are determined with the SPECTRO code, which performs VPT2 analysis[71]. We note here that the labeling of fundamentals differs from past theoretical work to reflect spectroscopic ordering. A first-order (Fermi) resonance was treated using standard effective Hamiltonian techniques[118,119,161] for $\nu_1(a_1) \approx 2\nu_2(a_1)$.

3.4 The Linear Least Squares solution of QFF

The linear least-squares (LLS) procedure seeks an n-by-1 vector f solution which minimizes $||Af - e||_2$ as indicated by its residual norm, $||r||_2$. The coefficient matrix, A, is an m-by-n matrix, the rows of which correspond to observed quantum chemical energies and whose columns correspond to the force constants of its potential energy function. In this research, each element of A is the product of symmetry internal displacement coordinates, a_{ij}, which when multiplied with the corresponding force constant, f_j, are summation elements of the familiar fourth-order Taylor series polynomial.

In this way, each row of A corresponds to the set of coefficients that when dotted with a set of unknown force constants leads to the observed energy at that displaced geometry, as shown below. In practice, the number of fit energies (m) greatly outnumber the number of sought force constants (n) which leads to an overdetermined system of equations. No general solution exists for such a system which is solved using a LLS fit in this research.

$$\begin{bmatrix} r_1 \\ r_2 \\ \vdots \\ r_m \end{bmatrix} = \begin{bmatrix} 1 & a_{11} & \dots & a_{1n} \\ 1 & a_{21} & \dots & a_{2n} \\ \vdots & \vdots & \vdots & \vdots \\ 1 & a_{m1} & \dots & a_{mn} \end{bmatrix} \cdot \begin{bmatrix} f_0 \\ f_1 \\ \vdots \\ f_n \end{bmatrix} - \begin{bmatrix} e_1 \\ e_2 \\ \vdots \\ e_m \end{bmatrix}$$

Two procedures are used which solve LLS problems: the normal equations and a truncated singular value decomposition (SVD). Solving the normal equations means solving the LLS problem for a square matrix with the same solution. Multiplying the rectangular A by its transpose A^T produces a non-singular matrix which can then be directly inverted.

$$A^T A f = A^T e \tag{3.5}$$

$$f = (A^T A)^{-1} A^T e = A^+ e \tag{3.6}$$

The solution in Equation 3.6 mimics an exactly soluble system through the Moore-Penrose inverse (pseudoinverse), A^+. Truncated SVD provides a more eloquent approach to the problem by decomposing A into two orthogonal matrices U and V^T, as well as a third diagonal one containing its singular values, Σ, as $A = U\Sigma V^T$. The properties of each matrix can be exploited to find A^+ without multiplying A by its transpose. Its full-rank solution is shown in Equation 3.7.

$$f = A^+ e = V\Sigma^{-1}U^T e \tag{3.7}$$

3.5 Results and Discussion

3.5.1 Diagnosing the Reduction Problem

The "reduction problem" of c-C_3H_2, simply stated, is a precipitous decrease (>20 cm^{-1}) observed in the CCSD(T)/CBS out-of-plane bending fundamental frequencies, $\nu_5(b_2)$ and $\nu_9(a_2)$, relative to CCSD(T)/XZ (X = T, Q) results[180,184–186,188]. The defining aspects of this problem are the same as a similar problem which has been present in the literature for some time. Specifically, the vibrational frequencies of bending coordinates which have inversion symmetry may exhibit unusually large decreases when using correlated wavefunctions with certain basis sets. Acetylene, ethylene, and benzene have all been shown to experience this problem for coordinates that bend multiply-bonded carbons out-of-plane[189–192].

Two key factors are at work which make the past and present problem categorically different. First, the reduction problem of the past seems to stem from an imbalance in the basis set which is most obvious when using very small (X=2) basis sets with correlated methods. However, this problem is partially or wholly eliminated with the inclusion of the relevant basis functions[191,193]. Such a line of reasoning is completely backwards in the present case as there is no qualitative difference in CCSD(T)/TZ and CCSD(T)/QZ quality predictions based on previous works[180,184]. The implication here is that extrapolation to the CCSD(T)/CBS limit should exhibit no such basis set imbalance. The second factor is that

only the anharmonic vibrational frequencies of c-C_3H_2 are affected by the reduction. In all past instances, it was the harmonic frequencies that first showed this issue which in turn would affect the prediction of fundamentals with VPT2. This is not the case here where a remarkable consistency, <2 cm^{-1}, is seen between the CCSD(T)/QZ quality and CcCR harmonic frequencies of the out-of-plane bends (Table 3.1). Such consistency suggests the reduction problem is not one of theory and basis set (i.e. electronic structure) but perhaps one of PES construction as only the anharmonic regions of the QFF seem affected.

Table 3.1: Harmonic Frequencies (cm^{-1}) and Total Energy Distribution

Mode	This Work[a]	Lee et al.[b]	Gong et al.[c]	TED(%)[a]		
$\omega_1(a_1)$	3290.7	3290.7	3288.6	S_3 (97.0)		
$\omega_2(a_1)$	1629.9	1629.9	1621.4	S_1 (79.0)	S_2 (17.7)	
$\omega_3(a_1)$	1312.8	1312.4	1305.1	S_2 (68.6)	$-S_4$ (18.5)	$-S_1$ (12.9)
$\omega_4(a_1)$	904.2	904.4	904.9	S_4 (81.1)	S_2 (13.1)	$-S_1$ (5.8)
$\omega_5(a_2)$	997.8	995.7	994.6	S_5 (100.0)		
$\omega_6(b_1)$	3255.9	3256.5	3249.5	S_7 (99.8)		
$\omega_7(b_1)$	1096.7	1093.1	1087.0	S_6 (81.5)	$-S_8$ (18.4)	
$\omega_8(b_1)$	914.3	911.4	902.1	S_8 (81.5)	S_6 (18.3)	
$\omega_9(b_2)$	787.8	789.4	786.2	S_9 (100.0)		

[a] CcCR results as defined in Equation 3.3.
[b] CCSD(T)/QZ+Δ_{core} results from Ref. 184.
[c] CCSD(T)/ANO2 results from Ref. 194.

3.5.2 Resolving the Reduction Problem

The generation of global PESs can be an exhaustive effort with trial and error but the near-equilibrium region that a QFF captures is generally well described by equidistant grids which rely on standard displacement sizes. The use of 0.005 for both stretches (Å) and bends (rad) has been shown to be an effective compromise between truncation and condition errors of the resulting QFF in past research[36,37,133,195]. However, the one-size-fits-all approach may become ineffective in cases where energy differences are very small. Table 3.2 provides an example of the finite-difference solution of F_{5555} which is the diagonal symmetry-adapted internal coordinate quartic force constant for the symmetric out-of-plane bend, $S_5(a_2)$. Note

that this work does not use finite-difference to solve for the force constants of c-C_3H_2 but the QFFs provided sample the single-points required to provide this illustrative example. The most important finding in this example is the limitation on significant figures once the sum Σ $cE(nh_b)$ is found; the final force constant will only have three significant digits at maximum. The variability of the last digit in each of the symmetry-related quantum chemical energies, $E(n) \stackrel{!}{=} E(-n)$, suggests only two of these digits are reliable. If the force constant is already small, as in the case of F_{5555}, then any loss of numerical precision in the result can render the constant meaningless.

Table 3.2: Finite Difference Calculation of F_{5555} with $h_b = 0.005$ rad

n	c	$E(nh_b)$	$cE(nh_b)$
4	1.0	−115.391 397 088 232	−115.391 397 088 232
2	−4.0	−115.391 401 559 836	461.565 606 239 344
0	6.0	−115.391 403 050 415	−692.348 418 302 490
−2	−4.0	−115.391 401 559 833	461.565 606 239 332
−4	1.0	−115.391 397 088 249	−115.391 397 088 249
		Σ $cE(nh_b)$	−0.000 000 000 295

$$F_{5555} = (2h_b)^{-4}[E(4h_b) - 4E(2h_b) + 6E(0) - 4E(-2h_b) + E(4h_b)]$$
$$= (1{\times}10^8 \text{rad}^{-4})(-2.95{\times}10^{-10}\ E_h)(4.35974394\ \text{aJ}/E_h) = -0.129\ \text{aJ/rad}^4$$

The importance of such a small force constant may be lost on the reader at first. Indeed, the very fact it is small indicates its contribution to the polynomial result will be negligible. However, Table 3.1 contains the harmonic total energy distribution (TED) which is a measure of how the symmetry-adapted internal coordinates correspond to the normal coordinates of the system. Here we can see that both $S_5(a_2)$ and $S_9(b_2)$ correspond one on one to their normal coordinate counterparts. Given this, and the fact each coordinate is the sole member of its irreducible representation, we can assume the one-dimensional (diagonal) potentials will be directly proportional to one another noting that the transformation from internal to normal coordinates is a non-linear transformation. The diagonal reduced normal coordinate quartic force constant (ϕ_{rrrr}) is the leading term of x_{rr} where the anharmonic correction is $\Delta\nu_r = 2x_{rr} + \frac{1}{2}\Sigma_{r\neq s}\ x_{rs}$ as discussed elsewhere[115,196]. The ramification of this detail is shown in Table 3.3 where small absolute changes in F_{5555} and F_{9999} correspond to large changes in

anharmonicity. A change as small as -0.1 aJ/rad^4 in either internal force constant results in an average change of ca. -20 cm^{-1} in the fundamentals.

Table 3.3: Sensitivity of Out-of-Plane Bending Quartic Force Constants (aJ/rad^4, cm^{-1}) and Anharmonic Frequencies (cm^{-1})

δ	F_{5555}	ϕ_{5555}	ν_5	$\Delta\nu_5$	δ	F_{9999}	ϕ_{9999}	ν_9	$\Delta\nu_9$
-0.8000	-0.0355	179.90	981.28	15.31	-0.8000	-0.0180	551.96	776.95	10.38
-0.6000	-0.0710	138.60	976.12	20.48	-0.6000	-0.0359	530.11	774.21	13.11
-0.4000	-0.1066	97.30	970.96	25.64	-0.4000	-0.0539	508.25	771.48	15.85
-0.2000	-0.1421	56.00	965.79	30.80	-0.2000	-0.0718	486.40	768.75	18.58
0.0000	-0.1776	14.70	960.63	35.96	0.0000	-0.0898	464.55	766.02	21.31
0.2000	-0.2131	-26.61	955.47	41.13	0.2000	-0.1077	442.70	763.29	24.04
0.4000	-0.2487	-67.91	950.31	46.29	0.4000	-0.1257	420.84	760.56	26.77
0.6000	-0.2842	-109.21	945.14	51.45	0.6000	-0.1436	398.99	757.83	29.50
0.8000	-0.3197	-150.51	939.98	56.62	0.8000	-0.1616	377.14	755.09	32.23

All force constants held constant except F_{5555} or F_{9999}.
δ is a constant used to proportionally scale F_{5555} or F_{9999}.
$F_{\text{new}} = F_{\text{ref}} + \delta F_{\text{ref}}$
$\Delta\nu = \nu - \omega$.

This subtlety is not revealed by the usual goodness-of-fit metrics, namely the residual sum-of-squares (RSS), because they evaluate the fit in the initial, internal, coordinate system and not the one required for VPT2[196]. The RSS is a measure of fit defined as $\Sigma_i^m(E_{i,\text{calc}} - E_{i,\text{obs}})^2$ where $E_{i,\text{calc}}$ is the energy predicted by the fit QFF, and $E_{i,\text{obs}}$ are the observed quantum chemical energies at each displaced geometry. Since F_{5555} and F_{9999} are small, they would have little to no effect on the quality of the RSS. The very good potential fit of the original QFF of Fortenberry et al., RSS = 2.0 $\times 10^{-17}$, is a testament to this and largely explains the earlier emphasis on electronic structure instead of the nuclear motion aspects of the reduction problem[185,186]. The main finding of this analysis is that the reduction problem of c-C_3H_2 is a consequence of numerical error in the quartic internal force constants of $S_5(a_2)$ and $S_9(b_2)$. This problem only manifests itself in the VPT2 results because a reduced normal coordinate Hamiltonian is employed[196,197].

Three possibilities for the loss of numerical significance are: 1) when the total energy exceeds double precision (>15 decimal digits), 2) numerical errors related to the algorithm

used to solve for the force constants, 3) too small of a displacement size. The first is not significant in the present case, due to the small total energy but the second is salient as the normal equations, which are known to effectively square the condition number of a matrix, were used to solve the LLS problem in past work on the system[185,186]. The SVD solution to the LLS problem avoids this increase in the condition number and as a result should exhibit less numerical error. The last point, too small of a displacement size, warrants testing as an increasing displacement size is known to reduce condition error as long as the size is small enough to still be considered a perturbation. As such, two new force fields are generated to supplement the original results of Fortenberry et al.[185,186] using a larger bending coordinate displacement size (h_b) of 0.010 rad. Only the bending coordinates were adjusted as these correspond to the frequencies which show significant change in prior research.

3.5.3 Discussion of Results

Table 3.4 contains the fundamental frequencies predicted using SVD and the normal equations for both CcCR and CcC composite theories. The aug-CBS columns use aug-cc-pVXZ (X=T,Q,5) and the CBS column uses cc-pVXZ (X=T,Q,5) for CBS extrapolation. Neither the core correlation nor scalar relativistic corrections use augmented basis sets in either set of data. The Δh_b column in Table 3.4 accounts for the use of a larger bending coordinate displacement (h_b). It is formally defined as the aug-CBS fundamentals predicted using h_b = 0.010 rad subtracted from the aug-CBS results using h_b = 0.005 rad. The final column of each table block in Table 3.4 contains the difference associated with the use of augmented basis sets for the CBS component of the composite energy. This Δaug column is found by subtracting the CBS (h_b = 0.010 rad) fundamentals from the aug-CBS (h_b = 0.010 rad) fundamentals.

The results in Table 3.4 indicate the following relationships: 1) An increased bending coordinate displacement size, h_b, is required for numerically stable results. This is clearly evident from the enormous values of Δh_b for $\nu_5(a_2)$ and $\nu_9(b_2)$ in every single block of Table

Table 3.4: Cyclopropenylidene (c-C_3H_2) Fundamental Frequencies (cm^{-1})

Singular Value Decomposition						Normal Equations					
CcCR	aug-CBS			CBS		CcCR	aug-CBS			CBS	
	($h_b = 0.005$)	($h_b = 0.010$)	Δh_b	($h_b = 0.010$)	Δaug		($h_b = 0.005$)	($h_b = 0.010$)	Δh_b	($h_b = 0.010$)	Δaug
$\nu_1(a_1)$	3152.0	3151.2	0.8	3153.1	−1.9	$\nu_1(a_1)$	3153.2	3150.9	2.3	3151.9	−1.0
$\nu_2(a_1)$	1599.8	1600.3	−0.5	1599.7	0.7	$\nu_2(a_1)$	1600.0	1599.1	0.9	1599.2	0.0
$\nu_3(a_1)$	1280.8	1280.0	0.8	1279.3	0.7	$\nu_3(a_1)$	1277.4	1279.5	−2.2	1278.5	1.0
$\nu_4(a_1)$	881.8	881.6	0.2	882.8	−1.2	$\nu_4(a_1)$	876.5	881.0	−4.4	881.9	−0.9
$\nu_5(a_2)$	960.6	979.3	−18.6	980.2	−0.9	$\nu_5(a_2)$	945.7	976.8	−31.2	976.3	0.6
$\nu_6(b_1)$	3120.6	3119.8	0.8	3120.2	−0.4	$\nu_6(b_1)$	3119.2	3118.9	0.4	3118.7	0.2
$\nu_7(b_1)$	1066.7	1066.0	0.7	1065.5	0.4	$\nu_7(b_1)$	1065.5	1065.5	0.0	1065.3	0.1
$\nu_8(b_1)$	896.1	891.7	4.4	892.0	−0.4	$\nu_8(b_1)$	891.3	890.7	0.6	890.9	−0.2
$\nu_9(b_2)$	766.0	776.2	−10.2	777.0	−0.8	$\nu_9(b_2)$	750.8	774.5	−23.7	773.8	0.7
CcC	aug-CBS			CBS		CcC	aug-CBS			CBS	
	($h_b = 0.005$)	($h_b = 0.010$)	Δh_b	($h_b = 0.010$)	Δaug		($h_b = 0.005$)	($h_b = 0.010$)	Δh_b	($h_b = 0.010$)	Δaug
$\nu_1(a_1)$	3152.5	3152.3	0.3	3153.7	−1.4	$\nu_1(a_1)$	3148.2	3150.0	−1.8	3153.6	−3.7
$\nu_2(a_1)$	1600.4	1600.5	−0.2	1599.9	0.6	$\nu_2(a_1)$	1598.1	1599.9	−1.9	1600.4	−0.5
$\nu_3(a_1)$	1281.4	1280.9	0.5	1280.4	0.5	$\nu_3(a_1)$	1277.2	1280.1	−2.9	1279.9	0.2
$\nu_4(a_1)$	881.8	881.7	0.2	882.3	−0.7	$\nu_4(a_1)$	875.1	880.9	−5.9	882.9	−2.0
$\nu_5(a_2)$	963.5	980.4	−16.9	979.0	1.4	$\nu_5(a_2)$	916.2	976.2	−60.0	979.3	−3.2
$\nu_6(b_1)$	3121.2	3121.0	0.2	3119.9	1.1	$\nu_6(b_1)$	3116.9	3119.2	−2.3	3120.3	−1.1
$\nu_7(b_1)$	1067.6	1066.6	1.0	1066.3	0.2	$\nu_7(b_1)$	1064.2	1066.0	−1.8	1066.3	−0.3
$\nu_8(b_1)$	897.0	892.5	4.5	892.3	0.2	$\nu_8(b_1)$	883.8	891.0	−7.2	892.3	−1.3
$\nu_9(b_2)$	769.3	778.3	−8.9	775.9	2.4	$\nu_9(b_2)$	720.7	774.0	−53.3	777.4	−3.4

h_b is the displacement size (rad) used for the bending coordinates, S_i (i=4,5,8,9).
All stretching coordinates, S_i (i=1,2,3,6,7), use a displacement size of 0.005 Å.
Δh_b is defined as aug-CBS ($h_b = 0.005$) − aug-CBS ($h_b = 0.010$).
Δaug is defined as aug-CBS ($h_b = 0.010$) − CBS ($h_b = 0.010$).

3.4. 2) Augmented basis functions for the CBS energy minimally alter the results, ca. 2 cm^{-1}, when using SVD. 3) The scalar relativistic correction (R) has a little to no effect on the data where a shift of ca. 1 cm^{-1} is observed at most when using SVD. 4) Using SVD instead of the normal equations to solve the LLS problem mitigates the numerical error for the out-of-plane bending modes relying on $h_b = 0.005$ rad. However, it does not resolve the reduction problem alone as an increase in h_b seems to further stabilize the results. The difference of ca. 4 cm^{-1} observed between the SVD and normal equation CcCR out-of-plane predictions for $h_b = 0.010$ rad, as well as the broader range of disagreement for $h_b = 0.005$ rad, suggests the use of SVD is important for high-level applications such as this work as the error relative to gas-phase experiments is expected to be less than these differences[36].

Table 3.5 contains past and present results for the infrared spectrum of c-C_3H_2. Here we see that the fundamental frequencies of Lee et al. are as consistent with the CcCR results as their harmonic counterparts, suggesting that the system is exceptionally well-described by the CCSD(T)/QZ method when a core-correction, $\Delta_{\text{core}} = (E_{\text{MTc}} - E_{\text{MT}})$, is made to the harmonic force field[184]. The CCSD(T)/ANO2 adaptive vibrational configuration interaction (AVCI) results of Gong et al. appear to be too low for most stretches, compared to the CcCR results, but good agreement is seen in the bends with the exception of $\nu_8(b_1)$. Table 3.1 shows a similar difference between the harmonic frequencies of Lee et al.[184] and Gong et al.[194] for the stretches, suggesting basis set effects are likely the source of the disagreement. The CcCR results appear to provide quality similar to matrix isolation only varying from Huang et al.[198] and McMahon et al.[199] by a few wavenumbers with the exception of $\nu_9(b_2)$. A ca. 4 cm^{-1} difference for the band origin of $\nu_9(b_2)$ is present between the two argon matrix experiments, which have similar temperatures, where we can only speculate on a matrix shift. The consistent agreement in theoretical predictions for $\nu_9(b_2)$ is re-assuring but ultimately a gas-phase observation will be required to pinpoint its origin.

Table 3.5: Summary of Infrared Results for c-C_3H_2 (cm^{-1})

	Theory		
Mode	This Work[a]	Lee et al.[b]	Gong et al.[c]
$\nu_1(a_1)$	3142.7*	3145.0*	3138.3
$\nu_2(a_1)$	1599.7	1600.2	1591.5
$\nu_3(a_1)$	1279.3	1279.4	1271.7
$\nu_4(a_1)$	882.8	882.2	883.5
$\nu_5(a_2)$	980.2	976.3	976.8
$\nu_6(b_1)$	3120.2	3123.5	3116.2
$\nu_7(b_1)$	1065.5	1063.0	1055.8
$\nu_8(b_1)$	892.0	889.2	914.3
$\nu_9(b_2)$	777.0	776.0	776.4
	Experiment		
Mode	Huang et al.[d]	McMahon et al.[e]	Hirahara et al.[f]
$\nu_1(a_1)$	-	-	-
$\nu_2(a_1)$	-	-	-
$\nu_3(a_1)$	1278.8	1278	1277.371 132(95)
$\nu_4(a_1)$	886.4	883	-
$\nu_5(a_2)$	-	-	-
$\nu_6(b_1)$	-	-	-
$\nu_7(b_1)$	1061.5	-	-
$\nu_8(b_1)$	-	895	-
$\nu_9(b_2)$	787.4	783	-

[a] CcCR results as defined in Equation 3.3. VPT2.
[b] CCSD(T)/QZ+Δ_{core} results from Ref. 184. VPT2.
[c] CCSD(T)/ANO2 results from Ref. 194. AVCI(3)+VMP2.
[d] Argon matrix (10K) results from Ref. 198.
[e] Argon matrix (8K) results from Ref. 199.
[f] Gas-phase result from Ref. 200.
* Treated for $\nu_1(a_1) \approx 2\nu_2(a_1)$. Eigenvalue is 81%/19% ($\nu_1/2\nu_2$).

3.6 Conclusions

In this work, we have established the misdiagnosis of the CcCR (a composite theory including CBS-extrapolation, core correlation, and scalar relativistic corrections) infrared spectrum of cyclopropenylidene. Previous studies on c-C_3H_2 using CcCR observed a large decrease in the out-of-plane bending modes, $\nu_5(a_2)$ and $\nu_9(b_2)$, relative to past theoretical results which was suggested to originate from a problematic coupling between the basis set and correlation methods. We find here that numerical instability of the symmetry-adapted internal coordinate quartic force constants for these two coordinates is the true source of the reduction.

Three details are critical: 1) the quartic force constants are very small in symmetry-adapted coordinates making them extremely susceptible to numerical errors, 2) the symmetry-adapted coordinates correspond directly to the normal coordinates for both modes, which introduces this error into the VPT2 results, and 3) too small of a displacement size was used to generate the force field along these internal coordinates, exacerbating the error. Our analysis shows that using a larger displacement size for the bending coordinates and solving the LLS problem with SVD instead of the normal equations are equally important in resolving the reduction problem and, more importantly, achieving the highest accuracy *ab initio* results. It is also found that the residual sum-of-squares (RSS) is not a suitable metric to evaluate the reliability of the VPT2 results in unique cases such as this one as a very small RSS indicates accuracy in the fit coordinate system but not necessarily the transformed one used in VPT2.

CHAPTER 4

THE BARRIER TO PLANARITY OF METHIDE AND ITS ANHARMONIC FORCE FIELD

[1] Morgan, W. James. To be submitted to the *Journal of Chemical Physics*.

4.1 Abstract

We report a six-dimensional quartic force field for methide, CH_3^-, which is complete basis set (CBS) extrapolated, corrected for core-correlation, includes scalar relativistic effects, and considers high-level electron correlation. Triple augmentation of basis sets up to cc-pV5Z are used in the CBS-extrapolation where electron correlation up to non-iterative quadruple excitations in coupled cluster theory [CCSDT(Q)] is applied. Relative to the variationally predicted result of $\nu_2^+ = 475.2\ \mathrm{cm}^{-1}$ determined in this work, it is found that previous *ab initio* predictions for the symmetric inversion fundamental are either qualtiatively too high due to a lack of augmentation or too low due to issues related to scaling. Recent photoelectron experiments are discussed in context of this new finding where some ambiguity exists in the experimental determination of this fundamental. The ground state inversion splitting is found to be $\Delta_{\mathrm{inv}} = 18.0\ \mathrm{cm}^{-1}$ in good agreement with previous studies. High-accuracy *ab initio* predictions are provided for the other fundamental modes of methide as well as its fully deuterated isotopologue, CD_3^-. A new estimate for the transition barrier is provided as $E_{\mathrm{TS}} = 388.7\ \mathrm{cm}^{-1}$ which includes harmonic zero-point vibrational energy contributions and diagonal Born-Oppenheimer corrections. A brief discussion of isoelectronic species is also provided which highlights differences between methide, ammonia, and hydronium.

4.2 Introduction

All rovibrational wavefunctions in a polyatomic system with equivalent minima are linear combinations of localized wavefunctions which are defined about each minimum energy structure. A coordinate must exist on this potential energy surface (PES) which predominantly describes the hindered motion that moves one minimum energy structure to the next. Transition state barriers exist along this nonrigid coordinate for each minimum beyond the first and the geometry at these maxima exhibit higher symmetry than the wells they connect.

Thus, the coordinate spans a delocalized vibrational domain containing two or more localized ones which possess the point group symmetry of the equilibrium configuration of the molecule. A direct consequence of this large amplitude motion, relative to the small amplitude vibrations which are well defined in the localized domains, is the splitting of energy levels. All rovibrational wavefunctions exist within this delocalized region, even the ground vibrational state corresponding to no vibrational quanta, and as a result all rovibrational energy levels split. However, if the magnitude of the splitting is not large enough to be detected spectroscopically then the split energy levels are considered degenerate and the equilibrium point group symmetry is used to define them[201].

Quantum mechanical tunneling is directly responsible for this type of energy splitting in small amplitude vibrations as well as nonrigid rovibrational states with energies below the barrier(s). Several factors contribute to the magnitude of these splittings but the most impactful is the height (relative energy) of the transition state barrier(s)[202]. Ammonia, NH_3, is a textbook example of this phenomenon due to the low barrier of inversion (1764 cm^{-1}) separating two equivalent C_{3v} minima[203,204]. A two-state system for the ground state emerges from the symmetric and anti-symmetric combinations of localized wavefunctions corresponding to the "up" or "down" equilibrium positions of the "umbrella" (inversion) coordinate. The energy difference between these states, known as the ground state inversion splitting (Δ_{inv}), emits in the microwave region and was central to the development of the first maser; the progenitor of the laser[205]. Ammonia has been studied countless times in a plethora of temperature regimes where both theory and experiment contribute to the broader understanding of its rovibrational transitions[203,204]. Unfortunately, there are few systems which have inversion properties similar to ammonia which are also easily studied in the laboratory. For example, the isovalent phosphine (PH_3) is predicted to have a barrier much larger than ammonia at ca. 11-12 000 cm^{-1}. Recent *ab initio* work has suggested that only the overtones of phosphine's inversion mode may have a detectable splitting, $\geq 1 \times 10^{-5}$ cm^{-1}, but sub-Doppler resolution spectroscopy with resolution half of this limit found no

evidence of such a splitting for the second overtone[206,207].

Isoelectronic systems to ammonia, on the other hand, are predicted to have inversion barriers even smaller than ammonia itself[208,209]. Hydronium, H_3O^+, and methide, CH_3^-, both appear to have pyramidal structures with more shallow inversion angles than either ammonia or phosphine, which produces a shorter and wider pyramid. Consequently, the central atom atop these pyramids must travel a shorter distance to tunnel, which is aided by their light mass relative to phophorous, and should experience faster tunneling rates. This is evident from the much larger ground state inversion splitting of 55.3462(55) cm^{-1} observed in the inversion spectrum of hydronium[210] where its inversion barrier is suggested[209] to be below 650 cm^{-1}. However, methide is substantially harder to isolate due its high reactivity and the features of its spectra are much less sharp due the inherent limitations of studying anions[211,212]. Despite these challenges, a recent photoelectron spectroscopy experiment[212] has reported the Δ_{inv} of methide to be 21(5) cm^{-1} and *ab initio* results in the same article estimate a barrier of 383 cm^{-1}.

The present work seeks to confirm previous *ab initio* results for the equilibrium and transition state (planar) properties of methide as well as provide additional context for the discussion of possible electron autodetachment. Methide exhibits extreme basis set dependence for geometries and vibrational frequencies, especially when moving along the inversion coordinate, which requires at least doubly augmented basis functions for effective convergence[213]. The addition of these basis functions to each atom quickly increases the computational cost and can lead to issues of linear dependence[213]. As such, many past theoretical works have been limited in either the cardinality of the basis (total number of basis functions) or its augmentation (the number of diffuse basis functions)[208,212]. This has resulted in the absence of a PES in the literature which is constructed using highly augmented but, also, very large basis sets which can be used to variationally predict the split vibrational energy levels. Such predictions are provided here using a six-dimensional (6D) quartic force field (QFF) constructed from complete-basis set (CBS) extrapolated coupled

cluster singles, doubles, and non-iterative triples [CCSD(T)] energies which are also corrected for core-correlation, scalar relativity, and electron correlation up to quadruple excitations in coupled cluster theory. A prediction for the barrier height is provided from a planar methide structure optimized using the same high level of theory. Lastly, a brief comparison of ammonia, hydronium, and methide is provided in the context of their geometric parameters and barrier heights.

4.3 Theoretical Methods

Restricted Hartree-Fock (RHF) wavefunctions are used to describe methide (CH_3^-) at its C_{3v} ground state and D_{3h} transition state. Both unrestricted Hartree-Fock (UHF) and resctricted open-shell Hartree-Fock (ROHF) wavefunctions are employed when evaluating methyl radical ($^{\bullet}CH_3$) energies at relevant D_{3h} anion geometries. Coupled cluster singles, doubles, and non-iterative triples, CCSD(T), as well as singles, doubles, triples, and non-iterative quadruples, CCSDT(Q), are used to describe electron correlation[23,150]. Truncated forms of the triply-augmented correlation-consistent polarized-valence t-aug-cc-pVXZ (X = T, Q, 5) basis sets are used where the s, p, and d diffuse functions of d-aug and t-aug are present on carbon but only those of d-aug are present on hydrogen[41,42]. A discussion of diagnostic computations related to this choice is presented in Section 4.4.1.

Table 4.1: Basis Set Truncation

	aug-cc-pv$X$Z	d-aug	t-aug
C	$spdf/g/h$	spd	spd
H	$spd/f/g$	spd	-

Slashes indicate X = T/Q/5.

No diffuse functions beyond d are included on any atoms except for those present in the aug-cc-pVXZ (X = T, Q, 5), or aXZ, basis set. For simplicity, these truncated basis sets will still be referred to as t-aug-cc-pVXZ and abbreviated ta$X$Z where their specific truncations are shown in Table 4.1. Cases where the original implementation of the augmented basis sets

are employed are specifically mentioned where relevant. Even-tempered extrapolations are used to generate augmented basis functions to and beyond triple augmentation as needed.

The near-equilibrium geometry is defined here as a CCSD(T)/ta5Z structure corrected with the geometric differences between an all-electron CCSD(T) structure using the Martin-Taylor (MT) basis set, CCSD(T)/MTc, and one within the frozen-core approximation, CCSD(T)/MT[153,154].

$$\mathbf{x}_{\mathrm{ne}} = \mathbf{x}_{\mathrm{ta5Z}} + (\mathbf{x}_{\mathrm{MTc}} - \mathbf{x}_{\mathrm{MT}}) \tag{4.1}$$

The MT basis has been augmented with the same diffuse s, p, d functions present in the truncated taTZ basis for all computations.

An initial estimate for the ground state equilibrium geometry is found by first optimizing a near-equilibrium geometry ($\mathbf{x}_{\mathrm{ne}}$). A fourth-order Taylor series representation of methide's potential energy surface (PES), known as a quartic force field (QFF), is produced from a linear least-squares fitting of energies computed at geometries displaced from $\mathbf{x}_{\mathrm{ne}}$. A four-dimensional grid of geometries is generated by displacing the four symmetry-adapted internal coordinates, $S_1 - S_4$, up to fourth-order using displacement sizes of 0.005 Å and 0.005 radians for bond stretch and angle bending coordinates, respectively. Only the S_{3a} and S_{4a} components of the degenerate (e) coordinates are displaced in this work. Each C−H bond is represented by R_i whereas H−C−H bond angles are represented as θ_i.

$$\begin{aligned}
S_1(a_1) &= (R_1 + R_2 + R_3)/\sqrt{3} \\
S_2(a_1) &= (\theta_1 + \theta_2 + \theta_3)/\sqrt{3} \\
S_{3a}(e) &= (2R_1 - R_2 - R_3)/\sqrt{6} \\
S_{4a}(e) &= (2\theta_1 - \theta_2 - \theta_3)/\sqrt{6} \\
S_{3b}(e) &= (R_2 - R_3)/\sqrt{2} \\
S_{4b}(e) &= (\theta_2 - \theta_3)/\sqrt{2}
\end{aligned} \tag{4.2}$$

Energies are then computed at each point using a highly-corrected composite level of theory abbreviated as CcCRE: an energy that is complete basis set extrapolated (C), corrected for core-correlation (cC), includes scalar relativistic effects (R), and considers high-level electron correlation (E)[36,37,155].

$$E_{\mathrm{CcCRE}} = E^{(\mathrm{T})}_{\mathrm{CBS}} + (E^{(\mathrm{T})}_{\mathrm{MTc}} - E^{(\mathrm{T})}_{\mathrm{MT}}) + (E^{(\mathrm{T})}_{\mathrm{rel}} - E^{(\mathrm{T})}_{\mathrm{nonrel}}) + (E^{(\mathrm{Q})}_{\mathrm{aTZ}} - E^{(\mathrm{T})}_{\mathrm{aTZ}}) \tag{4.3}$$

$$E_{\mathrm{CcCRE}} = E_{\mathrm{CBS}} + \Delta E_{\mathrm{core}} + \Delta E_{\mathrm{rel}} + \Delta E_{\mathrm{hlc}} \tag{4.4}$$

The leading term of Equation 4.3 is defined by the total energy three-point extrapolation of Martin and Lee shown in Equation 4.5 using the taTZ, taQZ, and ta5Z basis sets[50].

$$E(X) = A + B(X + 1/2)^{-4} + C(X + 1/2)^{-6} \tag{4.5}$$

Scalar relativistic computations rely on all-electron CCSD(T) using an aug-cc-pCVTZ-DK basis set that is augmented in the same way as the MT basis set. The energy denoted as $E^{(\mathrm{T})}_{\mathrm{rel}}$ in Equation 4.3 relies on the second-order Douglas-Kroll-Hess (DKH) method whereas $E^{(\mathrm{T})}_{\mathrm{nonrel}}$ does not implement these DKH corrections but is computed at the same level of theory. The final correction, shown in Equation 4.4 as ΔE_{hlc} for high-level electron correlation, is taken as the difference between CCSDT(Q)/aTZ and CCSD(T)/aTZ; these basis sets are the default implementation of aug-cc-pVTZ. Note that the high-level correction accounts for iterative triples and noniterative quadruples as $\Delta E_{\mathrm{hlc}} = (E^{(\mathrm{Q})}_{\mathrm{aTZ}} - E^{\mathrm{T}}_{\mathrm{aTZ}}) + (E^{\mathrm{T}}_{\mathrm{aTZ}} - E^{(\mathrm{T})}_{\mathrm{aTZ}})$.

An initial QFF is linear least-squares fit from 241 composite energy points to find 52 force constants. A Newton-Raphson optimization of this initial QFF is performed to minimize the gradient and determine the minimum energy structure[214]. After optimization, no individual gradient element is larger than 9.2×10^{-8} aJ/Å^{n}rad^m and the RMS is 4.6×10^{-8} aJ/Å^{n}rad^m where $n + m = 1$. The potential is then refit to this new minimum where the CcCRE QFF's residual sum of squares (RSS) is 4.1×10^{-18} E_h. The full 6D representation of the

QFF is then produced from equivalence relationships of force constants detailed in previous works[215–217] taking advantage of the degeneracy of the e irreducible representation of the C_{3v} point group. Three quartic force constants ($F_{4b4b3a3a}$, $F_{3b3b4a4a}$, and $F_{4b3b4a3a}$) are determined by finite difference where $F_{4b4b3a3a}$ and $F_{3b3b4a4a}$ are averaged and set equal. Less corrected composite models such as CcCR, CcC, and C are fit and refit in the same manner as above by simply omitting the corresponding correction(s) to CBS energy, E_{CBS}, shown in Equation 4.4. All QFFs show a RSS better than or equal to that of the CcCRE QFF.

Figure 4.1: Methide's Geometric Parameters

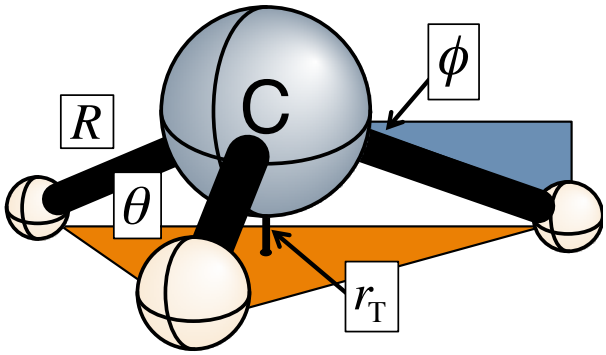

The D_{3h} planar transition state geometry of methide is optimized with a force RMS threshold of 1.0×10^{-7} E_h/a_0 using five-point numerical gradients defined with the CcC, CcCR, and CcCRE composite energies as described in a previous work[161]. A second-order expansion of the PES about each planar structure using the symmetry-adapted coordinates of BH_3, detailed elsewhere[35], is generated with the same procedure as the ground state. An estimation of the classical transition state barrier height is provided as the difference between the composite (CcCRE, CcCR, or CcC) electronic energies of the equilibrium C_{3v} and D_{3h} structures, ΔE_{e}, corrected with the difference in zero-point vibrational energies, Δ_{ZPVE}, and diagonal Born-Oppenheimer corrections (DBOC), Δ_{DBOC}. The harmonic zero-point vibrational energy (ωZPVE) is used for each structure where the imaginary frequency of the

transition state is excluded. The DBOC values used here are taken from the Supporting Information of Ref. 212 and computed in CFOUR 2.0[58] with SCF/d-aug-cc-pVTZ corrected using CCSD/aug-cc-pVTZ. The final form of the predicted classical transition state barrier height, E_{TS}, is shown in Equation 4.6 where each difference is taken with the energy of the D_{3h} structure minus that of the C_{3v} structure.

$$E_{\mathrm{TS}} = \Delta E_{\mathrm{e}} + \Delta_{\mathrm{ZPVE}} + \Delta_{\mathrm{DBOC}} \tag{4.6}$$

INTDER 2005 is used to transform geometries, displacements, and force constants between symmetry-adapted internal and Cartesian coordinates[72]. SPECTRO is used to provide spectroscopic constants through second-order vibrational perturbation theory (VPT2) analyses and treat Fermi resonances where applicable[71]. Variational predictions of vibrational energy levels are provided using VTET[157] after transformation of the quartic force field into Morse-Cosine coordinates[70,133]. All single-point energies and amplitudes are converged to 1.0×10^{-12} E_h. One- and two-electron integrals are retained if greater than 1.0×10^{-20}. Non-composite geometries, such as those used to determine the near-equilibrium geometry or those of isoelectronic species, are optimized with a force RMS threshold of 1.0×10^{9} E_h/a_0 in Molpro using five-point gradients. The ΔE_{hlc} for closed-shell species are computed using CCSD(T)/aTZ and CCSDT(Q)/aTZ which rely on the ECC and NCC modules of CFOUR 2.0, respectively[24,58]. All other closed-shell computations are performed with Molpro 2010.1.67[218]. The ΔE_{hlc} for open-shell species are computed with MRCC2018[159] for both unrestricted Hartree-Fock (UHF) and restricted open-shell Hartree-Fock (ROHF) references. The remaining open-shell computations rely on UCCSD(T) and RCCSD(T) as implemented in Molpro[218]. Multi-configurational self-consistent field (MCSCF) and multi-reference configuration interaction with Davidson corrections (MRCI+Q) computations are performed in Molpro using a full valence active space[218]. Natural bond orbital (NBO) analysis was performed with NBO 6.0 and interfaced with PSI4[55,219].

4.4 Results and Discussion

4.4.1 Basis Set Augmentation

Diagnostic computations to determine the required diffuse functions for CH_3^- are performed with the augmented correlation-consistent polarized-valence triple zeta basis sets, aug-cc-pVTZ (aTZ). The augmentation level of a cc-pVXZ basis set corresponds to the number of diffuse function sets which are added to the basis set. Each set contains a single uncontracted diffuse function for each angular momentum present in the basis set. The number of functions in each set vary by atom.

Table 4.2: Effects of Basis Set Augmentation on CH_3^-

Type	C	H	R	θ	$\omega_1(a_1)$	$\omega_2(a_1)$	$\omega_3(e)$	$\omega_4(e)$
All	+7	+0	1.1005	110.639	2923.3	649.1	3031.0	1417.7
All	+7	+1	1.1006	110.642	2923.2	649.4	3031.0	1417.6
All	+7	+2	1.1006	110.645	2923.3	649.3	3031.0	1417.6
spd	+7	+0	1.1005	110.639	2923.3	649.1	3031.0	1417.7
spd	+7	+1	1.1006	110.596	2923.2	652.5	3030.3	1417.7
spd	+7	+2	1.1006	110.591	2923.1	652.6	3030.3	1417.6
All	+2	+0	1.1005	110.639	2923.3	649.2	3031.0	1417.8
All	+2	+1	1.1006	110.640	2923.2	649.5	3030.9	1417.7
All	+2	+2	1.1006	110.646	2923.3	649.1	3030.9	1417.6
spd	+2	+0	1.1007	110.536	2922.4	655.0	3029.3	1417.9
spd	+2	+1	1.1006	110.596	2923.2	652.4	3030.4	1417.7
spd	+2	+2	1.1006	110.593	2923.1	652.5	3030.3	1417.6

Values under C and H refer to the augmentation level of aTZ.
+0 is the default aTZ basis on that atom whereas +2 is t-aug-cc-pVTZ.
All or *spd* refers to which angular momenta functions are added to aTZ.
Only extrapolated s, p, and d functions are added to aTZ for *spd* rows.

Table 4.2 contains the geometries and harmonic frequencies of CH_3^- using various augmented basis sets, some of which have been truncated to only add diffuse functions of s, p, or d angular momentum. It is shown that adding up to seven additional augmentation levels to aug-cc-pVTZ (i.e. 8-aug-cc-pVTZ) has a negligible effect on the geometries or harmonic frequencies of CH_3^- compared to t-aug-cc-pVTZ. Augmenting the hydrogen atoms past aug-

cc-pVTZ has a small effect on the geometry that does not appreciably manifest itself in the frequencies for basis sets which include all angular momenta functions. This is not the case for the truncated augmented basis sets (*spd*) which tend to require d-aug-cc-pVTZ on the hydrogens to provide consistent results. An approximately 0.05 degree difference is seen in the H−C−H bond angles between the truncated (*spd*) and full (All) augmented basis sets which incurs a 3 cm^{-1} penalty in the inversion frequency, $\omega_2(a_1)$, at this level of theory but the remaining vibrations are unaffected by this geometric change.

Table 4.3: A Comparison of CcCRE Methide Harmonic Frequencies (cm^{-1})

	spd/*spd*	*spdf*/*spd*	*spdfg*/*spdf*
$\omega_1(a_1)$	2938.7	2938.8	2938.6
$\omega_2(a_1)$	651.8	651.6	652.5
$\omega_3(e)$	3048.3	3048.6	3048.2
$\omega_4(e)$	1417.4	1417.4	1418.0

CcCRE composite energy shown in Equation 4.4
Column headers are the extrapolated functions on C/H.
Table 4.1 shows the truncation of *spd*/*spd*.

The choice of limiting the number and type of diffuse functions through truncation is a necessary one because the QFFs solved in this work are limited by the numerical significance of the single-point energies. It was determined that the full t-aug-cc-pVXZ (X = T, Q, 5) basis sets are unusable due to limited convergence ($<1\times10^{-12}$ E_h) but could be used to validate the harmonic portion of the potential because only low-order derivatives are required. Table 4.3 shows the effect of extrapolating higher angular momenta functions beyond *spd* when augmenting the aTZ basis set is negligible.

4.4.2 Methide Ground State

4.4.2.1 Geometries and Harmonic Frequencies

The geometric parameters of CH_3^- are shown in Figure 4.1. The equilibrium and zero-point structures of CH_3^- as well as the associated rotational constants and vibrational frequencies are reported in Table 4.4. All three of the equilibrium structures reported in this work rely on

composite energies that include at least CBS-extrapolation and core-correlation corrections. The least corrected of the three, the CcC structure, displays a slightly shorter C−H bond length, R_e, and wider H−C−H bond angle, θ_e, than the best estimate of Dixon et al. which is directly extrapolated from optimized CCSD(T)/cc-pVXZ (X = D, T, Q) geometries. This behavior is inline with a better description of the valence space with increasing basis size completeness as well as the inclusion of core-correlation[161]. Inclusion of scalar-relativistic effects in the CcCR geometry contracts both R_e and θ_e where the inversion angle, ϕ_e, defined as the angle of the equivalent hydrogen atoms to a plane containing the central carbon atom, absorbs this change by increasing slightly relative to the CcC structure. As anticipated with the consideration of high-level electron correlation, which includes iterative triple and non-iterative quadruple excitations, the CcCRE geometry exhibits longer bond lengths but the inversion angle flattens as the H−C−H bond angles expand. All three of the vibrationally-averaged structures (R_0, θ_0) show increases of ca. 0.013 Å in the bond lengths whereas the bond angles expand in a decreasing fashion as more corrections are applied, 0.033, 0.023, and 0.017°, compared to their equilibrium counterparts. The differences between CcCRE, CcCR, and CcC structures are small suggesting the geometry is well-converged.

The harmonic vibrational frequencies decrease with further corrections except for the inversion mode, $\omega_2(a_1)$, of CcCR which has the largest inversion angle of the three composite energy structures. Scalar relativity has a negligible effect on harmonic frequencies as the difference between CcCR and CcC is under a wavenumber in all cases. However, inclusion of the ΔE_{hlc} correction (see Equation 4.3) in CcCRE shifts the CcCR results by 1.6 cm^{-1} in the degenerate bend, $\omega_4(e)$, ca. 3 cm^{-1} in the C−H stretches, $\omega_1(a_1)$ and $\omega_3(e)$, and 4.2 cm^{-1} in the inversion mode. These results are substantially higher than the CCSD(T)/aTZ harmonic frequencies of Dixon et al. as seen in Table. 4.4. The CCSD(T)/aTZ results of Dixon et al. appear to lack sufficient diffuse functions to properly describe most vibrations of this system[208]. There is over a 50 cm^{-1} difference, on average, between our reported C−H stretches and the previous CCSD(T)/aTZ predictions; a difference that grows to 132 cm^{-1}

Table 4.4: Methide Structures (Å ,°), Rotational Constants (cm^{-1}), and VPT2 Vibrational Frequencies (cm^{-1})

	CcC	CcCR	CcCRE	Previous[a,b]
R_e	1.096 25	1.096 22	1.096 39	1.101
θ_e	110.675	110.650	110.701	109.4
ϕ_e	18.239	18.265	18.211	-
$A_e = B_e$	8.765 96	8.765 08	8.765 16	-
C_e	5.143 32	5.145 15	5.140 40	-
$\omega_1(a_1)$	2942.6	2941.7	2938.7	2890.6
$\omega_2(a_1)$	655.3	656.0	651.8	783.8
$\omega_3(e)$	3052.4	3051.6	3048.3	2980.9
$\omega_4(e)$	1418.7	1419.0	1417.4	1420.8
R_0	1.109 03	1.109 03	1.109 24	-
θ_0	110.708	110.673	110.718	-
$A_0 = B_0$	8.683 81	8.681 99	8.680 92	-
C_0	5.048 30	5.050 38	5.045 74	-
$\nu_1(a_1)*$	2827.9	2828.5	2822.7	2787.8
$\nu_2(a_1)$	577.9	579.2	574.5	600.8
$\nu_3(e)$	2877.1	2875.1	2871.0	2850.7
$\nu_4(e)$	1387.0	1387.7	1384.9	1380.3

* treated for the $2\nu_4 \approx \nu_1$ Fermi interaction.
* perturbed values of $\nu_1(a_1)$ = 2808.3, 2808.8, 2803.7 cm^{-1}.
[a] CBS limit geometry and CCSD(T)/aTZ harmonics from Ref. 208.
[b] CCSD(T)/daTZ VPT2 fundamentals from Ref. 212.

in the inversion mode. The degenerate bending mode, on the other hand, is near-equivalent between the present and previous work despite the present work using a much higher level of theory.

4.4.2.2 Anharmonic Frequencies

The double-well nature of the methide PES, which is due to equivalent minima resulting from opposite equilibrium positions of the inversion mode, renders VPT2 fundamental frequencies only so useful because the split symmetric (ν^+) and anti-symmetric (ν^-) vibrational energy levels are not accounted for in a standard VPT2 analysis. This utility is further complicated by Fermi interactions which appears to affect the symmetric C−H stretch through $2\nu_4(a_1 \oplus a_2 \oplus e) \approx \nu_1(a_1)$, an issue experienced previously in studies on the isoelectronic ammonia[215]. Regardless, the fundamentals should be a good measure of anharmonicity and the

analysis offers other quantities such as the vibrationally averaged structures in Table 4.4 and the anharmonicity constants found in Table 4.5. The inversion fundamental shows strong

Table 4.5: Anharmonicity Constants of CH_3^-

	CcC	CcCR	CcCRE
x_{11}	-29.678	-29.758	-30.034
x_{12}	46.236	46.676	46.984
x_{13}	-107.715	-107.896	-108.68
x_{14}^*	-15.511	-15.33	-15.54
x_{22}	-76.828	-76.688	-77.425
x_{23}	59.173	59.272	60.117
x_{24}	-6.014	-6.05	-6.088
x_{33}	-52.599	-52.672	-53.115
x_{34}	-7.879	-8.722	-8.366
x_{44}^*	-4.07	-3.615	-4.207
g_{33}	14.603	14.603	14.673
g_{34}	-2.505	-2.539	-2.518
g_{44}^*	-0.805	-0.967	-0.767
x_{14}	-15.511	-15.33	-15.54
x_{44}	-4.07	-3.615	-4.207
g_{44}	-0.805	-0.967	-0.767

Values with asterisks are deperturbed.

anharmonicity, decreasing over 70 cm^{-1} (or 10%) from $\omega_2(a_1)$ to $\nu_2(a_1)$. It is apparent from the magnitude of the $x_{i2} = x_{2i}$ anharmonicity constants that the relatively large diagonal anharmonicity from x_{22} is offset by large couplings to the C−H stretches through off-diagonal anharmonicity where x_{12} and x_{23} are the only positive constants observed. Reasonable agreement, within ca. 20 cm^{-1}, is found between the CCSD(T)/daTZ VPT2 fundamentals of Oliveira et al. and those reported here. The exception to this agreement is the resonance affected $\nu_1(a_1)$ but the perturbed (before removal of resonance denominators and subsequent diagonalization of the resonance matrix) values are within this range. As with the harmonic frequencies, the best agreement is seen in the degenerate bend, $\nu_4(e)$, between the CcCRE results and the lower level CCSD(T)/daTZ with the former being higher than the latter by 4.6 cm^{-1}. Both CcCRE C−H stretches are much larger in magnitude, ca. 20 cm^{-1}, than the CCSD(T)/daTZ values whereas the CcCRE inversion mode is much lower, lying 26.3

cm^{-1} below those of previous work[212]. The much larger basis set size, additional diffuse functions, and corrections for core-correlation in the present work are responsible for the observed differences.

Variational predictions of methide's fundamental vibrations as well as the symmetric overtone of the inversion mode are shown in Table 4.6. Previous variational results are provided by Oliveira et al. using a four-dimensional (4D) CCSD(T)/daTZ potential which is scaled according to a high-level transition barrier height prediction[212]. This 4D PES omits the degenerate bend, $\nu_4(e)$, and its prediction of the anharmonic ZPVE should not be directly compared to the CcCR or CcCRE ZPVE results because of the qualitative difference shown in Table 4.6. However, the six-dimensional (6D) anharmonic VPT2 ZPVE of 6125.7 cm^{-1} from the same work agrees well with the present results, only varying 12.5 cm^{-1} from the CcCRE ZPVE. The ground state inversion splitting, Δ_{inv}, predicted in this work is ca. 18 cm^{-1} which is lower than the scaled 4D PES prediction of Oliveira et al. by 7 cm^{-1}. Only a small difference, 0.7 cm^{-1}, is observed between the CcCR and CcCRE Δ_{inv} values with the latter being higher as shown in Table 4.6. Both the CcCR and CcCRE values are within the reported experimental uncertainty of the recent photoelectron spectroscopy determination, also reported by Oliveira et al., where the CcCRE value of 18.0 cm^{-1} only differs by 3 cm^{-1} from the experimental value of 21(5) cm^{-1}. The experimental value of Oliveira et al. was determined through a weighted least-squares minimization of Δ_{inv} which exhibits a higher degree of uncertainty than an individual gaussian peak fitting and is only afforded by comparison to the high-resolution methyl radical observations of Yamada et al[212,220].

The lower level of the inversion fundamental, ν_2^+, is the only experimentally determined vibrational frequency available for methide. Its experimental value is from a vibrational hotband, a peak with lower energy than the origin band in the photoelectron spectrum, observed by Oliveira et al.[212] The experimental value of ν_2^+ appears to originate from the difference between the origin peak corrected with Δ_{rot}, an approximate origin shift due to rotational structure[221], and the vibrational hotband as ν_2^+= 757(9) - 10(4) - 303(10) =

Table 4.6: CH_3^- VTET Vibrational Frequencies (cm^{-1})

		CcCR	CcCRE	Past Theory[a]	Experiment[b]
ZPVE		6147.9	6138.2	4708.4	-
Δ_{inv}		17.3	18.0	25.0	21(5)
$\nu_2(a_1)$	+	478.8	475.2	412.3	444(13)
	-	689.5	688.2	646.1	-
$2\nu_2(a_1)$	+	1066.1	1064.4	1007.9	-
	-	1467.8	1466.6	1403.3	-
$\nu_4(e)$	+	1380.5	1377.5	-	-
	-	1401.3	1399.0	-	-
$\nu_1(a_1)$	+	2813.9	2808.8	2780.4	-
	-	2827.1	2822.3	2797.4	-
$\nu_3(e)$	+	2884.2	2880.1	2876.8	-
	-	2890.9	2887.1	2886.7	-

CcCRE energy shown in Equation 4.4.
[a] Scaled CCSD(T)/d-aug-cc-pVTZ DVR predictions.
[b] Photoelectron velocity-map imaging spectroscopy.
Values for past theory and experiment reported in Ref. 212.

444(13) cm^{-1}. No similar correction appears to be made for the rotational structure of the hotband peak itself. The $\boldsymbol{D}_{3h}$(M) molecular symmetry of the ground state of the anion and the symmetric inversion fundamental of the anion are the same. Both benefit from the textbook understanding of ammonia's inversion spectrum where the only difference present is the zero spin of carbon leading to fewer nuclear spin states[222]. The only significant feature which may affect the rotational contour of observed peaks is a series of missing rovibrational states in the $K = 0$ "stack" corresponding to $J = 2n$ (this is in contrast to the methyl radical's $J = 2n+1$, $K = 0$ missing levels). We would suspect any shift in the origin band and hotband centroids of methide's ground and inversion fundamental vibrational states due to rotational structure would be similar to one another. Thus, the effect of rotational structure on the relative band spacing should be less than 10(4) cm^{-1} (Δ_{rot}). With these considerations, it may be more accurate to neglect this term entirely by representing the experimental value of the symmetric inversion fundamental as the difference of their fit origins as $\nu_2^+ = 757(9)$ - 303(10) = 454(13) cm^{-1}.

Table 4.6 shows that the CcCRE QFF predicts ν_2^+ to be 475.2 cm^{-1} which is higher

than the reported experimental result by 31 cm^{-1} and the suggested experimental value of 454(13) cm^{-1} by 21 cm^{-1}. The scaled 4D PES of Oliveira et al. predicts a ν_2^+ value lower than the experimental result by 32 cm^{-1}. This means that both the scaled 4D and CcCRE variational predictions are outside experimental uncertainity by 18 cm^{-1} on opposite sides of the reported experimental value. A brief comparison of the CcCR and CcCRE energy levels shows a downward trend from CcCR to CcCRE of a few wavenumbers. There is no evidence showing increased electron correlation or basis set effects would amount to the precipitous decrease observed in the scaled 4D PES results. This suggests that the scaled 4D PES energy level predictions are not as reliable as its predicted ground state inversion splitting which agrees well with this work and the experimental value. The scaled 4D PES predicts other energy level splittings, the difference between ν^+ and ν^-, that reflect this relative accuracy when compared to the CcCRE results. There is only a difference of ca. 5 cm^{-1} for ν_1, ν_3, and $2\nu_2$ between the scaled 4D and CcCRE splittings but, this difference increases to 21 cm^{-1} when comparing the difference between ν_2^+ and ν_2^-.

The differences between past and present theoretical predictions can be explained by the different levels of theory, the basis set sensitivity of the system, and issues of scaling which emphasize Δ_{inv}. However, the disagreement of our results with experiment is indicative that either the reported experimental uncertainties are perhaps larger than suggested for methide or that some critical physics is not included in our theoretical methods. The highly corrected nature of the composite method used in this work, shown in Equation 4.4, implies the latter is unlikely. Only the truncation of the basis set should present any error in the completeness of the theory due to the highly diffuse nature of methide's highest occupied molecular orbital. Table 4.3 shows that, at least to second order, this truncation does not affect the vibrational frequencies and would not be the source of this discrepancy.

Examination of the fully deuterated isotopologue of methide, as shown in Table 4.7, provides more evidence for the quality of the present results. The CcCRE ground state inversion splitting for CD_3^- of $\Delta_{inv} = 5.1$ cm^{-1} differs by less than a wavenumber from the

experimental result, $\Delta_{\text{inv}} = 6(4)$ cm^{-1}, of Oliveira et al. and is well within the experimental uncertainity. The same trends between the CcC and CcCR methide results are present for CD_3^- where differences amount to ca. 5 cm^{-1}. The experimental result for the lower level of the deuterated inversion mode is 373(12) cm^{-1}. This result is 18 cm^{-1} lower than the CcCRE prediction of 390.9 cm^{-1} which lies 6 cm^{-1} above the upper bound of uncertainity on the experimental value. The approximate rotational correction, Δ_{rot}, appears to be applied only to the origin peak, once again, as ν_2^+ = 674(8) - 7(3) - 294(8) = 373(12) cm^{-1}. As seen with methide, removing this term provides far better agreement to the theoretically predicted CcCRE result. The CcCRE value lies 11 cm $^{-1}$ above the suggested experimental value of ν_2^+ = 674(8) - 294(8) = 380(11) cm^{-1}. Oliveira et al. report ν_2^+ = 335.9 cm^{-1} from their scaled 4D PES of CD_3^- which is far from the lower bound of either experimental value's uncertainity suggesting that the scaled predictions of this mode are too low.

Table 4.7: CD_3^- VTET Vibrational Frequencies (cm^{-1})

		CcCR	CcCRE	Past Theory	Experiment
ZPVE		4533.8	4526.9	3459.1	-
Δ_{inv}		4.8	5.1	7.9	6(4)
$\nu_2(a_1)$	+	394.7	390.9	335.9	373(12)
	-	495.2	493.5	459.9	-
$2\nu_2(a_1)$	+	763.9	761.2	713.8	-
	-	1026.7	1024.9	979.3	-
$\nu_4(e)$	+	1017.4	1015.5	-	-
	-	1022.9	1021.3	-	-
$\nu_1(a_1)$	+	1991.5	1988.1	2011.1	-
	-	1997.1	1993.8	2015.1	-
$\nu_3(e)$	+	2163.0	2160.2	2141.8	-
	-	2164.6	2161.9	2145.0	-

CcCRE energy shown in Equation 4.4.
[a] Scaled CCSD(T)/d-aug-cc-pVTZ DVR predictions.
[b] Photoelectron velocity-map imaging spectroscopy.
Values for past theory and experiment reported in Ref. 212.

Several points may be made regarding the approximate rotational contour shift (Equation 4.7) employed in previous work. It has error related to the accuracy of the *ab initio* methide rotational constants chosen. For example, the equilibrium rotational constants are predicted

to be larger than their vibrationally-averaged counterparts.

$$\Delta_{\text{rot}} = k_B T(B'/B'' + C'/2C'' - 3/2) + (B'' - B')/3 \tag{4.7}$$

Using either set of CcCRE rotational constants, shown in Table 4.4, and the methyl radical rotational constants of Yamada (Table II of Ref.[220]) produces a smaller shift than reported by Oliveira et al. where 5 and 7 cm^{-1} are predicted for $T = 150$ K with equilibrium and vibrationally-averaged rotational constants, respectively. The relationship between the equilibrium and vibrationally averaged rotational constants is generally consistent across temperatures in this prediction. Values of 19 cm^{-1} and 25 cm^{-1} are computed at 500 K where the vibrationally-averaged rotational constants produce a value that is ca. 30% larger than those at equilibrium. The fitting of variationally computed rovibrational energy levels to the A/S-reduced Watson Hamiltonian would provide the most accurate rotational constant predictions barring superior experimental values as the VPT2 values of B_0 and C_0 does not distinguish between inversion states.

The difference between the anti-symmetric and symmetric ground inversion states for experimentally determined rotational constants of the isoelectronic ammonia, NH_3, amount to 0.005 cm^{-1} for B, with the upper (anti-symmetric) state B constant being smaller[223]. Studies on hydronium, H_3O^+, show a much larger difference on the order of 0.2 cm^{-1} for B and 0.1 cm^{-1} for C. Similarly to ammonia, the upper state B value is smaller than its lower state counterpart but this is reversed for hydronium's C constants[224]. This relationship will likely persist for the rotational constants of methide but the magnitude of the shifts remain undetermined. In either case, it is perhaps more appropriate to compute this rotational shift using only *ab initio* rotational constants at the same level of theory when the upper or lower state constants are unavailable. The ratios will likely be over- or under-estimated when combining experimentally determined rotational constants with those from theory but as long as the theory adequately describes the states of interest, a purely *ab initio* answer will

be computed "on equal footing" within the Born-Oppenheimer approxmation. The utility of this dfference in $\Delta_{\rm rot}$ will largely depend on the resolution of the experiment.

4.4.3 Planar Transition State

The molecular geometries and harmonic vibrational frequencies of planar methide as well as the transition state barrier heights (Equation 4.6) are presented in Table 4.8 for the CcC, CcCR, and CcCRE levels of theory. A noticeable contraction of 0.016 Å is observed in the equilibrium C−H bond length of all three D_{3h} methide transition structures relative to their C_{3v} minima. Geometric changes seen in the ground state structures between theories are also present in the planar geometry where CcCR exhibits the shortest bonds and CcCRE the longest. The difference between CcC and CcCR bond lengths is exaggerated relative to the ground state minima in this case where the a_1 inversion coordinate in C_{3v} belongs to a_2'' in D_{3h} symmetry. Changes between the CcC and CcCR harmonic frequencies are even smaller than observed in the ground state where the results are nearly identical. Inclusion of high-level correlation, on the other hand, shifts the C−H stretches by ca. 3 $\rm cm^{-1}$ each, the degenerate bend by 1 $\rm cm^{-1}$, and the imaginary (inversion) mode by less than half a wavenumber. This shift results in the harmonic ZPVE being slightly lower in the CcCRE results relative to the CcC and CcCR force fields.

Table 4.8: Transition State Harmonic Frequencies and Barrier Heights ($\rm cm^{-1}$)

	CcC	CcCR	CcCRE
R_e	1.080 36	1.080 24	1.080 45
$\omega_1(a_1')$	3088.2	3088.3	3085.1
$\omega_2(a_2'')$	491.4i	491.3i	490.9i
$\omega_3(e')$	3247.8	3247.8	3244.2
$\omega_4(e')$	1384.4	1384.8	1383.5
ωZPVE	6176.3	6176.8	6170.3
$\Delta E_{\rm e}$	497.6	500.1	490.4
$E_{\rm TS}$	392.9	396.4	388.7

$\Delta E_{\rm e} \equiv E_{\rm e}(D_{3h}) - E_{\rm e}(C_{3v})$.
$E_{\rm TS} = \Delta E_{\rm e} + \Delta_{\rm ZPVE} + \Delta_{\rm DBOC}$

Evaluating the electronic energy difference between the ground and transition stationary states, defined in this work as ΔE_{e}, provides a similar result for all three composite theories; ca. 500 cm^{-1}. The inclusion of scalar relativistic corrections (CcCR) only slightly raises the CcC result with the addition of high level electron correlation (CcCRE) lowering ΔE_{e} to 490.4 cm^{-1}, the best estimate in this work. The transition state (inversion) barrier height is defined $E_{\mathrm{TS}} = \Delta E_{\mathrm{e}} + \Delta_{\mathrm{ZPVE}} + \Delta_{\mathrm{DBOC}}$ as described in Section 4.3. A slight difference persists in the prediction of E_{TS} for CcC and CcCR where the CcCRE result is lower by approximately the difference observed in ωZPVE between the theories. The CcCRE result is very close to the highly-corrected theoretical prediction of Oliveira et al. differing by only 2.7 cm^{-1}. Thus, the present and previous work have reached a consensus on the magnitude of E_{TS}, which is generally consistent amongst all values at ca. 390 cm^{-1}. Dixon et al. have previously predicted this barrier to be 720.5 cm^{-1} which is almost twice the values present herein. The CCSD(T)/aQZ ΔE_{e} value of 856.9 cm^{-1} reported by Dixon et al. suggests a lack of additional diffuse functions likely played a large role in the overestimation of the barrier as the electron density would be unnecessarily constrained at the planar structure.

As discussed in previous work, one anticipates methide will lose its extra electron at a given geometry if the methyl radical ($^{\bullet}\mathrm{CH}_3$) exists at a lower energy for that geometry; i.e. the potential energy surfaces of methide and methyl radical cross before that point[208,212]. Assuming both PESs are smooth leading to any crossing, the simplest way to address possible electron autodetachment at methide's planar (D_{3h}) transition state is to evaluate the methyl radical's energy at methide's optimized planar structure using the same level of theory. This is a trivial solution to a much more complicated dynamical problem but provides minor insight into the topic. Table 4.9 provides the optimized C−H bond length of the methide transition state using CCSD(T)/ta$X$Z (X = T,Q,5), full-valence active space MRCI+Q/ta$X$Z (X = T,Q,5), and (up to) CcCRE. The energy difference between the methide transition state and the methyl radical at this geometry is defined here as ΔE_{ROHF} or ΔE_{UHF} when using a ROHF or UHF reference for $^{\bullet}\mathrm{CH}_3$, respectively. The values are

presented as anion minus radical and a positive ΔE indicates that the radical exists below the energy of the anion at the optimized geometry (R_e) of methide's planar transition state. The effects of basis set size (cardinality) are the same between the CCSD(T) and MRCI+Q results where a decrease of ca. 100 and 35 cm^{-1} is seen in ΔE_{ROHF} from TZ→QZ→5Z including ΔE_{UHF} in the case of CCSD(T). While MRCI+Q runs higher than CCSD(T) by ca. 100 cm^{-1}, they reach the same conclusion that the methyl radical is lower in energy at methide's optimized planar structure. Both the CcCR and CcC results are very close to the CCSD(T)/ta5Z predictions. However, the consideration of high-level correlation in CcCRE causes a much larger change which lowers the result over half relative to the other composite theories. The UHF-based results tend to run ca. 30 cm^{-1} higher than ROHF except in case of CcCRE where the difference is only 12.4 cm^{-1}. Thus, at the highest level of theories used here it is anticipated an electronic energy difference of under 100 cm^{-1} (half a milliHartree) separates planar methide and the methyl radical PES.

Table 4.9: Planar $CH_3^-/{}^{\bullet}CH_3$ Electronic Energy Differences (cm^{-1}) and Structures (Å)

	R_e	ΔE_{ROHF}	ΔE_{UHF}
CCSD(T)/taTZ	1.083 89	291.7	323.1
CCSD(T)/taQZ	1.082 61	183.3	215.8
CCSD(T)/ta5Z	1.082 15	148.0	180.5
MRCI+Q/taTZ	1.083 83	393.0	-
MRCI+Q/taQZ	1.082 46	292.0	-
MRCI+Q/ta5Z	1.081 97	259.9	-
CcC	1.080 36	133.3	166.5
CcCR	1.080 24	140.4	173.6
CcCRE	1.080 45	64.2	74.6

R_e is the optimized CH_3^- (D_{3h}) geometry.
Energy differences shown as anion - radical.
A full valence active space is used in MRCI.
CcCRE energy shown in Equation 4.4.

One can speculate on the topic of electron autodetachment by simply noting that the imaginary mode of the anion transition state will not contribute to its zero-point vibrational energy. This implies that as long as the methyl radical is below any inflection points along its PES that it will have all real contributions to its zero-point vibrational energy. The

latter requirement is shown to be true by past work as the predicted geometries of methyl radical and planar methide are very close to one another in their equilibrium positions[212]. The methyl radical vibrational energy should then exceed that of methide in the region of planarity by at least ca. 200-300 cm^{-1} ($\omega_2/2$) assuming its ZPVE is higher than that of planar methide. It is clear from the present work that methide's planar transition state will have a lower ZPVE (CcCRE ωZPVE = 6170.3 cm^{-1}) than its minimum energy structure (CcCRE ωZPVE = 6261.0 cm^{-1}) where the ωZPVE of methide exceeds its planar counterpart by ca. 100 cm^{-1}. Past work also shows the anharmonic ZPVE of methyl radical exceeds that of methide's equilibrium state by several hundred wavenumbers[212]. Thus, methyl radical should exhibit a higher ZPVE than methide's planar transition state. From these results, it appears methide may be bound at planarity through vibrational effects, similar to those seen with its electron affinity, despite evidence to suggest its transition state exists slightly above the methyl radical on its electronic PES.

4.4.4 Isoelectronic Species

A brief comparison of species isoelectronic to methide is presented in Table 4.10. All species have ten electrons in a C_{3v} electron configuration of $(1a_1)^2(2a_1)^2(1e)^4(3a_1)^2$ with a ground state term symbol of $^1A_1$. Note that the equilibrium geometries presented in Table 4.10 are optimized with CCSD(T)/taTZ for methide but CCSD(T)/aTZ for ammonia and hydronium. The inversion angle ϕ is defined here again as the angle between a plane containing the central atom, parallel to the plane of the hydrogens, and each hydrogen. The distance r_T is defined as the center of the central atom to the plane of the hydrogens and represents half the distance this atom would have to travel to tunnel to the equivalent minimum position on the PES (not considering vibrational effects). The geometric parameters follow what is expected of the periodic trend of electronegativity (EN) with carbon being the least electronegative and oxygen the most in this series of central atoms. Methide has the longest bond lengths and hydronium the shortest both aided by their overall charges. A natural

bond orbital (NBO) analysis shows how the bonding MO's are distributed on atomic centers, by percent, with BD(X/H) where X is the central atom and H is one of the equivalent hydrogens. The polarizing effect of increasing EN is present here as well where the negatively charged methide shows a more diffuse distribution and the positively charged hydronium is dominated by the central oxygen atom. Ammonia is in the center of this EN trend.

Table 4.10: Isoelectronic Species to Methide (Å , °, and cm^{-1})

	CH_3^-	NH_3	H_3O^+
R_e	1.100	1.015	0.979
θ_e	110.6	106.4	111.4
ϕ_e	18.3	22.4	17.5
r_T	0.35	0.39	0.29
BD(X/H)	56/44	67/33	80/20
LP(s/p)	15/85	24/76	18/82
ΔE_e[†]	495 (490)	1937 (1785)	803 (651)
E_{TS}[‡]	418 (389)	1641 (1483)	410 (258*)
Δ_{inv}[§]	21	0.8	55

See text for a description of the variables.
CCSD(T)/taTZ (CH_3^-) or CCSD(T)/aTZ (NH_3, H_3O^+) unless noted.
[†] adiabatic electronic energy difference. [‡] $\Delta E_e + \Delta\omega$ZPVE.
Values in parenthesis are high-level results from this work, Ref 203, and Ref. 209.
* is computed with ΔE_e from Ref. 209 + CCSD(T)/aTZ ωZPVE from this work.
[§] cm^{-1}. Ref. 212, Ref. 203, and Ref. 224.

Both of the ionic species have shorter and wider pyramidal structures than the neutral ammonia as evidenced by their much smaller inversion angles and wider HXH bond angles. Another noticeable difference provided by the NBO analysis is seen in the highest occupied molecular orbital (HOMO) where the s and p character of this sp^3 non-bonding lone pair (LP) varies among species. The HOMO of ammonia shows a greater amount of s character than its ionic counterparts both of which show stronger p character. This orbital is very low energy (by magnitude) in methide but does not show the characteristic features of a system with a loosely bound electron despite slightly more Rydberg character than the other two species[225]. The similarity between the sp^3 HOMO of the ground state and the completely p-type HOMO of the D_{3h} transition structure may play a role in the height of the barrier and, thus, rate of tunneling. This appears to be the case for the ionic species

where planar methide resides 495 cm^{-1} above its ground state using CCSD(T)/taTZ and hydronium's planar transition state is 803 cm^{-1} above its minima using CCSD(T)/aTZ. High-accuracy predictions of each electronic barrier are shown in the parenthesis next to their CCSD(T)/taTZ or CCSD(T)/aTZ counterpart in Table. 4.10. It is obvious from the small difference seen between the CCSD(T)/taTZ ΔE_e of 495 cm^{-1} and the CcCRE result of 490 cm^{-1} that correlation and basis set effects play a limited role in the relative difference between the C_{3v} and D_{3h} stationary points. This result is consistent with previous studies on the convergence of methide properties where the highly diffuse basis functions play a more important role than the cardinality of the basis set[213]. This is not the case for ammonia and hydronium which both show appreciable drops of 152 cm^{-1} from their CCSD(T)/aTZ values when compared to the empirically refined HSL2 PES of ammonia and the highly corrected result of Rajamaki et al.[203,226]

The barrier heights for each of these species are compared using CCSD(T)/taTZ or CCSD(T)/aTZ harmonic vibrational frequencies as $E_{TS} = \Delta E_e + \Delta\omega ZPVE$. What becomes apparent at this level of theory is that $\Delta\omega ZPVE$ increases along the periodic row of the isoelectronic species. Methide shows the smallest $\Delta\omega ZPVE$ which only decreases by ca. 20 cm^{-1} at the CcCRE level of theory; both results have magnitude under 100 cm^{-1}. The CCSD(T)/aTZ and HSL2 $\Delta\omega ZPVE$ for NH_3 are nearly equivalent as -296 and -301 cm^{-1}, respectively, where this correction is three times that observed in methide. The $\Delta\omega ZPVE$ of hydronium is the largest in magnitude of the considered molecules and appears to be at least half that of the adiabatic electronic energy difference between the optimized ground and planar structures, ΔE_e. Harmonic vibrational frequencies were not reported by Rajamaki et al. for hydronium so the high-level E_{TS} for H_3O^+ is found using the CCSD(T)/aTZ $\Delta\omega ZPVE$[226]. Using this high-level ΔE_e result of 650.4 cm^{-1} and the CCSD(T)/aTZ $\Delta\omega ZPVE$ of -393 cm^{-1} produces the smallest barrier height of all the isoelectronic species at 258 cm^{-1}. The low height of this barrier combined with its width, the smallest of the three species by way of r_T, means it should exhibit the smallest non-classical region along the inversion coordinate.

This results in the largest ground state inversion splitting of the isoelectronic species at 55.34840(71) cm^{-1} despite possessing the heaviest mass[224]. The photoelectron result of Δ_{inv} = 21(5) cm^{-1} from Oliveira et al. is less than half that of hydronium, where the CcCRE results suggest an even lower value of 18.0 cm^{-1}, even though the H_3O^+ and CH_3^- have comparable barriers and equilibrium properties.

4.5 Conclusions

A full dimensional 6D QFF for methide, CH_3^-, is presented in this work which includes CBS-extrapolation, core correlation corrections, scalar relativistic corrections, and consideration of high-level electron correlation up to non-iterative quadruple excitations of coupled cluster theory. Variational predictions of the upper and lower states of each vibrational level is provided and the ground state inversion splitting is predicted to be 18.0 cm^{-1} in good agreement with the experimental determination of 21(5) cm^{-1}. The lower level of the inversion fundamental, ν_2^+, is predicted to be higher than the value of 444(13) cm^{-1} suggested by recent photoelectron experiments[212]; a difference which is excaberated by the application of an approximate rotational contour correction to the experimental origin band. The best prediction of the present results is ν_2^+ = 475.2 cm^{-1} where previous *ab initio* results seem to underestimate the fundamental despite showing level splittings in good agreement with those reported here[212]. Better agreement is seen with the fully deuterated isotopologue, CD_3^-, between the present results and the experimental determinations of Δ_{inv} and ν_2^+. The prediction of the barrier to planarity from the *ab initio* results of Oliveira et al. agrees well with the current high-level result of 388.7 cm^{-1}. It is noted that the electronic contribution to this barrier height is relatively converged when using sufficiently diffuse basis functions on smaller basis sets as shown in previous work[213]. This is not the case for species isoelectronic to methide where the barrier height predictions of ammonia and hydronium both benefit substantially more from increasing levels of correlation and basis set completeness; in partic-

ular, higher angular momentum functions. A more complete understanding of methide and its inversion fundamental awaits higher resolution results.

Bibliography

[1] Stanton, J. F.; Gauss, J. A Discussion of Some Problems Associated with the Quantum Mechanical Description of Open-Shell Molecules. *Adv. Chem. Phys.* **2003**, *125*, 101.

[2] Burleigh, D. C.; McCoy, A. B.; Sibert III, E. L. An accurate quartic force field for formaldehyde. *J. Chem. Phys.* **1996**, *104*, 480.

[3] Carter, S.; Pinnavaia, N.; Handy, N. C. The vibrations of formaldehyde. *Chem. Phys. Lett.* **1995**, *240*, 400–408.

[4] Carter, S.; Handy, N. C. The Geometry of Formaldehyde. *J. Mol. Spectrosc.* **1996**, *179*, 65–72.

[5] Yachmenev, A.; Yurchenko, S. N.; Jensen, P.; Thiel, W. A new "spectroscopic" potential energy surface for formaldehyde in its ground electronic state. *J. Chem. Phys.* **2011**, *134*, 244307.

[6] Polyanksy, O. L.; Császár, A. G.; Shirin, S. V.; Zobov, N. F.; Barletta, P.; Tennyson, J.; Schwenke, D. W.; Knowles, P. J. High-Accuracy ab Initio Rotation-Vibration Transitions for Water. *Science* **2003**, *128*, 539–542.

[7] Császár, A. G.; Czakó, G.; Furtenbacher, T.; Tennyson, J.; Szalay, V.; Shirin, S. V.; Zobov, N. F.; Polyanksy, O. L. On equilibrium structures of the water molecule. *J. Chem. Phys.* **2005**, *122*, 214305.

[8] Barletta, P.; Shirin, S. V.; Zobov, N. F.; Polyanksy, O. L.; Tennyson, J.; Valeev, E. F.; Császár, A. G. CVRQD ab initio ground-state adiabatic potential energy surfaces for the water molecule. *J. Chem. Phys.* **2006**, *125*, 204307.

[9] Karton, A.; Martin, J. M. L. Performance of W4 theory for spectroscopic constants and electrical properties of small molecules. *J. Chem. Phys.* **2010**, *133*, 144102.

[10] Owens, A.; Yurchenko, S. N.; Yachmenev, A.; Thiel, W. A global potential energy surface and dipole moment surface for silane. *J. Chem. Phys.* **2015**, *143*, 244317.

[11] Polyansky, O. L.; Ovsyannikov, R. I.; Kyuberis, A. A.; Lodi, L.; Tennyson, J.; Yachmenev, A.; Yurchenko, S. N.; Zobov, N. F. Calculation of rotation-vibration energy levels of the ammonia molecule based on *ab initio* potential energy surfaces. *J. Mol. Spectrosc.* **2016**, *327*, 21–30.

[12] Nikitin, A. V.; Rey, M.; Rodina, A.; Krishna, B. M.; Tyuterev, V. G. Full-Dimensional Potential Energy and Dipole Moment Surfaces of GeH_4 Molecule and Accurate First-Principle Rotationally Resolved Intensity Predictions in the Infrared. *J. Phys. Chem. A* **2016**, *120*, 8983–8997.

[13] Nikitin, A. V.; Rey, M.; Tyuterev, V. G. First fully *ab initio* potential energy surface of methane with a spectroscopic accuracy. *J. Chem. Phys.* **2016**, *145*, 114309.

[14] Allen, W. D.; East, A. L. L.; Császár, A. G. In *Structures and Conformations of Non-Rigid Molecules*; Laane, J., Dakkouri, M., van der Veken, B., Oberhammer, H., Eds.; Kluwer Academic Publishers: Dordrecht, 1993; Chapter 17, pp 343–374.

[15] Császár, A. G.; Allen, W. D.; Schaefer III, H. F. In pursuit of the *ab initio* limit for conformational energy prototypes. *J. Chem. Phys.* **1998**, *108*, 9751–9764.

[16] East, A. L. L.; Johnson, C. S.; Allen, W. D. Characterization of the $\tilde{X}\ A'$ state of isocyanic acid. *J. Chem. Phys.* **1993**, *98*, 1299–1328.

[17] East, A. L. L.; Allen, W. D. The heat of formation of NCO. *J. Chem. Phys.* **1993**, *99*, 4638–4650.

[18] Matthews, D. A.; Gauss, J.; Stanton, J. F. Revisitation of Nonorthogonal Spin Adaptation in Coupled Cluster Theory. *J. Chem. Theo. Comp.* **2013**, *1*, 1011.

[19] Noga, J.; Bartlett, R. J. The full CCSDT model for molecular electronic structure. *J. Chem. Phys.* **1987**, *86*, 7041.

[20] Noga, J.; Bartlett, R. J. Erratum: The full CCSDT model for molecular electronic structure [J. Chem. Phys. 86, 7041 (1987)]. *J. Chem. Phys.* **1988**, *89*, 3401.

[21] Oliphant, N.; Adamowicz, L. Coupled-cluster method truncated at quadruples. *J. Chem. Phys.* **1991**, *95*, 6645.

[22] Kucharski, S. A.; Bartlett, R. J. The coupled-cluster single, double, triple, and quadruple excitation method. *J. Chem. Phys.* **1992**, *97*, 4282.

[23] Bomble, Y. J.; Stanton, J. F.; Kállay, M.; Gauss, J. Coupled-cluster methods including noniterative corrections for quadruple excitations. *J. Chem. Phys.* **2005**, *123*, 054101.

[24] Matthews, D. A.; Stanton, J. F. Non-orthogonal spin-adaptation of coupled cluster methods: A new implementation of methods including quadruple excitations. *J. Chem. Phys.* **2015**, *142*, 064108.

[25] Matthews, D. A.; Stanton, J. F. Accelerating the convergence of higher-order coupled cluster methods. *J. Chem. Phys.* **2015**, *143*, 204103.

[26] Reisner, D. E.; Field, R. W.; Kinsey, J. L.; Dai, H.-L. Stimulated emission spectroscopy: A complete set of vibrational constants for $\tilde{X}_1$ A_1 formaldehyde. *J. Chem. Phys.* **1984**, *80*, 5968–5978.

[27] Polik, W. F.; Guyer, D. R.; Moore, C. B. Stark level-crossing spectroscopy of S 0 formaldehyde eigenstates at the dissociation threshold. *J. Chem. Phys.* **1990**, *92*, 3453–3470.

[28] Polik, W. F.; Guyer, D. R.; Miller, W. H.; Moore, C. B. Eigenstate-resolved unimolecular reaction dynamics: Ergodic character of S_0 formaldehyde at the dissociation threshold. *J. Chem. Phys.* **1990**, *92*, 3471–3484.

[29] Bouwens, R. J.; Hammerschmidt, J. A.; Grzeskowiak, M. M.; Stegink, T. A.; Yorba, P. M.; Polik, W. F. Pure vibrational spectroscopy of S_0 formaldehyde by dispersed fluorescence. *J. Chem. Phys.* **1996**, *104*, 460–479.

[30] Brünken, S.; Müller, H. S. P.; Lewen, F.; Winnewisser, G. High accuracy measurements on the ground state rotational spectrum of formaldehyde (H_2CO) up to 2 THz. *Phys. Chem. Chem. Phys* **2003**, *5*, 1515–1518.

[31] Lohilahti, J.; Horneman, V.-M. FTFIR-spectrum of the ground state of D_2CO. *J. Mol. Struc.* **2004**, *228*, 1–6.

[32] Gordan, I. E. et al. The HITRAN2016 Molecular Spectroscopic Database. *J. Quant. Spectrosc. Radiat. Transfer* **2017**, *203*, 3–69.

[33] Müller, H. S. P.; Gendriesch, R.; Margulés, L.; Lewen, F.; Winnewisser, G.; Bocquet, R.; Demaison, J.; Wötzel, U.; Mäder, H. Spectroscopy of the formaldehyde isotopomer $H_2^{13}CO$ in the microwave to terahertz region. *Phys. Chem. Chem. Phys* **2000**, *2*, 3401–3404.

[34] Puzzarini, C.; Heckert, M.; Gauss, J. The accuracy of rotational constants predicted by high-level quantum-chemical calculations. I. molecules containing first-row atoms. *J. Chem. Phys.* **2008**, *128*, 194108.

[35] Schuurman, M. S.; Allen, W. D.; Schaefer III, H. F. The *Ab Initio* Limit Quartic Force Field of BH_3. *J. Comp. Chem.* **2005**, *26*, 1106–1112.

[36] Huang, X.; Lee, T. J. A procedure for computing accurate ab initio quartic force fields: Application to HO_2^+ and H_2O. *J. Chem. Phys.* **2008**, *129*, 044312.

[37] Huang, X.; Lee, T. J. Accurate *ab initio* quartic force fields for NH_2 and CCH^- and rovibrational spectroscopic constants for their isotopologs. *J. Chem. Phys.* **2009**, *131*, 104301.

[38] Fortenberry, R. C.; Huang, X.; Francisco, J. S.; Crawford, T. D.; Lee, T. J. The *trans*-HOCO radical: fundamental vibrational frequencies, quartic force fields, and spectroscopic constants. *J. Chem. Phys.* **2011**, *135*, 134301.

[39] Morgan, W. J.; Fortenberry, R. C. Quartic force fields for excited electronic states: Rovibronic reference data for the $1\ ^2A'$ and $1\ ^2A$" states of the isoformyl radical, HOC. *Spec. Chem. Acta* **2015**, *135*, 965–972.

[40] Ringholm, M.; Jonsson, D.; Ruud, K. A general, recursive, and open-ended response code. *J. Comp. Chem.* **2014**, *35*, 622–623.

[41] Peterson, K. A.; Dunning, T. H. Benchmark calculations with correlated molecular wave functions. VII. Binding energy and structure of the HF dimer. *J. Chem. Phys.* **1995**, *102*, 2032–2041.

[42] Kendall, R. A.; Dunning, T. H.; Harrison, R. J. Electron affinities of the first-row atoms revisited. Systematic basis sets and wave functions. *J. Chem. Phys.* **1992**, *96*, 6796–6806.

[43] Woon, D. E.; Dunning, T. H.; Peterson, K. A. Gaussian basis sets for use in correlated molecular calculations. V. Core-valence basis sets for boron through neon. *J. Chem. Phys.* **2001**, *114*, 9244.

[44] Feller, D. The use of systematic sequences of wave functions for estimating the complete basis set, full configuration interaction limit in water. *J. Chem. Phys.* **1993**, *98*, 7059.

[45] Helgaker, T.; Klopper, W.; Koch, H.; Noga, J. Basis-set convergence of correlated calculations on water. *J. Chem. Phys.* **1997**, *106*, 9639–9646.

[46] Schwartz, C. Importance of Angular Correlations between Atomic Electrons. *Phys. Rev.* **1962**, *126*, 1015–1019.

[47] Kutzelnigg, W.; Morgan III, J. D. Rates of convergence of the partial-wave expansions of atomic correlation energies. *J. Chem. Phys.* **1992**, *96*, 4484.

[48] Kutzelnigg, W.; Morgan III, J. D. Erratum: Rates of convergence of the partial-wave expansions of atomic correlation energies [J. Chem. Phys. 96, 4484 (1992)]. *J. Chem. Phys.* **1992**, *97*, 8821.

[49] Feller, D.; Peterson, K. A.; Hill, J. G. On the effectiveness of CCSD(T) complete basis set extrapolations for atomization energies. *J. Chem. Phys.* **2011**, *135*, 044102.

[50] Martin, J. M. L.; Lee, T. J. The atomization energy and proton affinity of NH3. An ab initio calibration study. *Chem. Phys. Lett.* **1996**, *258*, 136–143.

[51] Schwenke, D. W. The extrapolation of one-electron basis sets in electronic structure calculations: How it should work and how it can be made to work. *J. Chem. Phys.* **2005**, *122*, 014107.

[52] Tajti, A.; Szalay, P. G.; Császár, A. G.; Kállay, M.; Gauss, J.; Valeev, E. F.; Flowers, B. F.; Vázquez, J.; Stanton, J. F. HEAT: High accuracy extrapolated ab initio thermochemistry. *J. Chem. Phys.* **2004**, *121*, 11599.

[53] Bomble, Y. J.; Vázquez, J.; Kállay, M.; Michauk, C.; Szalay, P. G.; Császár, A. G.; Gauss, J.; Stanton, J. F. High-accuracy extrapolated ab initio thermochemistry. II. Minor improvements to the protocol and a vital simplification. *J. Chem. Phys.* **2006**, *125*, 064108.

[54] Harding, M. E.; Vázquez, J.; Ruscic, B.; Wilson, A. K.; Gauss, J.; Stanton, J. F. High-accuracy extrapolated ab initio thermochemistry. III. Additional improvements and overview. *J. Chem. Phys.* **2008**, *128*, 114111.

[55] Turney, J. M. et al. Psi4: an open-source *ab initio* electronic structure program. *Wiley Interdisciplinary Reviews: Computational Molecular Science* **2012**, *2*, 556–565.

[56] Cowan, R. D.; Griffin, D. C. Approximate relativistic corrections to atomic radial wave functions. *J. Opt. Soc. Am.* **1976**, *66*, 1010.

[57] Klopper, W. Simple recipe for implementing computation of first-order relativistic corrections to electron correlation energies in framework of direct perturbation theory. *J. Comp. Chem* **1997**, *18*, 20–27.

[58] CFOUR, a quantum chemical program package written by J.F. Stanton, J. Gauss, M.E. Harding, P.G. Szalay with contributions from A.A. Auer, R.J. Bartlett, U. Benedikt, C. Berger, D.E. Bernholdt, Y.J. Bomble, O. Christiansen, M. Heckert, O. Heun, C. Huber, T.-C. Jagau, D. Jonsson, J. Jusélius, K. Klein, W.J. Lauderdale, D.A. Matthews, T. Metzroth, D.P. O'Neill, D.R. Price, E. Prochnow, K. Ruud, F. Schiffmann, S. Stopkowicz, A. Tajti, J. Vázquez, F. Wang, J.D. Watts and the integral packages MOLECULE (J. Almlöf and P.R. Taylor), PROPS (P.R. Taylor), ABACUS (T. Helgaker, H.J. Aa. Jensen, P. Jørgensen, and J. Olsen), and ECP routines by A. V. Mitin and C. van Wüllen. For the current version, see `http://www.cfour.de`.

[59] Stanton, J. F.; Gauss, J. Analytic second derivatives in high-order many- body perturbation and coupled-cluster theories: Computational considerations and applications. *Int. Rev. Phys. Chem.* **2000**, *19*, 61–95.

[60] Jagau, T.-C.; Gauss, J.; Ruud, K. Analytic evaluation of the dipole Hessian matrix in coupled-cluster theory. *J. Chem. Phys.* **2013**, *139*, 154106.

[61] Heckert, M.; Kállay, M.; Gauss, J. Molecular equilibrium geometries based on coupled-cluster calculations including quadruple excitations. *Mol. Phys.* **2005**, *103*, 2109–2115.

[62] Heckert, M.; Kállay, M.; Tew, D. P.; Klopper, W.; Gauss, J. Basis-set extrapolation

techniques for the accurate calculation of molecular equilibrium geometries using coupled cluster theory. *J. Chem. Phys.* **2006**, *125*, 044108.

[63] Halkier, A.; Helgaker, T.; Jørgensen, P.; Klopper, W.; Olsen, J. Basis-set convergence of the energy in molecular Hartree-Fock calculations. *Chem. Phys. Lett.* **1999**, *302*, 437–446.

[64] Jensen, S. R.; Flå, T.; Jonsson, D.; Monstad, R. S.; Ruud, K.; Frediani, L. Magnetic properties with multiwavelets and DFT: the complete basis set limit achieved. *Phys. Chem. Chem. Phys.* **2016**, *18*, 21145–21161.

[65] Martin, J. M. L.; Lee, T. J.; Taylor, P. R. An Accurate ab initio Quartic Force Field for Formaldehyde and Its Isotopomers. *J. Mol. Spectrosc.* **1993**, *160*, 105–116.

[66] Allen, W. D. INTDIF2008, an abstract program written for Mathematica (Wolfram Research Inc., Champaign, Illinois, USA) to perform general numerical differentiation to high orders of electronic structure data, Athens, Georgia, USA. 2008.

[67] Pavanello, M.; Adamowicz, L.; Alijah, A.; Zobov, N. F.; Mizus, I. I.; Polyansky, O. L.; Tennyson, J.; Szidarovszky, T.; Császár, A. G. Calibration-quality adiabatic potential energy surfaces for H_3^+ and its isotopologues. *J. Chem. Phys.* **2012**, *136*, 184303.

[68] Polyansky, O. L.; Alijah, A.; Zobov, N. F.; Mizus, I. I.; Ovsyannikov, R. I.; Tennyson, J.; Lodi, L.; Szidarovszky, T.; Császár, A. G. Spectroscopy of H_3^+ based on a new high-accuracy global potential energy surface. *Phil. Trans. R. Soc. A* **2012**, *370*, 5014–5027.

[69] NITROGEN, Numerical and Iterative Techniques for Rovibronic Energies with General Internal Coordinates, a program by P. B. Changala, http://www.colorado.edu/nitrogen.

[70] Dateo, C. E.; Lee, T. J.; Schwenke, D. W. An accurate quartic force-field and vibrational frequencies for HNO and DNO. *J. Chem. Phys.* **1994**, *101*, 5853–5859.

[71] Gaw, J. F.; Willets, A.; Green, W. H.; Handy, N. C. In *Advances in Molecular Vibrations and Collision Dynamics*; Bowman, J. M., Ratner, M. A., Eds.; JAI Press, Inc.: Greenwich, Connecticut, 1991; pp 170–185.

[72] Allen, W. D.; coworkers, 2005; $INTDER$ 2005 is a general program written by W. D. Allen and coworkers, which performs vibrational analysis and higher-order non-linear transformations.

[73] Allen, W. D.; Császár, A. G.; Szalay, V.; Mills, I. M. General derivative relations for anharmonic force fields. *Mol. Phys.* **1996**, *89*, 1213–1221.

[74] Thorvaldsen, A. J.; Ruud, K.; Kristensen, K.; Jørgensen, P.; Coriani, S. *J. Chem. Phys.* **2008**, *129*, 214108.

[75] Ringholm, M.; Jonsson, D.; Ruud, K. *J. Comput. Chem.* **2014**, *35*, 622.

[76] Aidas, K. et al. The Dalton quantum chemistry program system. *WIREs Comput. Mol. Sci.* **2013**, *4*, 269.

[77] Dalton. a molecular electronic structure program. Release Dalton2013, see http://daltonprogram.org/, 2013.

[78] Gao, B.; Thorvaldsen, A. J.; Ruud, K. *Int. J. Quantum Chem.* **2011**, *111*, 858.

[79] Gao, B.; Thorvaldsen, A. J. Gen1Int Version 0.2.1. a library to evaluate the derivatives of one-electron integrals with respect to the geometry perturbations, external electric and magneti fields, and total rotational angular momentum at zero fields with contracted rotational London atomic orbitals, released under the GNU Lesser General Public License, 2012.

[80] Thorvaldsen, A. J. CGTO-DIFF-ERI. a library for the evaluation of geometry-differentiated two-electron integrals (d^n/dR_k^n) under the GNU Lesser General Public License, 2012.

[81] Reine, S.; Tellgren, E. I.; Helgaker, T. *Phys. Chem. Chem. Phys.* **2011**, *9*, 4771.

[82] Jørgensen, P.; Jensen, H. J. A.; Olsen, J. *J. Chem. Phys.* **1988**, *89*, 3654.

[83] Kristensen, K.; Jørgensen, P.; Thorvaldsen, A. J.; Helgaker, T. *J. Chem. Phys.* **2008**, *129*, 214103.

[84] Amat, G.; Nielsen, H. Higher order rotation-vibration energies of polyatomic molecules. IV. *J. Chem. Phys.* **1958**, *29*, 665–672.

[85] Sibert, E. L. Theoretical studies of vibrationally excited polyatomic molecules using canonical Van Vleck perturbation theory. *J. Chem. Phys.* **1988**, *88*, 4378–4390.

[86] Krasnoshcheckov, S.; Isayeva, E.; Stepanov, N. Numerical-analytic implementation of the higher-order canonical Van Vleck perturbation theory for the interpretation of medium-sized molecule vibrational spectra. *J. Phys. Chem. A* **2012**, *116*, 3691–3709.

[87] Werner, H.-J. et al. MOLPRO, version 2010.1, a package of ab initio programs. 2010; see http://www.molpro.net.

[88] Helgaker, T.; Gauss, J.; Jørgensen, P.; Olsen, J. The prediction of molecular equilibrium structures by the standard electronic wave functions. *J. Chem. Phys.* **1997**, *106*, 6430.

[89] Peterson, K. A.; Dunning Jr., T. H. The CO molecule: the role of basis set and correlation treatment in the calculation of molecular properties. *J. Molec. Struc.* **1997**, *400*, 93–117.

[90] He, Y.; Cremer, D. Molecular Geometries at Sixth Order Møller-Plesset Perturbation Theory. At What Order Does MP Theory Give Exact Geometries? *J. Phys. Chem. A* **2000**, *104*, 7679–7688.

[91] Bak, K. L.; Gauss, J.; Jørgensen, P.; Olsen, J.; Helgaker, T.; Stanton, J. F. The accurate determination of molecular equilibrium structures. *J. Chem. Phys.* **2001**, *114*, 6548.

[92] Cremer, D.; Kraka, E.; He, Y. Exact geometries from quantum chemical calculations. *J. Mol. Struc.* **2000**, *567-568*, 275–293.

[93] Helgaker, T.; Ruden, T. A.; Jørgensen, P.; Olsen, J.; Klopper, W. *A priori* calculation of molecular properties to chemical accuracy. *J. Phys. Org. Chem.* **2004**, *17*, 913–933.

[94] Halkier, A.; Jørgensen, P.; Gauss, J.; Helgaker, T. CCSDT calculations of molecular equilibrium geometries. *Chem. Phys. Lett.* **1997**, *274*, 235–241.

[95] Eriksen, J. J.; Matthews, D. A.; Jørgensen, P.; Gauss, J. Communication: The performance of non-iterative coupled cluster quadruples models. *J. Chem. Phys.* **2015**, *143*, 041101.

[96] Lohilahti, J. Rotation-Vibration Spectroscopic Studies of Formaldehyde and Formic Acid Molecules. Ph.D. thesis, University of Oulu, 2006.

[97] Rauhut, G.; Knizia, G.; Werner, H.-J. Accurate calculation of vibrational frequencies using explicitly correlated coupled-cluster theory. *J. Chem. Phys.* **2009**, *130*, 054105.

[98] Demaison, J. Experimental, semi-experimental and ab initio equilibrium structures. *Mol. Phys.* **2007**, *105*, 3109–3138.

[99] Flygare, W. H. Magnetic Interactions in Molecules and an Analysis of Molecular Electronic Charge Distribution from Magnetic Parameters. *Chem. Rev.* **1973**, *74*, 653–687.

[100] Krause, H.; Sutter, D. H.; Palmer, M. H. The Molecular Zeeman Effect of Imines. I. I. Methanimine, its Molecular g-Tensor, its Magnetic Susceptibility Anisotropics, its Molecular Electric Quadrupole Moment, its Electric Field Gradient at the Nitrogen Nucleus, and its Nitrogen Spin-Rotation Coupling. *Z. Naturforsch* **1989**, *44a*, 1063–1078.

[101] Margulés, L.; Demaison, J.; Sreeja, P. B.; Guillemin, J.-C. Submillimeterwave spectrum of CH_2PH and equilibrium structures of CH_2PH and CH_2NH. *J. Molec. Spectrosc.* **2006**, *238*, 234–240.

[102] Müller, H. S. P.; Lewen, F. Submillimeter spectroscopy of $H_2C^{17}O$ and a revisit of the rotational spectra of $H_2C^{18}O$ and $H_2C^{16}O$. *J. Mol. Spectrosc.* **2017**, *331*, 28–33.

[103] Carter, S.; Handy, N. C.; Demaison, J. The rotational levels of the ground vibrational state of formaldehyde. *Mol. Phys.* **1997**, *90*, 729–737.

[104] Martin, J. M. L.; Taylor, P. R. Basis set convergence for geometry and harmonic frequencies. Are h functions enough? *Chem. Phys. Lett.* **1994**, *225*, 473–479.

[105] Martin, J. M. L. On the effect of core correlation on the geometry and harmonic frequencies of small polyatomic molecules. *Chem. Phys. Lett.* **1995**, *242*, 343–350.

[106] Tew, D. P.; Klopper, W.; Heckert, M.; Gauss, J. Basis Set Limit CCSD(T) Harmonic Vibrational Frequencies. *J. Phys. Chem. A.* **2007**, *111*, 11242–11248.

[107] Ruden, T. A.; Helgaker, T.; Jørgensen, P.; Olsen, J. Coupled-cluster connected quadruples and quintuples corrections to the harmonic vibrational frequencies and equilibrium bond distances of HF, N_2, F_2, and CO. *J. Chem. Phys.* **2004**, *121*, 5874–5884.

[108] Cortez, M. H.; Brinkmann, N. R.; Polik, W. F.; Taylor, P. R.; Bomble, Y. J.; Stanton, J. F. Factors Contributing to the Accuracy of Harmonic Force Field Calculations of Water. *J. Chem. Theo. Comp.* **2007**, *3*, 1267–1274.

[109] Kállay, M.; Gauss, J. Analytic second derivatives for general coupled-cluster and configuration-interaction models. *J. Chem. Phys.* **2004**, *120*, 6841–6848.

[110] Martin, J. M. L.; Taylor, P. R. The geometry, vibrational frequencies, and total atomization energy of ethylene. A calibration study. *Chem. Phys. Lett.* **1996**, *248*, 336–344.

[111] Persson, B. J.; Taylor, P. R.; Martin, J. M. L. Ab initio Calibration Study of the Heat of Formation, Geometry, and Anharmonic Force Field of Fluoroacetylene. *J. Phys. Chem. A* **1998**, *102*, 2483–2492.

[112] Feller, D.; Peterson, K. A. High level coupled cluster determination of the structure, frequencies, and heat of formation of water. *J. Chem. Phys.* **2009**, *131*, 154306.

[113] Kahn, K.; Kirtman, B.; Noga, J.; Ten-no, S. High level coupled cluster determination of the structure, frequencies, and heat of formation of water. *J. Chem. Phys.* **2010**, *133*, 074106.

[114] Cross, P. C.; Wilson Jr., E. B.; Decius, J. C. *Molecular Vibrations: The Theory of Infrared and Raman Vibrational Spectra*; Dover Publications, 1980.

[115] Clabo Jr., D. A.; Allen, W. D.; Remington, R. B.; Yamaguchi, Y.; Schaefer III, H. F. A systematic study of molecular vibrational anharmonicity and vibration-rotation interaction by self-consistent field higher derivative methods. Asymmetric top molecules. *Chem. Phys.* **1988**, *123*, 187–239.

[116] Nielsen, H. H. The Vibration-Rotation Energies of Polyatomic Molecules. Part II. Accidental Degeneracies. *Phys. Rev* **1945**, *68*, 181–191.

[117] Martin, J. M. L.; Lee, T. J.; Taylor, P. R.; François, J.-P. The anharmonic force field of ethylene, C_2H_4, by means of accurate *ab initio* calculations. *J. Chem. Phys.* **1995**, *103*, 2589–2602.

[118] Matthews, D. A.; Vázquez, J.; Stanton, J. F. Calculated stretching overtone levels and Darling-Dennison resonances in water: a triumph of simple theoretical approaches. *Mol. Phys.* **2007**, *105*, 2659–2666.

[119] Matthews, D. A.; Stanton, J. F. Quantitative analysis of Fermi resonances by harmonic derivatives of perturbation theory corrections. *Mol. Phys.* **2009**, *107*, 213–222.

[120] Lehmann, K. K. Beyond the x-K relations. *Mol. Phys.* **1989**, *66*, 1129–1137.

[121] Lehmann, K. K. ERRATUM: Beyond the x-K relations. Calculations of $1-1$ and $2-2$ resonance constants with applications to HCN and DCN. *Mol. Phys.* **1992**, *75*, 739.

[122] Martin, J. M. L.; Taylor, P. R. *Spectrochim. Acta, Part A.* **1997**, *53*, 1039–1050.

[123] Rosnik, A. M.; Polik, W. F. VPT2+K spectroscopic constants and matrix elements of the transformed vibrational Hamiltonian of a polyatomic molecule with resonances using Van Vleck perturbation theory. *Mol. Phys.* **2014**, *112*, 261–300.

[124] McCaslin, L.; Stanton, J. Calculation of fundamental frequencies for small polyatomic molecules: a comparison between correlation consistent and atomic natural orbital basis sets. *Mol. Phys.* **2013**, *111*, 1492–1496.

[125] Perrin, A.; Valentin, A.; Daumont, L. New analysis of the $2\nu_4$, $\nu_4+\nu_6$, $2\nu_6$, $\nu_3+\nu_4$, $\nu_3+\nu_6$, ν_1, ν_5, $\nu_2+\nu_4$, $2\nu_3$, $\nu_2+\nu_6$, and $\nu_2+\nu_3$ bands of formaldehyde $H_2^{12}C^{16}O$: Line positions and intensities in the 3.5μm spectral region. *J. Mol. Struc.* **2006**, *780-781*, 28–44.

[126] Tchana, F. K.; Perrin, A.; Lacome, N. New analysis of the ν_2 band of formaldehyde ($H_2^{12}C^{16}O$): Line positions for the nu_2, nu_3, nu_4 and nu_6 interacting bands. *J. Mol. Spectrosc.* **2007**, *245*, 141–144.

[127] J.-M.Flaud,; Lafferty, W. J.; Sams, R. L.; Sharpe, S. W. High resolution spectroscopy of $H_2{}^{12}C^{16}O$ in the 1.9 to 2.56μm spectral range. *Mol. Phys.* **2006**, *104*, 1891–1903.

[128] Lohilahti, J.; Alanko, S. High resolution infrared study of D_2CO in the region of 1780−2400 cm^{-1}: assignment and preliminary analysis. *J. Mol. Struc.* **2006**, *780-781*, 182–205.

[129] Lohilahti, J.; Alanko, S. The ν_2 band of Formaldehyde-d_2. *J. Mol. Spectrosc.* **2001**, *205*, 248–251.

[130] Perrin, A.; Flaud, J.-M.; Predoi-Cross, A.; Winnewisser, M.; Winnewisser, B. P.; Mellau, G.; Lock, M. igh-Resolution Analysis of the ν_3, ν_4, and ν_6 Bands of D_2CO Measured by Fourier Transform Spectroscopy. *J. Mol. Spectrosc.* **1998**, *187*, 61–69.

[131] Ellsworth, K.; Lajiness, B. D.; Lajiness, J. P.; Polik, W. F. Dispersed fluorescence spectroscopy of S_0 vibrational levels of formaldehyde-*d*. *J. Mol. Spectrosc.* **2008**, *252*, 205–213.

[132] Rauhut, G. Efficient calculation of potential energy surfaces for the generation of vibrational wave functions. *J. Chem. Phys.* **2004**, *121*, 9313–9322.

[133] Fortenberry, R. C.; Huang, X.; Yachmenev, A.; Thiel, W.; Lee, T. J. On the Use of Quartic Force Fields in Variational Calculations. *Chem. Phys. Lett.* **2013**, *574*, 1–12.

[134] Ruffle, D. P.; Hartquist, T. W.; Caselli, P.; Williams, D. A. The sulphur depletion problem. *Mon. Notices Royal Astron. Soc.* **1999**, *306*, 691–695.

[135] Agúndez, M.; Marcelino, N.; Cernicharo, J.; Tafalla, M. Detection of interstellar HCS and its metastable isomer HSC: new pieces in the puzzle of sulfur chemistry. *Astron. Astrophys.* **2018**, *611*, L1.

[136] Vastel, C.; Quénard, D.; Gal, R. L.; Wakelam, V.; Andrianasolo, A.; Caselli, P.; Vidal, T.; Ceccarelli, C.; Lefloch, B.; Bachiller, R. Sulphur chemistry in the L1544 prestellar core. *Mon. Notices Royal Astron. Soc.* **2018**, *478*, 5514–5532.

[137] Vidal, T. H. G.; Loison, J.-C.; Jaziri, A. Y.; Ruaud, M.; Gratier, P.; Wakelam, V. On the reservoir of sulphur in dark clouds: chemistry and elemental abundance reconciled. *Mon. Notices Royal Astron. Soc.* **2017**, *469*, 435–447.

[138] Cernicharo, J.; Lefloch, B.; Agúndez, M.; Bailleux, S.; Margulés, L.; Roueff, E.; Bachiller, R.; Marcelino, N.; Tercero, B.; Vastel, C.; Caux, E. Discovery of the Ubiquitous Cation NS^+ in Space Confirmed by Laboratory Spectroscopy. *Astrophys. J. Lett.* **2018**, *853*, L22.

[139] Fuente, A.; Goicoechea, J. R.; Pety, J.; Ga, R. L.; Martín-Doménech, R.; Gratier, P.; Guzmán, V.; Roueff, E.; Loison, J. C.; noz Caro, G. M. M.; Wakelam, V.; Gerin, M.; Riviere-Marichalar, P.; Vidal, T. First Detection of Interstellar S_2H. *Astrophys. J. Lett.* **2017**, *851*, L49.

[140] Fuente, A.; Cernicharo, J.; Roueff, E.; Gerin, M.; Pety, J.; Marcelino, N.; Bachiller, R.; Lefloch, B.; Roncero, O.; Aguado, A. Ionization fraction and the enhanced sulfur chemistry in Barnard 1. *Astron. Astrophys.* **2016**, *593*, A94.

[141] Agúndez, M.; Wakelam, V. Chemistry of Dark Clouds: Databases, Networks, and Models. *Chem. Rev.* **2013**, *113*, 8710–8737.

[142] Neufeld, D. A.; Godard, B.; Gerin, M.; des Forêts, G. P.; Bernier, C.; Falgarone, E.; Graf, U. U.; Güsten, R.; Herbst, E.; Lesaffre, P.; Schilke, P.; Sonnentrucker, P.; Wiesemeyer, H. Sulphur-bearing molecules in diffuse molecular clouds: new results from SOFIA/GREAT and the IRAM 30 m telescope. *Astron. Astrophys.* **2015**, *577*, A49.

[143] Azzam, A. A. A.; Tennyson, J.; Yurchenko, S. N.; Naumenko, O. V. ExoMol molecular line lists – XVI. The rotation–vibration spectrum of hot H_2S. *Mon. Notices Royal Astron. Soc.* **2016**, *460*, 4063–4074.

[144] Webb, A. D.; Dixon, R. N.; Ashfold, M. N. R. Imaging studies of the photodissociation

of H2S+ cations. I. Illustrations of the role of nuclear spin. *J. Chem. Phys.* **2007**, *127*, 224307.

[145] Webb, A. D.; Kawanaka, N.; Dixon, R. N.; Ashfold, M. N. R. Imaging studies of the photodissociation of H2S+ cations. II. *J. Chem. Phys.* **2007**, *127*, 224308.

[146] Duxbury, G.; Jungen, C.; Alijah, A.; Maier, J.; Klapstein, D. The Renner–Teller effect observed in the and electronic states of H_2S^+. *Mol. Phys.* **2014**, *112*, 3072–3084.

[147] Hochlaf, M.; Weitzel, K.-M.; Ng, C. Y. Vacuum ultraviolet pulsed-field ionization-photoelectron study of H_2S in the energy range of 10–17 eV. *J. Chem. Phys.* **2004**, *120*, 6944.

[148] Han, S.; Kang, T. Y.; Kimb, S. K. Rotationally resolved spectroscopy of the $\widetilde{A}^2A_1 \leftarrow \widetilde{X}^2B_1$ transition of H_2S^+ above the barrier to linearity using the mass-analyzed threshold ionization photofragment excitation technique. *J. Chem. Phys.* **2010**, *132*, 124304.

[149] Lahmar, S.; Lakhdar, Z. B.; Chambaudb, G.; Rosmus, P. Theoretical spectroscopic data for the X^2B_1 and A^2A_1 states of H_2S^+. *J. Mol. Struc.* **1995**, *333*, 29–37.

[150] Raghavachari, K.; Trucks., G. W.; Pople, J. A.; Head-Gordon, M. A fifth-order perturbation comparison of electron correlation theories. *Chem. Phys. Lett.* **1989**, *157*, 479–483.

[151] Dunning, T. H. Gaussian basis sets for use in correlated molecular calculations. I. The atoms boron through neon and hydrogen. *J. Chem. Phys.* **1989**, *90*, 1007–1023.

[152] Dunning, T. H.; Peterson, K. A.; Wilson, A. K. Gaussian basis sets for use in correlated molecular calculations. X. The atoms aluminum through argon revisited. *J. Chem. Phys.* **2001**, *114*, 9244.

[153] Martin, J. M. L.; Taylor, P. R. Basis set convergence for geometry and harmonic frequencies. Are h functions enough? *Chem. Phys. Lett.* **1994**, *225*, 473–479.

[154] Martin, J. M. L. On the effect of core correlation on the geometry and harmonic frequencies of small polyatomic molecules. *Chem. Phys. Lett.* **1995**, *242*, 343–350.

[155] Fortenberry, R. C.; Huang, X.; Francisco, J. S.; Crawford, T. D.; Lee, T. J. The *trans*-HOCO radical: Quartic force fields, vibrational frequencies, and spectroscopic constants. *J. Chem. Phys.* **2011**, *135*, 134301.

[156] Reiher, M.; Wolf, A. Exact decoupling of the Dirac Hamiltonian. II. The generalized Douglas–Kroll–Hess transformation up to arbitrary order. *J. Chem. Phys.* **2004**, *121*, 10945–10956.

[157] Schwenke, D. W. Variational calculations of rovibrational energy levels and transition intensities for tetratomic molecules. *J. Phys. Chem.* **1996**, *100*, 2867–2884.

[158] Werner, H.-J.; Knowles, P. J.; Knizia, G.; Manby, F. R.; Schütz, M. , et al. MOLPRO, version 2010.1, a package of ab initio programs. 2010; see http://www.molpro.net.

[159] Kállay, M. "MRCC, a quantum chemical program suite written by M. Kállay et al., J. Chem. Phys. 139, 094105 (2013), as well as: www.mrcc.hu.". 2018.

[160] Duxbury, G.; Horani, M.; Rostas, J. Rotational analysis of the electronic emission spectrum of the H_2S^+ ion radical. *Proc. R. Soc. Lond. A* **1972**, *331*, 109–137.

[161] Morgan, W. J.; Matthews, D. A.; Ringholm, M.; Agarwal, J.; Gong, J. Z.; Ruud, K.; Allen, W. D.; Stanton, J. F.; Schaefer III, H. F. Geometric Energy Derivatives at the Complete Basis Set Limit: Application to the Equilibrium Structure and Molecular Force Field of Formaldehyde. *J. Chem. Theory Comput.* **2018**,

[162] Huang, X.; Taylor, P. R.; Lee, T. J. Highly accurate quartic force field, vibrational

frequencies, and spectroscopic constants for cyclic and linear $C_3H_3^+$. *J. Phys. Chem. A* **2011**, *115*, 5005–5016.

[163] Zhao, D.; Doney, K. D.; Linnartz, H. LABORATORY GAS-PHASE DETECTION OF THE CYCLOPROPENYL CATION (c-$C_3H_3^+$). *Ap. J. Lett* **2004**,

[164] Berglund, M.; Wieser, M. E. Isotopic compositions of the elements 2009 (IUPAC Technical Report). *Pure Appl. Chem.* **2009**, *83*, 397–410.

[165] Viswanathan, R.; Dyke, T. R. Electric Dipole Moments and Nuclear Hyperfine Interactions of H_2S, HDS, and D_2S. *J. Mol. Spectrosc.* **1984**, *103*, 231–239.

[166] Minh, Y. C.; Brewer, M. K.; Irvine, W. M.; Friberg, P.; Johansson, L. E. B. Abundance and chemistry of interstellar $HOCO^+$. *Astron. Astrophys.* **1991**, *244*, 470–476.

[167] Vastel, C.; Phillips, T. G.; Ceccarelli, C.; Pearson, J. First detection of doubly deuterated hydrogen sulfide. *Astrophys. J.* **2003**, *593*, L97–L100.

[168] Benz, A. O. et al. Hydrides in young stellar objects: Radiation tracers in a protostar-disk-outflow system. *Astron. Astrophys.* **2010**, *521*, L35.

[169] Müller, H. S. P.; Goicoechea, J. R.; Cernicharo, J.; Agúndez, M.; Pety, J.; Cuadrado, S.; Gerin, M.; Dumas, G.; Chapillon, E. Revised spectroscopic parameters of SH^+ from ALMA and IRAM 30m observations. *Astron. Astrophys.* **2014**, *569*, L5.

[170] Belov, S. P.; Yamada, K. M. T.; Winnewisser, G.; Poteau, L.; Bocquet, R.; Demaison, J.; Polyansky, O.; Tretyakov, M. Y. Terahertz Rotational Spectrum of H_2S. *J. Mol. Spectrosc.* **1995**, *173*, 380–390.

[171] Azzam, A. A.; Yurchenko, S. N.; Tennyson, J.; Martin-Drumel, M.-A.; Pirali, O. Terahertz spectroscopy of hydrogen sulfide. *J. Quant. Spectrosc. Radiat. Transf.* **2013**, *130*, 341–351.

[172] Cazzoli, G.; Puzzarini, C. The rotational spectrum of hydrogen sulfide: The $H_2^{33}S$ and $H_2^{32}S$ isotopologues revisited. *J. Mol. Spectrosc.* **2014**, *298*, 31–37.

[173] Cazzoli, G.; Puzzarini, C.; Gauss, J. Rare isotopic species of hydrogen sulfide: the rotational spectrum of $H_2^{36}S$. *Astron. Astrophys.* **2014**, *566*, A52.

[174] Mürtz, P.; Zink, L. R.; Evenson, K. M.; Brown, J. M. Measurement of high-frequency rotational transitions of H_2O^+ in its ground state by far-infrared laser magnetic resonance (LMR) spectroscopy. *J. Chem. Phys.* **1998**, *109*, 9744.

[175] Ossenkopf, V. et al. Detection of interstellar oxidaniumyl: Abundant H_2O^+ towards the star-forming regions DR21, Sgr B2, and NGC6334. *Astron. Astrophys.* **2010**, *518*, L111.

[176] Menten, K. M.; Wyrowski, F.; Belloche, A.; Güsten, R.; Dedes, L.; Müller, H. S. P. Submillimeter absorption from SH^+, a new widespread interstellar radical, $^{13}CH^+$ and HCl. *Astron. Astrophys.* **2011**, *525*, A77.

[177] Gillis, J. R.; Edwards, T. H. Analysis of $2\nu_2$, ν_1, and ν_3 of H_2S. *J. Mol. Spectrosc.* **1981**, *85*, 55–73.

[178] Lane, W. C.; Edwards, T. H.; Gillis, J. R.; Bonomo, F. S.; Murcray, F. J. Analysis of ν_3 of H_2S. *J. Mol. Spectrosc.* **1982**, *95*, 365–380.

[179] Liu, A.-W.; Ulenikov, O.; Onopenko, G.; Gromova, O.; Bekhtereva, E.; Wan, L.; Hao, L.-Y.; Hu, S.-M.; Flaud, J.-M. Global fit of the high-resolution infrared spectrum of D_2S. *J. Mol. Spectrosc.* **2006**, *238*, 11–28.

[180] Dateo, C. E.; Lee, T. J. An accurate ab initio quartic force field and vibrational frequencies for cyclopropenylidene. *Spectrochim. Acta, Part A.* **1997**, *53*, 1065–1077.

[181] Spezzano, S.; Tamassia, F.; Thorwirth, S.; Thaddeus, P.; Gottlieb, C. A.; McCarthy, M. C. A high-resolution isotopic study of the rotational spectrum of c-C_3H_2. *Astrophys. J. Suppl. S.* **2013**, *200*, 1–11.

[182] Schmidt, S. R.; Zack, L. N.; Ziurys, L. M. Widespread CCH and c-C_3H_2 in the Helix Nebula: Unraveling the Chemical History of Hydrocarbons. *Astrophys. J. Lett.* **2018**, *864*, L31.

[183] Chantzos, J.; Spezzano, S.; Caselli, P.; Chacón-Tanarro, A.; Bizzocchi, L.; Sipilä, O.; Giuliano, B. M. A Study of the c-C_3HD/c-C_3H_2 Ration in Low-mass Star-forming Regions. *Astrophys. J.* **2018**, *863*, 126.

[184] Lee, T. J.; Huang, X.; Dateo, C. E. The effect of approximating some molecular integrals in coupled-cluster calculations: fundamental frequencies and rovibrational spectroscopic constants for isotopologues of cyclopropenylidene. *Mol. Phys.* **2010**, *107*, 1139–1152.

[185] Fortenberry, R. C.; Lee, T. J.; Layfield, J. P. The Failure of Correlation to Describe Out−of−Plane Carbon=Carbon Bending. *J. Chem. Phys.* **2017**, *147*, 221101.

[186] Fortenberry, R. C.; Novak, C. M.; Layfield, J. P.; Matito, E.; Lee, T. J. Overcoming the Failure of Correlation for Out−of−Plane Motions in a Simple Aromatic: Rovibrational Quantum Chemical Analysis of c-C_3H_2. *J. Chem. Theory Comput.* **2018**, *14*, 2155–2164.

[187] Császár, A. G. Anharmonic molecular force fields. *WIREs Comput. Mol. Sci.* **2012**, *2*, 273–289.

[188] Fortenberry, R. C.; Novak, C. M.; Lee, T. J. Rovibrational Analysis of c−SiC_2H_2: Further Evidence for Out−of−Plane Bending Issues in Correlated Methods. *J. Chem. Phys.* **2018**, *149*, 024303.

[189] Lee, T. J.; Allen, W. D.; Schaefer III, H. F. The analytic evaluation of energy first derivatives for two-configuration self-consistent-field configuration interaction (TCSCF-CI) wave functions. Application to ozone and ethylene. *J. Chem. Phys.* **1987**, *87*, 7062.

[190] Ahern, A. M.; Garrell, R. L.; Jordan, K. D. Theoretical investigation of the normal-mode vibrational frequencies and intensities of ethylene. *J. Phys. Chem.* **1988**, *92*, 6228–6232.

[191] Simandiras, E. D.; Rice, J. E.; Lee, T. J.; Amos, R. D.; Handy, N. C. On the necessity of f basis functions for bending frequencies. *J. Phys. Chem.* **1988**, *88*, 3187.

[192] Martin, J. M. L.; Taylor, P. R.; Lee, T. J. The harmonic frequencies of benzene. A case for atomic natural orbital basis sets. *Chem. Phys. Lett.* **1997**, *29*, 414–422.

[193] Green, W. H.; Jayatilaka, D.; Willetts, A.; Amos, R. D.; Handy, N. C. The prediction of spectroscopic properties from quartic correlated force fields: HCCF, HFCO, SiH_3^+. *J. Chem. Phys.* **1990**, *93*, 4965.

[194] Gong, J. Z.; Matthews, D. A.; Changala, P. B.; Stanton, J. F. Fourth-order vibrational perturbation theory with the Watson Hamiltonian: Report of working equations and preliminary results. *J. Chem. Phys.* **2018**, *149*, 114102.

[195] Iott, J.; Haftka, R. T.; Adelman, H. M. *Selecting Step Sizes in Sensitivity Analysis by Finite Differences*; 1985.

[196] Mills, I. M. In *Molecular Spectroscopy - Modern Research*; Rao, K. N., Mathews, C. W., Eds.; Academic Press: New York, 1972; pp 115–140.

[197] Aliev, M. R.; Watson, J. K. G. In *Molecular Spectroscopy: Modern Research*; Rao, K. N., Ed.; Academic Press: New York, 1985; Vol. 3; pp 2–63.

[198] Huang, J. W.; Graham, W. R. M. Fourier transform infrared study of tricarbon hydride radicals trapped in Ar at 10 K. *J. Chem. Phys.* **1990**, *93*, 1583.

[199] Seburg, R. A.; Patterson, E. V.; Stanton, J. F.; McMahon, R. J. Structures, Automerizations, and Isomerizations of C_3H_2 Isomers. *J. Am. Chem. Soc.* **1997**, *119*, 5847–5846.

[200] Hirahara, Y.; Masuda, A.; Kawaguchi, K. Fourier transform infrared spectroscopy of the ν_3 band of cyclopropenylidene, C_3H_2. *J. Chem. Phys.* **1991**, *95*, 3975.

[201] Watson, J. K. G. The correlation of the symmetry classifications of states of nonrigid molecules. *Can. J. Phys* **1965**, *43*, 1996–2007.

[202] Bell, R. P. *The Tunnel Effect in Chemistry*, 1st ed.; University Press, 1980.

[203] Huang, X.; Schwenke, D. W.; Lee, T. J. Rovibrational spectra of ammonia. I. Unprecedented accuracy of a potential energy surface used with nonadiabatic corrections. *J. Chem. Phys.* **2011**, *134*, 044320.

[204] Sung, K.; Brown, L. R.; Huang, X.; Schwenke, D. W.; Lee, T. J.; Coy, S. L.; Lehmann, K. K. Rovibrational spectra of ammonia. I. Unprecedented accuracy of a potential energy surface used with nonadiabatic corrections. *J. Quant. Spectrosc. Rad. Trans.* **2012**, *113*, 1066–1083.

[205] Gordon, J. P.; Zeiger, H. J.; Townes, C. H. The Maser–New Type of Microwave Amplifier, Frequency Standard, and Spectrometer. *Phys. Rev.* **1955**, *99*, 1264.

[206] Sousa-Silva, C.; Tennyson, J.; Yurchenko, S. N. Communication: Tunnelling splitting in the phosphine molecule. *J. Chem. Phys.* **2016**, *145*, 091102.

[207] Okuda, S.; Sasada, H. Search for inversion splitting in the $3\nu_2$ band of phosphine. *J. Molec. Spectrosc.* **2018**, *346*, 27–31.

[208] Dixon, D. A.; Feller, D.; Peterson, K. A. Accurate Calculations of the Electron Affinity and Ionization Potential of the Methyl Radical. *J. Phys. Chem. A* **1997**, *101*, 9405–9409.

[209] Rajamäki, T.; Noga, J.; Valiron, P.; Halonen, L. Inversion levels of H_3O^+ as a probe for the basis set convergence in traditional and explicitly correlated coupled-cluster calculations. *Mol. Phys.* **2004**, *102*, 2259–2268.

[210] Liu, D.-J.; Oka, T. Experimental Determination of the Ground-State Inversion Splitting of H_3O^+. *Phys. Rev. Lett.* **1985**, *54*, 1787–1789.

[211] Ellison, G. B.; Engelking, P. C.; Lineberger, W. C. An Experimental Determination of the Geometry and Electron Affinity of CH_3. *J. Am. Chem. Soc.* **1978**, *100*, 2556–2558.

[212] Oliveria, A. M.; Lu, Y.-J.; Lehman, J. H.; Changala, P. B.; Baraban, J. H.; Stanton, J. F.; Lineberger, W. C. Photoelectron Spectroscopy of the Methide Anion: Electron Affinities of $^{\bullet}CH_3$ and $^{\bullet}CD_3$ and Inversion Splittings of CH_3^- and CD_3^-. *J. Am. Chem. Soc.* **2015**, *137*, 12939–12945.

[213] Bowman, M. C.; Zhang, B.; Morgan, W. J.; Schaefer III, H. F. A Remarkable Case of Basis Set Dependence: The Equilibrium Geometry and Harmonic Vibrational Frequencies of the Methyl Anion. *Mol. Phys.* **2018**,

[214] Morgan, W. J.; Fortenberry, R. C.; Schaefer III, H. F.; Lee, T. J. Vibrational Analysis of the Ubiquitous Interstellar Molecule Cyclopropenylidene (c-C_3H_2): The Importance of Numerical Stability. *Mol. Phys*

[215] Martin, J. M. L.; Lee, T. J. An accurate ab initio quartic force field for ammonia. *J. Chem. Phys.* **1992**, *97*, 8361.

[216] Henry, L.; Amat, G. The Cubic Anharmonic Potential Energy Functin of Polyatomic Molecules. *J. Molec. Spectrosc.* **1960**, *5*, 319–325.

[217] Henry, L.; Amat, G. The Quartic Anharmonic Potential Energy Functin of Polyatomic Molecules. *J. Molec. Spectrosc.* **1965**, *15*, 168–179.

[218] Werner, H.-J.; Knowles, P. J.; Knizia, G.; Manby, F.; Schütz, M. Molpro: a general-purpose quantum chemistry program package. *WIREs Comput. Mol. Sci* **2012**, *2*, 242–253.

[219] Glendening, E. D.; J, K. B.; Reed, A. E.; Carpenter, J. E.; Bohmann, J. A.; Morales, C. M.; Landis, C. R.; Weinhold, F. 2013; NBO 6.0. Theoretical Chemistry Institute, University of Wisconsin, Madison.

[220] Yamada, C.; Hirota, E.; Kawaguchi, K. Diode laser study of the ν_2 band of the methyl radical. *J. Chem. Phys.* **1981**, *75*, 5256–5264.

[221] Engelking, P. C. Approximate Rotational Band Shifts. *J. Phys. Chem.* **1986**, *90*, 4544–4545.

[222] Bunker, P. R.; Jensen, P. *Fundamentals of Molecular Symmetry*; IOP Publishing, 2005; pp 274–277.

[223] Poynter, R. L.; Kakar, R. K. The Microwave Frequencies, Line Parameters, and Spectral Constants for $^{14}NH_3$. *Astrophys. J. Suppl. Ser.* **1975**, *29*, 87–96.

[224] Tang, J.; Oka, T. Infrared Spectroscopy of H_3O^+: The ν_1 Fundamental Band. *J. Mol. Spectroc.* **1999**, *196*, 120–130.

[225] Simons, J. Molecular Anions. *J. Phys. Chem. A.* **2008**, *112*, 6401–6511.

[226] Rajamäki, T.; Miani, A.; Halonen, L. Six-dimensional ab initio potential energy surfaces for H_3O^+ and NH_3 Approaching the subwave number accuracy for the inversion splittings. *J. Chem. Phys.* **2003**, *118*, 10929–10937.